

# Zero<sup>th</sup>-Order Design Report for the Electron-Light Ion Collider at CEBAF

A. Afanasev, A. Bogacz, A. Bruell, L. Cardman, Y. Chao, S. Chattopadhyay, E. Chudakov, P. Degtarenko, J. Delayen, Ya. Derbenev, R. Ent, P. Evtushenko, A. Freyberger, J. Grames, A. Hutton, R. Kazimi, G. Krafft, R. Li, L. Merminga, M. Poelker, A. Thomas, C. Weiss, B. Wojtsekhowski, B. Yunn, Y. Zhang

**Thomas Jefferson National Accelerator Facility**  
Newport News, Virginia, USA

W. Fischer, C. Montag  
**Brookhaven National Laboratory**  
Upton, New York, USA

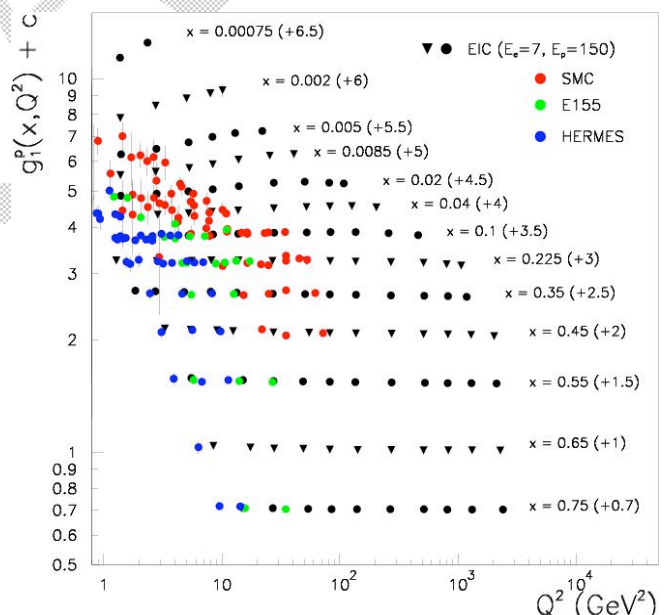
V. Danilov  
**Oak Ridge National Laboratory**  
Oak Ridge, Tennessee, USA

V. Dudnikov  
**Brookhaven Technology Group**  
New York, New York, USA

P. Ostroumov  
**Argonne National Laboratory**  
Argonne, Illinois, USA

V. Derenchuk  
**Indiana University Cyclotron Facility**  
Bloomington, Indiana, USA

A. Belov  
**Institute of Nuclear Research**  
Moscow-Troitsk, Russia



Editors: Ya. Derbenev, L. Merminga, Y. Zhang

# Table of Contents

## Executive Summary

## Introduction

### I Nuclear Physics with ELIC

- 1.1 The structure of the nucleon
- 1.2 The spin-flavor landscape of the nucleons
  - 1.2.1 The impact of quark and gluon motion on the nucleon spin
  - 1.2.2 How do hadronic final states form in QCD
- 1.3 Quarks and gluons in nuclei
- 1.4 Summary of luminosity requirements

### II General Description of ELIC at CEBAF

- 2.1 Nuclear physics requirements
- 2.2 Basic constituents and beam parameters
- 2.3 ELIC luminosity concepts
- 2.4 Electron facility
- 2.5 Positron source
- 2.6 Ion facility
- 2.7 Electron cooling
- 2.8 Interaction region
- 2.9 Polarization

### III Forming and Operating Electron/Positron Beams

- 3.1 Polarized electron source and injector
- 3.2 Positron source at CEBAF
- 3.3 Electron/positron storage ring
- 3.4 Lattice design and beam emittance
- 3.5 Spin control
- 3.6 Collective effects and beam stability

### IV Forming and Operating Ion Beams

- 4.1 Polarized light ion and heavy ion sources
- 4.2 Linear accelerator, pre-booster and large booster
- 4.3 Stacking ions
- 4.4 Collider ring
- 4.5 Cooling of ion beam
- 4.6 Transport, maintenance and manipulation of ion spin
- 4.7 Collective effects and beam stability

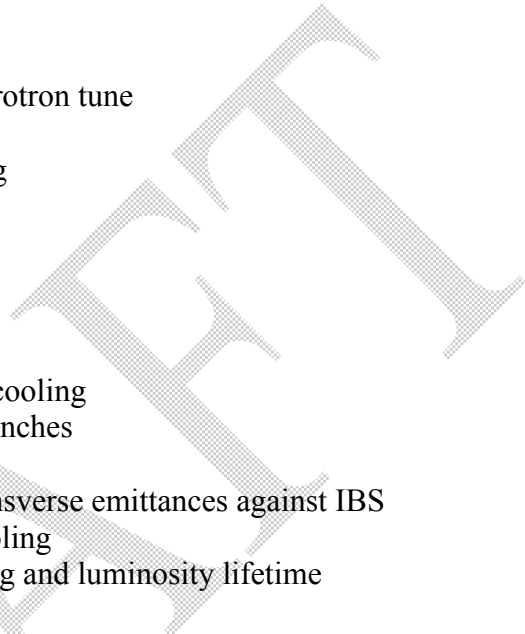
### V High Energy Electron Cooling of ELIC

- 5.1 Introduction: EC principles and physics
- 5.2 Basic parameters and general concept of HEEC for ELIC
- 5.3 ERL for HEEC

- 5.4 HEEC with circulator ring
- 5.5 Cooling and IBS rates
- 5.6 Staged cooling
- 5.7 Dispersive cooling
- 5.8 Flat beams cooling

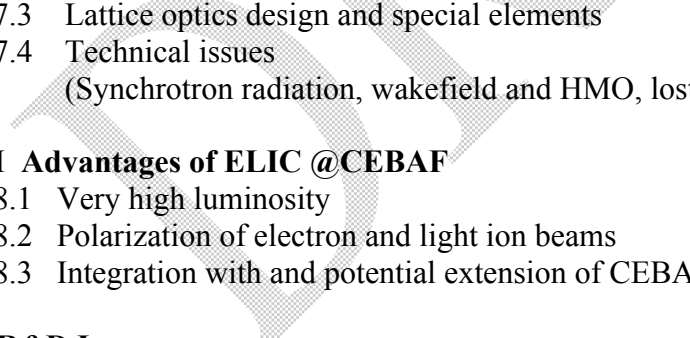
## **VI Concepts for High Luminosity**

- 6.1 Overview
- 6.2 Beam-beam effects
  - 6.2.1 Beam-beam resonances
  - 6.2.2 Beam-beam dependence on synchrotron tune
  - 6.2.3 Coherent stability
  - 6.2.4 Multiple IP interference and tuning
- 6.3 Laslett's limit on ion beam
- 6.4 Particle Scattering Processes
  - 6.4.1 Multiple intrabeam scatterings
  - 6.4.2 Touscheck effect on ion beam
  - 6.4.3 Background collision processes
- 6.5 Luminosity improvements with electron cooling
  - 6.5.1 Low beta star with short cooled bunches
  - 6.5.2 Crab crossing colliding beams
  - 6.5.3 Reduction and maintenance of transverse emittances against IBS
  - 6.5.4 Reduction of IBS by flat beam cooling
  - 6.5.5 Diminishing of Touschek scattering and luminosity lifetime
- 6.6 Summary



## **VII Interaction region**

- 7.1 Detector design considerations
- 7.2 Final focusing and crab crossing
- 7.3 Lattice optics design and special elements
- 7.4 Technical issues  
(Synchrotron radiation, wakefield and HMO, lost particle background)



## **VIII Advantages of ELIC @CEBAF**

- 8.1 Very high luminosity
- 8.2 Polarization of electron and light ion beams
- 8.3 Integration with and potential extension of CEBAF fixed target program

## **IX R&D Issues**

## **X Summary**

### **Appendix A**

- A1 Complete ELIC parameter list
- A2 Site Map

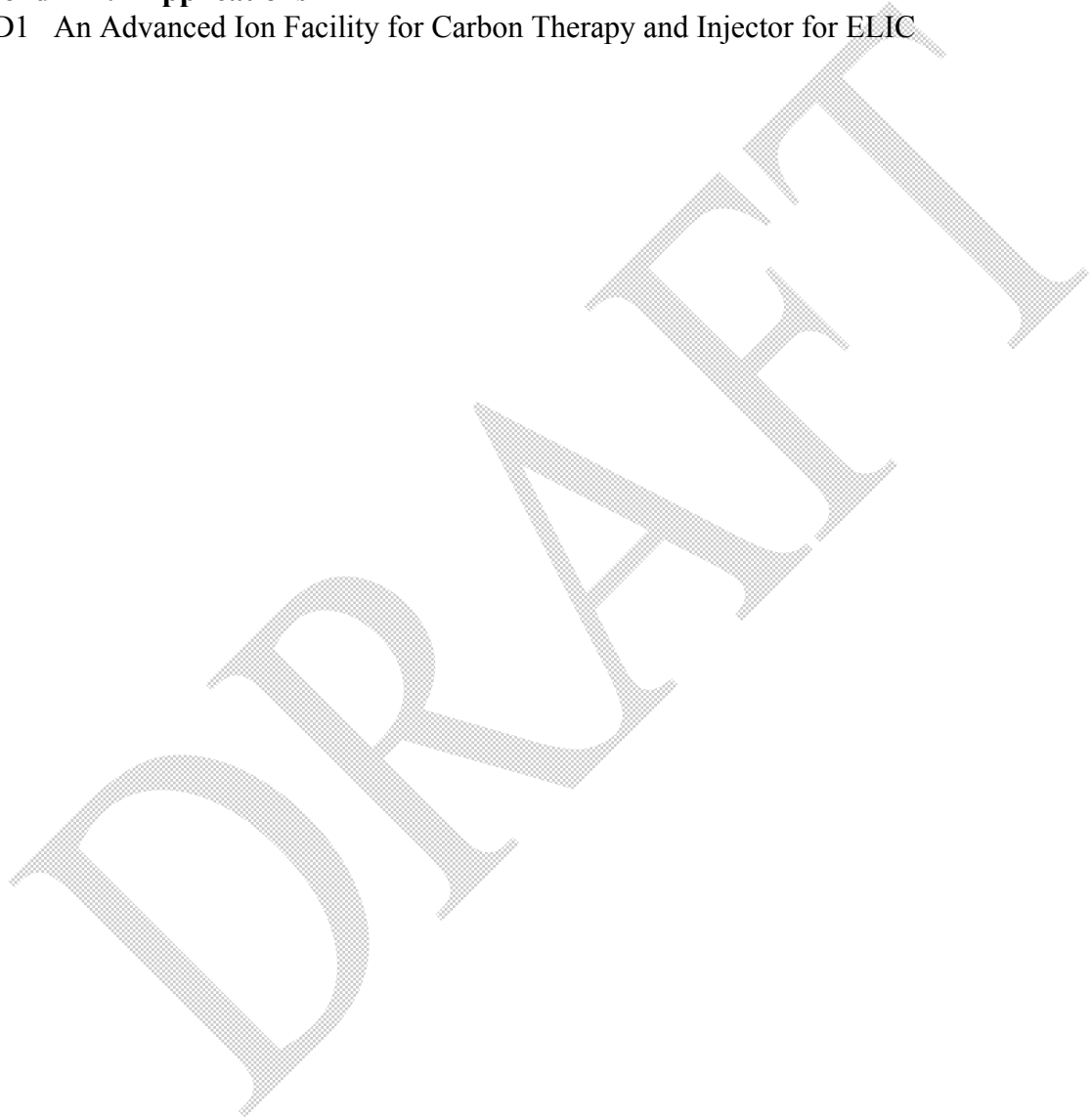
### **Appendix B: ELIC Linac-Ring: Advantages and Technical Challenges**

- B1 Design consideration: ring-ring vs. linac-ring
- B2 High average current polarized electron source and injector
- B3 Energy recovery linac
- B4 Electron circulator-collider ring

## **Appendix C: A High Luminosity Polarized $e^-e^-$ Collider**

### **Appendix D: Applications**

- D1 An Advanced Ion Facility for Carbon Therapy and Injector for ELIC



## Executive Summary

Thirty years after the establishment of QCD as the theory of the strong nuclear interaction, and despite significant progress towards understanding of the structure of hadronic matter, some crucial questions involving the role and behavior of quarks and gluons in atomic nuclei remain open. In particular, one would like to: 1) develop a quantitative understanding of the contribution of gluons to the binding and the spin of the nucleon; 2) learn how the dynamics of confinement leads to the formation of hadrons – a key aspect of the transition from the deconfined state of free quarks and gluons in the Big Bang to stable hadron matter; and 3) determine how the nuclear medium affects quarks and gluons.

The nuclear physics community worldwide has suggested that a high-luminosity, at or above  $10^{33} \text{ cm}^{-2} \text{ sec}^{-1}$ , polarized Electron-Ion Collider with variable center-of-mass range  $\sqrt{s}$  in the range of 20 to 100 GeV would allow us to probe the hadronic structure of matter and provide answers to these questions. The 2001 Long Range Plan for the next decade, outlining opportunities in nuclear science, put an Electron-Ion Collider forward as the next major facility to consider for the field. They emphasized the need to refine the scientific case, and to pursue the accelerator R&D necessary to ensure that the optimum technical design could be chosen. The 2002 Ad-hoc Facilities NSAC Subcommittee identified the research program of such a facility as “absolutely central to Nuclear Physics”.

A high luminosity, polarized Electron-Light Ion Collider, ELIC, which uses CEBAF, and requires the construction of a 30 to 150 GeV ion storage ring, has been proposed since 2001. ELIC’s unique and innovative design features directly aim at addressing the science program outlined above:

- ELIC, with the “figure-8” electron and ion collider rings designed to ensure spin preservation and ease of spin manipulation, is the first-ever collider specifically aimed at full exploitation of spin physics.
- The high luminosity of ELIC, at the  $10^{35} \text{ cm}^{-2} \text{ s}^{-1}$  level, is crucial for measurements of small cross sections, thus allowing us to probe at unknown essential features of the proton landscape - such as the impact of quark motion on the proton’s spin - through so-called deep exclusive measurements.
- Distributions of quarks inside the nucleus differ in non-trivial ways from those in a free nucleon. Extending the range of nuclei up to  $^{40}\text{Ca}$  allows to probe such effects over a large range of scales, and allows, for the first time, access to the modification of gluon distributions in nuclei.

This report, the ELIC Zero<sup>th</sup>-Order Design Report, is the first detailed document outlining the physics reach of ELIC, and summarizing the accelerator design, and R&D required to demonstrate the technical feasibility of ELIC. The accelerator design studies have resulted in a consistent set of parameters that meet the required performance goals. Accelerator physics issues have been investigated and important R&D topics have been identified. An R&D strategy planned to address the physics and technology challenges is outlined.

ELIC is an electron-light ion collider with center of mass energy of 20 to 65 GeV and luminosity up to  $8 \times 10^{34} \text{ cm}^{-2} \text{ s}^{-1}$ . This high luminosity collider is envisioned as a future upgrade of CEBAF, beyond

the 12 GeV Upgrade, and compatible with simultaneous operation of the 12 GeV CEBAF (or a potential extension to 24 GeV) for fixed-target experiments.

The CEBAF accelerator with polarized injector can be used as a full energy injector into a 3-7 GeV electron storage ring. A positron source is envisioned as an addition to the CEBAF injector, for generating positrons that can be accelerated in CEBAF, accumulated and polarized in the electron storage ring, and collide with ions with luminosity similar to the electron/ion collisions.

The ELIC facility is designed to produce a variety of polarized light ion species: p, d,  $^3\text{He}$  and Li, and unpolarized light to medium ion species. To attain the required ion beams, an ion facility must be constructed, a major component of which is a 150 GeV collider ring located in the same tunnel and below the electron storage ring. A critical component of the ion complex is an ERL-based continuous electron cooling facility, anticipated to provide low emittance and simultaneously very short ion bunches.

ELIC is designed to accommodate up to four interaction regions (IR's), consistent with realistic detector designs. Longitudinal polarization is guaranteed for protons, electrons, and positrons in all four IR's simultaneously and for deuterons in up to two IR's simultaneously.

An alternate design approach for ELIC is based on the linac-ring concept, in which CEBAF operates as a single-pass Energy Recovery Linac (ERL) providing full energy electrons for collisions with the ions. Although this approach promises potentially higher luminosity than the ring-ring option, it requires significant technological advances and associated R&D. A linac-ring ELIC design is described in the Appendix, as the ultimate Upgrade of ELIC, fully compatible with and a natural extension of the ring-ring scheme.

# I Nuclear Physics with ELIC

## Contents

- 1.1 The Structure Of The Nucleon**
- 1.2 The Spin-Flavor Landscape Of The Nucleons**
  - 1.2.1 The Impact Of Quark And Gluon Motion On The Nucleon Spin**
  - 1.2.2 How Do Hadronic Final States Form In QCD**
- 1.3 Quarks And Gluons In Nuclei**
- 1.4 Summary Of Luminosity Requirements**

Three decades after the establishment of QCD as the theory of the strong nuclear interaction, understanding the structure of the basic components of matter (protons, neutrons and nuclei) remains one of the great puzzles in nuclear physics. QCD stipulates that colored quarks are the basic constituents of strongly-interacting matter, and gluons are the mediators of this interaction through the exchange of color. In contrast to the well understood electromagnetic interaction where photons act only as mediators, gluons carry color and can thus interact with each other. This unique non-abelian character of QCD implies that, unlike any other many-body system, the individual quark and gluon constituents inside a proton cannot be removed from the system and examined in isolation.

This non-linearity of QCD at long distance scales (termed confinement) makes calculations and theoretical predictions difficult, as the world we encounter consists of nucleons and mesons, rather than the fundamental degrees of freedom of QCD — quarks and gluons. For the same reason, at short distance scales the quarks and gluons behave essentially as free particles (asymptotic freedom), and QCD renders reliable predictions in the high-energy limit.

A great achievement of nuclear and particle physics has been the quantitative verification of the QCD theory in hard scattering processes, at distance scales several times smaller than the size of the proton. At these short distances, the quarks and gluons have a very clear experimental signature, and their dynamics follows the prediction of perturbative QCD calculations. Such experiments have, *e.g.*, established that the quarks carry about 50% of the proton's momentum (the rest being carried by gluons), and - surprisingly - only 30% of the proton's spin. Furthermore, significant modification of the momentum distributions of quarks in a nucleus has been demonstrated (although not yet understood), but not much is known about other properties of quarks (and gluons) in a nucleus. Yet, at some level the quarks and gluons must be responsible for the binding of nuclei. Similarly, there are still glaring gaps in our knowledge of quarks and gluons inside the proton. What is the role of gluons and angular momentum in the description of the proton's spin? What is happening at very low momentum fractions where more and more gluons are expected to start overlapping each other? How large are the correlations between quarks and gluons inside the nucleon? And how are they distributed in transverse space? In addition, although the knowledge gained in regions where quarks and gluons behave as essentially free is impressive, we know that no free quarks exist, and the quarks and gluons must have strong correlations in certain kinematic regions.

Recent advances in computational technology, lattice field theory algorithms, continuum model building, accelerator beam quality, and detector design have led us to the threshold of developing a

true understanding of the fundamental mechanisms of QCD and the ability to solve QCD, also at a long distance scale, quantitatively. However, such an understanding requires an extensive series of precise measurements, utilizing a hard electron-quark collision not only to access deep inelastic scattering processes, but also the more selective (and hence having a smaller cross section) semi-inclusive and deep exclusive processes. For the latter, the consensus is that a momentum transfer squared of about  $Q^2 \sim 10$  GeV would be optimal, thus leading to the requirement for high luminosity. A large range in energy is similarly required, to cover the full region of  $x$  (the momentum fraction of the struck quark), from the region where gluons dominate to where solely quarks remain.

The feasibility of a high-luminosity (up to  $10^{30}$  cm $^{-2}$  sec $^{-1}$ ) electron-light ion collider in the center-of-mass energy range  $\sqrt{s}$  of 20-65 GeV, in combination with data that will have been obtained from a 12-GeV Upgrade fixed target facility, is optimal to finally understand the elusive structure of the nucleon. In particular, such a facility will provide the perfect tool to:

- develop a quantitative understanding of how quarks and gluons provide the binding and spin of the nucleon,
- understand how hadronic final states form from quarks and gluons,
- and, determine how the nuclear medium affects the properties of quarks and gluons.

The collider geometry offers two major advantages over fixed target e-p studies. First, the collider is capable to deliver a much increased center of mass energy thus providing a larger range in  $x$  and  $Q^2$  in the primary collision. Secondly, the collider eases the requirements for particle detection. In a fixed target experiment relativity boosts the reaction fragments to small laboratory angles, a problem that is absent in a collider geometry. In addition, low-energy nuclear fragments might not escape the fixed target nuclear environment, whereas these fragments can easily escape in the lower-luminosity e-p collision area.

At the design center-of-mass energy of 65 GeV, it will be possible to access values of  $x$  down to  $2.5 \cdot 10^{-4}$ , for  $Q^2 > 1$  GeV $^2$ , the typical kinematic limit for the deep inelastic scattering region (in deep inelastic scattering, the collision is assumed to occur on a free quark). From here, one can use scaling arguments to derive the accessible  $x$ - $Q^2$  ranges for variable center-of-mass energies  $s$ , since  $x$  scales as  $s^{-1}$ . Finally, having both beams polarized will allow full access to the spin structure of the nucleons.

## 1.1 The Structure of the Nucleon

Electron scattering directly probes the charged quarks residing in the proton. Following the seminal work of Freedman, Kendall, and Taylor at SLAC in the early 70's, three decades of deep inelastic scattering experiments have mapped the momentum distributions of light quarks over a large range in  $x$  and  $Q^2$ .

On the other hand, the study of the gluons within the nucleon is only possible at high energies, with the established technique being the determination of the gluon momentum distributions through the evolution equations of QCD. Great progress has been made here at the HERA collider which has

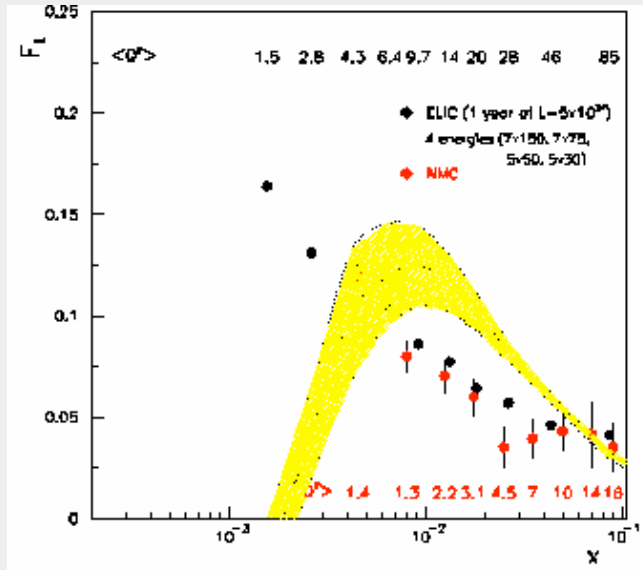
established the total dominance of gluons at low values of  $x$ . However, this technique is hampered by the lack of large ranges in  $Q^2$  for all values of  $x$ , rendering large uncertainties in  $G(x, Q^2)$  at large  $x$  and the region of small  $x$  and  $Q^2$ .

In the latter region, additional questions exist whether the conventional  $Q^2$  evolution is applicable. At small  $x$ , higher-order perturbative corrections may become important in the region of low  $Q^2$ , and possibly even the fixed-order perturbative expansion in the strong coupling constant  $\alpha_s$  may turn inadequate. Using global parton distribution fitting algorithms, gluon distributions in this region can even turn negative. With the question still outstanding whether the gluons inside the proton can also behave as pre-existing, valence-like, constituents, or are rather the sole products of perturbative gluon Bremsstrahlung and gluon-gluon splitting processes, it is exactly this low  $Q^2$  region where we would like to map the gluon content of the proton to study nucleon structure.

Measurement of the longitudinal structure function  $F_L$  would directly settle these issues.  $F_L$  gives direct access to the gluon momentum distributions in the region of small  $x$ , where  $F_L \approx \alpha_s(Q^2)xG(x, Q^2)$ , and good access in the region of large  $x$ . The Electron-Ion Collider, with its variable energy scheme, would allow truly unprecedented measurements of  $F_L$  (see Fig. 1). For the proton, this would render a substantial decrease of the uncertainties in  $G(x, Q^2)$ , especially in the region of interest, *i.e.*, at low values of  $x$  and moderate values of  $Q^2$ .

Figure 1 Projected data for the longitudinal structure function  $F_L$  at an Electron-Ion Collider, assuming an integrated luminosity of  $100 \text{ fb}^{-1}$ . Four different accelerator energies have been assumed: 7 GeV electrons colliding with 150 GeV protons, 7 GeV electrons and 75 GeV protons, and 5 GeV electrons colliding with 50 (30) GeV protons. A minimum of 3 measurements and a minimum range in  $\epsilon$  of 0.25 has been required for each  $(x, Q^2)$  point. Finally, the results have been averaged over  $Q^2$ .

At small Bjorken  $x$ ,  $F_L$  is directly related to the gluon momentum distribution  $G(x, Q^2)$ , as  $G(x, Q^2) = F_L(0.8, Q^2)$ . The present uncertainty in  $G(x, Q^2)$  is indicated by the shaded band representing  $F_L$  calculated from the CTEQ6M parton distribution (at the  $Q^2$  values of ELIC), where the turning over at small  $x$  reflects the collapse of the NLO calculation of the longitudinal proton structure function at small  $x$  and  $Q^2$ . The existing data from NMC are also shown (red circles). The average  $Q^2$  values of both the projected EIC measurement (black numbers at the top) and the existing NMC measurement (red numbers at the bottom) are given for each of the respective  $x$  values.



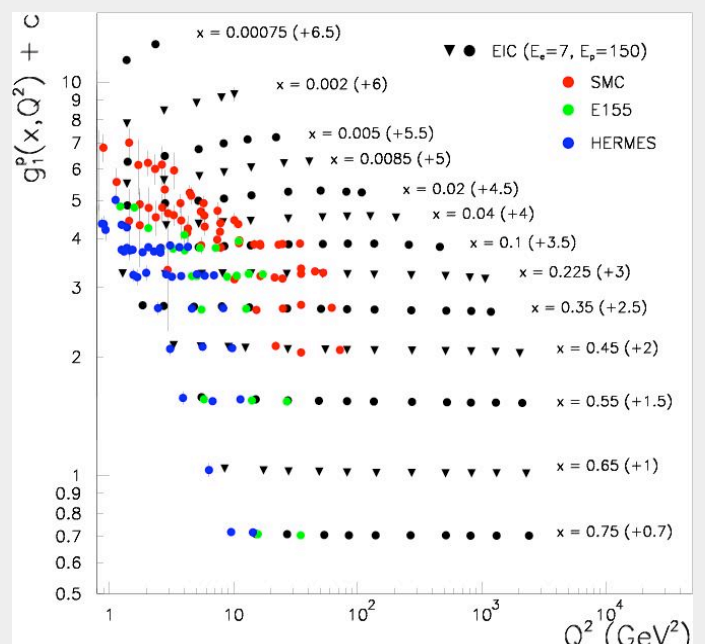
Since gluons do not carry isospin, the gluon distribution in protons and neutrons are expected to be identical. However, the gluon distribution in the deuteron will be modified due to binding. At small  $x$ , measurements give additional insight in the connection of nuclear shadowing and diffraction.  $F_L$  measurements are an obvious vehicle for this topic, as it is more difficult for a longitudinal photon to convert into a  $\gamma\gamma$  pair and diffractively scatter off a nucleon. Deuteron measurements would fold in an unprecedented study of the effects of nuclear binding on diffractive cross sections (the latter processes represent one of the major surprises of the HERA/DESY data: in about 15% of the hard collisions the entire nucleus was found to remain intact, a finding difficult to reconcile with a hard electron-quark scattering).

## 1.2. The Spin-Flavor Landscape of the Nucleons

One of the greatest successes of the Quark Model has been the description of the static properties of the nucleon and other baryons. Within this picture, the proton (neutron) consists of two up (down) and one down (up) valence quarks. Similarly, all baryons observed to-date can be classified as two or three quark states. However, with quarks and gluons forever confined, a more realistic description includes a sea of quarks, anti-quarks and gluons popping into existence one moment to disappear the next, with a few ever-present valence quarks. All of these have nearly light-speed momentum, and possibly large angular momentum. How all this activity can be related to the static properties of the nucleon remains a mystery.

Fig. 2. Projected data for the  $x$  and  $Q^2$  dependence of the polarized structure function  $g_1^p$  at an Electron-Ion Collider, assuming one year of running uses 7 GeV electrons colliding with 150 GeV protons. The integrated luminosity corresponds to  $500 \text{ fb}^{-1}$ . A minimum of the scattered electron of 1.5 GeV have been required.

The great improvement in range of both  $x$  and  $Q^2$  compared to previous fixed-target experiments is apparent, and will allow for determination of the polarized gluon contribution via  $Q^2$  evolution. Additional data at lower center-of-mass energies will improve upon the precision at the medium and large values of  $x$ . For  $x$  values in the valence-quark region, additional precision data, at lower  $Q^2$ , will be accumulated with the 12 GeV Upgrade at JLab.



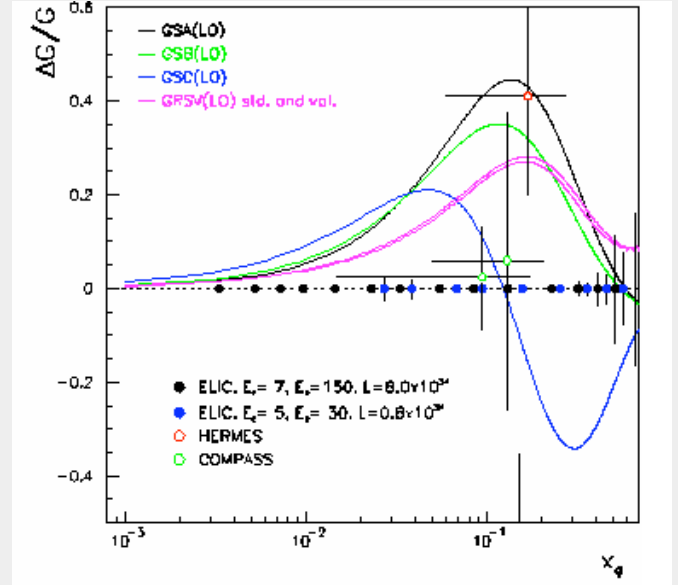
For example, the quark model picture seems to perfectly account for the nucleon spin, with three valence quarks with spin 1/2 arranged to form the spin-1/2 proton. However, deep inelastic scattering experiments have shown an entirely different picture. Over the last 20 years the unpolarized (or spin-averaged) electron scattering measurements have been extended to precision spin-dependent measurements, rendering data on the  $g_1$  structure function over a large range in  $x$  and about one decade in  $Q^2$ . The major surprise from these results was that quarks and anti-quarks together carry only about 30% of the nucleon's spin. Nowadays, the theoretical framework has been developed to allow a breakthrough in the determination how the inner constituents of the nucleons, the valence quarks, the sea of quarks and gluons, and their orbital motions, conspire to provide the spin-1/2 of the nucleon.

Similar as in the unpolarized case, the dependence on  $Q^2$  of the structure function  $g_1$  has been used to constrain the gluon contribution to the proton spin. However, the precision and range in  $Q^2$  are far from optimal for this procedure to precisely determine the gluon spin distribution. In addition, attempts to directly map the gluon spin distribution by di-jet production through the photon-gluon fusion process, or derivatives such as di-hadron production, have suffered from low center-of-mass energies and low transverse momenta of the final products in collision. The recent results of RHIC-Spin proton-proton scattering experiments have overcome some of these limitations, but suffer from imprecise determination of the event kinematics. Although this in principle could be resolved by using more exclusive methods, this method will suffer from strongly-reduced statistics. Hence, the gluon spin determinations will remain an outstanding puzzle to solve for ELIC.

The proposed ELIC will, on one hand, allow for precision measurements of the spin structure functions  $g_1$ , down to the smallest momentum fractions and over an unprecedented range of scales, as illustrated in Fig. 2. This will provide crucial benchmark data to better pin down our present understanding of the precise contributions to the nucleon spin of quark and anti-quark spin together. The increase range in  $x$  scales will similarly provide better constraints on the gluon contribution to the proton spin. The latter contributions can also be *directly* measured at the charm-quark mass scale with an EIC through low- $x$  electroproduction of  $\pi$  mesons. The high precision achievable in the determination of  $g_1$  at ELIC, using the latter method, is illustrated in Fig. 3.

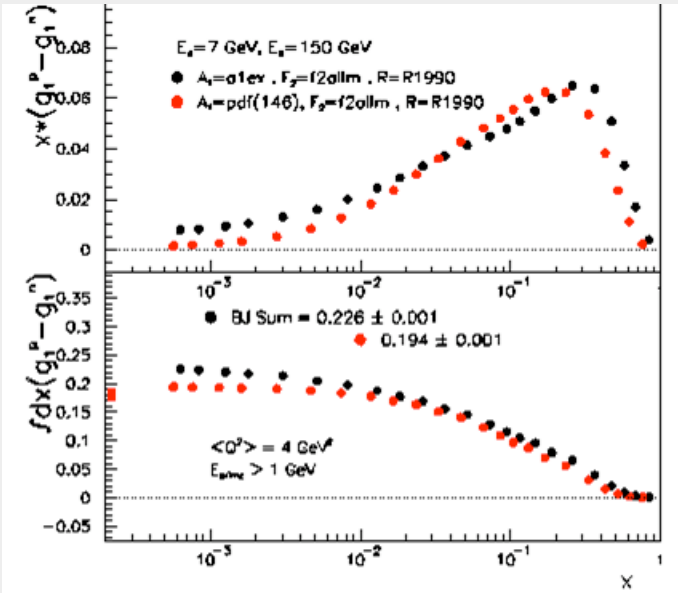
With the precision  $g_1$  spin structure function measurements in hand for both the proton and the neutron case (the latter extracted from spin-dependent electron-deuteron and electron- ${}^3\text{He}$  collisions), significant progress can also be made in the determination of the Bjorken sum rule. This sum rule relates the difference of  $g_1$  of proton and neutron, integrated over all  $x$ , to a static limit representing the neutron  $\beta$ -decay constant,  $\alpha_s$ . This Bjorken sum rule is a rare example of a fundamental relationship within QCD, with perturbative corrections known through order  $\alpha_s^3$ . ELIC would, assuming an independent precision method of ion polarization measurement is found, provide the statistical precision to constrain this sum rule to better than 1%, averaged over all  $x$ , and 3-4% at various values of constant  $\alpha_s$ . This would represent an increase in precision of a factor of 5-10. An example of such a measurement at ELIC is given in Fig. 4.

Fig. 3. Projected data at an Electron-Ion Collider for the  $x_G$  dependence of the polarization of the gluon distribution,  $\Delta G/G$ , measured via the quasi-real photoproduction of charmed mesons. Projections correspond to the "golden" channel of charm production, *i.e.*, the two-particle decay of a  $D^0$  meson into a  $K^-$  and a  $\pi^+$ . One year of running using 7 GeV electrons colliding with 150 GeV protons (black circles, for an integrated luminosity of  $500 \text{ fb}^{-1}$ ), and one year using 5 GeV electrons and 30 GeV protons (blue circles, integrated luminosity  $50 \text{ fb}^{-1}$ ) have been assumed. To suppress the background from any non-charm events, a minimum separation of  $100 \text{ cm}$  between the primary and the secondary vertex has been required. Additionally, a polar angle between 3 and 177 degrees and a maximum opening angle between the pion and the kaon of about 65 degrees have been assumed. Using these two different center-of-mass energies, the polarized gluon distribution will be measured precisely at a fixed scale of about  $10 \text{ GeV}^2$  over the wide range of  $0.002 < x_G < 0.5$ . Additional decay channels of the  $D^0$  and other charmed mesons will allow to study systematic uncertainties in this method.



With present knowledge of the spin structure of the nucleon mainly coming from polarized deep inelastic scattering, the polarization of the individual quark-flavors and anti-flavors were up to recently mainly studied using fits to the inclusive data. This technique is sensitive to the squared charges of the quarks and anti-quarks only, and thus requires additional assumptions, like SU(3) symmetry, leading to ambiguities in the interpretation. Semi-inclusive studies, where a hadron is detected in coincidence with the scattered lepton ("flavor tagging"), provide more direct access to the contributions from various quarks.

Fig. 4. Projected data at an Electron-Ion Collider for the difference between the polarized structure functions of the proton and the neutron (upper panel) and the cumulative integral of that difference, the Bjorken Sum (lower panel). An integrated luminosity of 250  $\text{fb}^{-1}$  for 7 GeV electrons colliding with 150 GeV protons has been assumed and data at all  $Q^2$  values above 1  $\text{GeV}^2$  have been included. The black and red symbols correspond to two parameterizations of the polarized  $g_1$  structure functions, both consistent with all presently available data. The expected statistical precision of the Bjorken Sum measured over the enormous kinematical range of  $0.0008 <$



$< 0.85$  is better than 1%. The contribution from the unmeasured regions is at most 7% for the chosen parameterizations. In the future, the functional form of  $g_1^p - g_1^n$  should be well constrained by data in the measured region and by Lattice QCD. Combining the data shown here with data at lower center-of-mass energies will allow a determination of the Bjorken Sum at various fixed values of  $Q^2$ . Ultimately, the uncertainty in this measurement is expected to be dominated by the uncertainty in the determination of the ion polarization.

Assuming factorization of the hard electron-quark scattering and quark-hadron fragmentation processes, double spin asymmetries for the production of different hadrons allow the separate determination of the contribution of the various quarks to the nucleon spin. Indeed, over the last decade there has been considerable progress in disentangling the contributions from different quark flavors to the proton spin by flavor tagging in semi-inclusive scattering, spearheaded by the HERMES collaboration. Further information on the  $^+$ ,  $^-$ ,  $^+$ ,  $^-$ ,  $^+$ , and  $^-$  at relatively large  $x$  will come from RHIC-Spin through its  $\gamma$ -physics program, and from the 12-GeV Upgrade at JLab. Crucial input on the sea quark and anti-quarks will remain for ELIC, to quantitatively answer whether these strongly spin “against” the proton, thereby counteracting valence quark contributions and rendering the small net contribution to the nucleon spin of the quarks. Whether  $^+$  quarks are positively polarized, and  $^-$  quarks negatively, as one might expect on the basis of the Pauli principle. And whether  $^-$  quarks are polarized or not. Such data will provide great intuitive insight in the degrees of freedom relevant within the nucleon landscape. Projected data of such ELIC determinations are shown in Fig. 5.

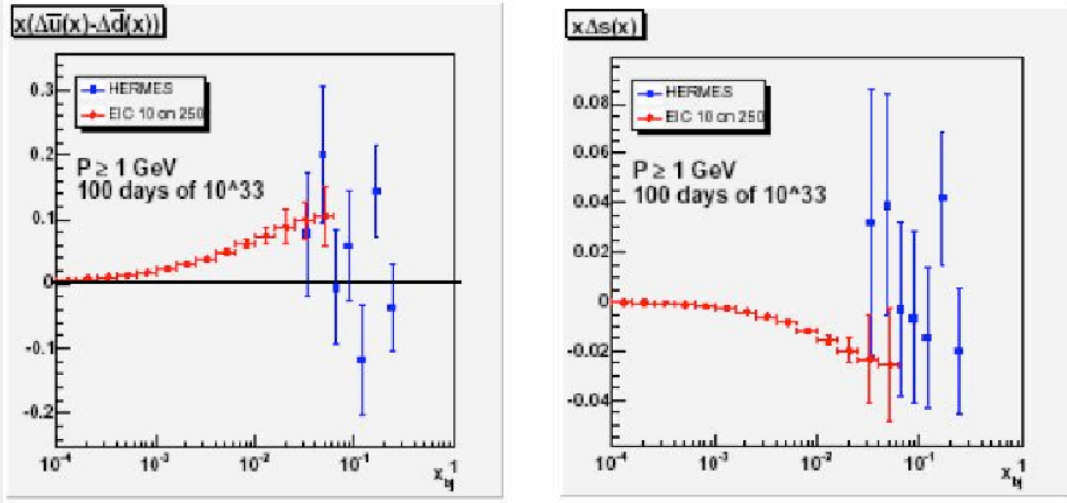


Fig. 5. Projected data at an Electron-Ion Collider for the difference between the polarized u and d sea quark distributions (left panel) and for the polarized strange sea quark distributions (right panel) as a function of  $x$ . The highest possible energy of 7 GeV electrons colliding with 150 GeV protons at an integrated luminosity of  $5 \text{ fb}^{-1}$  has been assumed and data at all  $Q^2$  values above  $1 \text{ GeV}^2$  have been included.

These measurements are based on pion and kaon double spin asymmetries and have been extracted using the LO purity formalism. Also shown are the existing results from HERMES (blue symbols). The improvement both in statistical precision and in  $x$  coverage is obvious and will allow a precision determination of the polarized sea quark distributions, crucial for the understanding of the nonperturbative and perturbative nature of the nucleon structure.

### 1.2.1 The Impact of Quark and Gluon Motion on the Nucleon Spin

With the realization that quarks and anti-quarks together only carry some 30% of the proton spin, and gluons likely not completing this picture, orbital angular momentum of quarks and gluons has become a central issue in nuclear physics. Recent major theoretical breakthroughs have made possible to determine such orbital motion within the nucleons, a completely novel area of study. These breakthroughs introduced more complete parton distribution functions termed “*Generalized Parton Distributions*” (GPDs) and “*Transverse Momentum Dependent Parton Distributions*” (TMDs), that both contain information not only on the longitudinal momentum but also on the transverse spatial (or momentum) distribution of quarks and gluons in a fast moving hadron. As such, they are sensitive to the orbital motion of quarks and gluons, not accessible in inclusive scattering.

The recently developed GPD formalism describes hard scattering processes that involve the *correlations* between quarks and gluons. This formalism offers an exciting bridge between elastic and deep inelastic scattering: in different limits of the GPDs, one recovers the familiar elastic form factors (where the quarks act coherently, and the proton remains intact) and quark (and gluon) distributions accessible in deep inelastic scattering. As such, they are perhaps the most fundamental characterization of the internal dynamics of nucleon structure. For example, a Fourier transform of the

GPDs in momentum transfer will render the distribution of quarks and gluons in the plane transverse to the proton direction, thus yielding a transverse spatial profile of the proton.

Since GPDs describe also transitions between the nucleon and different hadrons, this allows one to probe the overlap of their respective wave functions. This opens the way to study hadrons not available as beam particles. Although highly promising, measurements of GPDs are challenging. They depend on three separate kinematic variables, and require a series of fully exclusive processes, in which all of the reaction products are reconstructed, for deconvolution. Tremendous progress has been made, however, in raising the theoretical treatment of GPDs to levels approaching that achieved in over three decades of intense studies of the usual quark distributions. Factorization proofs (similar to that used in deep inelastic scattering to separate the hard electron-quark collision from the underlying nucleon structure) guarantee that the GPDs are indeed well-defined QCD objects.

Determination of valence quark GPDs are the flagship of the physics program at the 12-GeV Upgrade at JLab. With ELIC, it will be possible to extend the surveys of GPDs into the region where sea quarks and gluons abound. Electroproduction measurements of vector mesons, such as  $\pi^+$  mesons and

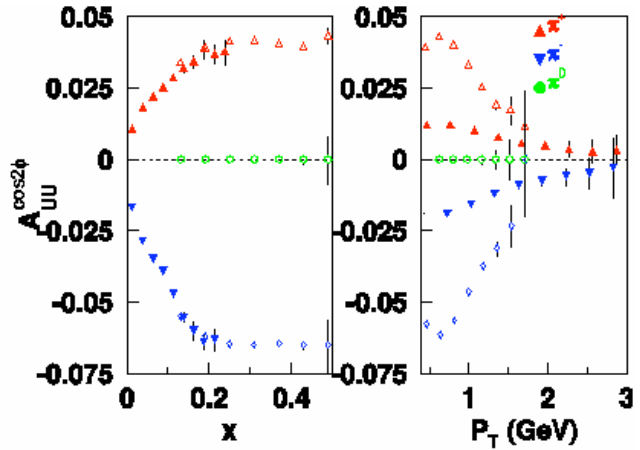
$\rho^0$  mesons, can be used to map the transverse spatial profile of gluons. Electroproduction measurements of charged pions can be extended to reach the limit,  $Q^2 > 10 \text{ GeV}^2$ , where we can safely believe access to GPDs is feasible for a quark-flavor separation.

To finalize the subject of GPDs, we note that positron beams will find their largest advantage in these challenging measurements. Here, it will be of great help to have both electron and positron beams to one's disposal, and also to have polarization of these beams. With these in hand, one can define charge and beam spin asymmetries, which will allow, *e.g.* in the case of the Deeply-Virtual Compton Scattering process, unprecedented access to both the real and imaginary parts of the matrix elements carrying the complete information on the nucleon wave function.

Azimuthal distributions of final state hadrons in semi-inclusive deep inelastic scattering provides an independent window on the orbital motion of quarks, through the framework of TMDs. TMDs in general describe transitions of nucleons with one polarization state to a quark with another polarization state. At the quark-gluon level, this provides a window into the physics of initial and final state interactions. TMDs were introduced to explain the surprisingly large asymmetries found in hadronic reactions and, more recently, in semi-inclusive deep inelastic scattering experiments at HERMES, COMPASS, and JLab, with polarized targets.

In perturbative QCD, which applies when the transverse momentum  $P_T$  of the detected hadron is large compared to  $\Lambda_{\text{QCD}}$  (the scale where  $\alpha_s \sim 1$ ), symmetries vanish at leading twist level. The observed spin-dependent and spin-independent azimuthal asymmetries occur at  $P_T$  below 1-2 GeV, not much larger than  $\Lambda_{\text{QCD}}$  or the typical quark-gluon transverse momenta of order 0.5 GeV. Thus, the measured asymmetries could arise from non-collinear parton (quark-gluon) or multi-parton correlations (“higher-twist” effects, suppressed at large  $P_T$ ). Presently, the intrinsic transverse momentum of partons in the nucleon is at the root of most explanations of these non-zero azimuthal asymmetries. Measurements at ELIC would be crucial, as they would extend measurements planned with the 12-GeV Upgrade at JLab into a region of large  $P_T$ , sufficiently large to provide an alternative “hard” scale for precise perturbative calculations. This is illustrated in Fig. 6.

Fig. 6. Projected data at an Electron-Ion Collider for the azimuthal asymmetry  $A_{UU}^{\cos 2\phi}$  of semi-inclusive pion production as a function of  $x$  (left panel) and transverse momentum  $p_T$  (right panel). This asymmetry is related to the Boer-Mulders function which describes the correlation between the transverse spin and momentum of quarks in an unpolarized target and is one prominent example for the many studies of transverse momentum dependent parton distributions (TMDs) which will be possible at an EIC. An integrated luminosity of  $100 \text{ fb}^{-1}$  for 5 GeV electrons colliding with 50 GeV protons has been assumed and data at all  $Q^2$  values above  $1 \text{ GeV}^2$  have been included. Also shown are expected results from CLAS and 12 GeV (open symbols).



Recent theoretical work has established a framework to provide a rigorous basis to study TMDs from the great wealth of existing and future semi-inclusive deep inelastic scattering data for different spin-dependent and spin-independent observables. The so-called “Sivers” function expresses the correlation between the transverse momentum of quarks, ejected from a transversely polarized nucleon, and the transverse spin of that nucleon. This Sivers function requires both orbital angular momentum as well as non-trivial phases from the final state interaction. To date, experimental results of this Sivers function are consistent with a heuristic model of  $u$  and  $d$  quarks orbiting the nucleon in opposite directions.

The so-called “Boer-Mulders” function describes the correlation between the transverse spin and momentum of a quark ejected from an unpolarized target. It is thus similar to the Sivers function except that the nucleon spin is swapped for the spin of the active quark. The most simple mechanism that can lead to a non-zero value of this function is a correlation between the spin of the quarks and their orbital angular momentum. The sign of this value would, with an on average attractive final state interaction, then reveal this correlation.

Related effects that give rise to the Sivers function, but now in the quark-hadron formation or fragmentation process, expressed in a “Collins” function, allow new insights in hadronization (see below), and may be used as a tool to provide a first measurement, over two decades of  $x$ , of the transversity distributions of the quarks. These distributions describe the quark polarizations within a transversely polarized proton, and do not mix with gluon distributions (there is no transversity of gluons in a nucleon). In the non-relativistic quark model, the transversity distribution  $\varepsilon_{u,d}$  should be equal to  $\varepsilon_{u,d}$ , the longitudinal spin distribution mentioned earlier, and this provides a “baseline” for our understanding of this, as yet unmeasured, distribution. The transversity distribution  $\varepsilon_{u,d}$  encodes more general, information about the relativistic effects in the nucleon’s transverse spin content. The first moment of  $\varepsilon_{u,d}$ , termed the tensor charge of the proton, offers a promising point of direct comparison with theory.

### 1.2.2. How do hadronic final-states form in QCD

We have known since the work of Einstein that matter can be created out of pure energy, a concept that is at the root of modern physics. However, how this basic law is intertwined with within QCD to explain the formation of final hadrons due to color confinement remains a mystery that is only explained heuristically by sketches of space-time processes involving string breaking. High-energy scattering allows physicists to study how a quark or gluon evolves into a hadron. The asymptotic physical states detected in experiment must be color-neutral hadrons, and hence must have picked up their quark (or anti-quark) partners from the debris of the high-energy collision. This process is known as hadronization.

Studying such processes provides new information on how the color field of the hadrons is restored in real time through the fundamental process of gluon emission. Studying the Collins function, described above, will give insight whether properties such as quark motion and quark spin play a role. This similarly poses a complex and challenging problem, as any effects can be produced by a combination of intrinsic quark transverse momenta, gluon radiation, and broadening effects in the fragmentation process itself.

Lastly, the collider geometry will allow measurement of all reaction products, with a dramatic increase in our knowledge of the essentially unknown target fragmentation process. This can, e.g., be used to study how, and to what extent, the spin of a quark is transferred to its hadronic daughters.

### 1.3. Quarks and Gluons in Nuclei

Most of the observable matter in the universe is contained in the form of atomic nuclei, with the interaction between protons and neutrons responsible for the *nuclear binding*. With the scale of nuclear binding, of the order of 10 MeV, small compared to the natural energy scale of QCD, hundreds of MeV, it was a large surprise when the European Muon Collaboration demonstrated a significant modification of the quark momentum distributions in the nuclear medium.

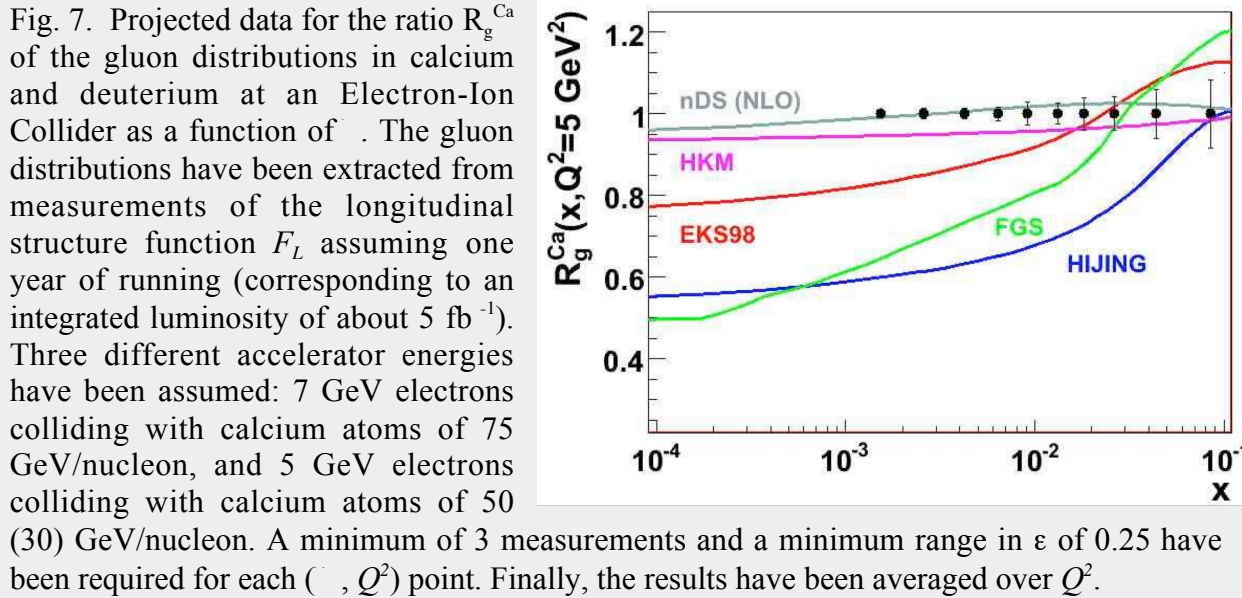
To date, this remains the single unambiguous experimental result highlighting that a nucleus is not merely a simple set of nucleons. By now, this EMC-effect has been mapped out to large detail for many nuclei, and over a tremendous range in Bjorken  $\beta$  and  $Q^2$ . Three separate physics regions emerge: (i) for  $\beta > 0.2$  one obtains a reduction of  $F_2$  in nuclei, followed by a steep rise at  $\beta \sim 0.7$ . This is the original “EMC effect”, where the rise at large  $\beta$  is due to Fermi smearing effects; (ii) at  $\beta < 0.1$  there is a small enhancement of the nuclear structure function  $F_2$  with respect to the free nucleon. This region is termed the *anti-shadowing* region; (iii) at lower  $\beta$  the nuclear ratio drops to below unity (the *shadowing* region), ultimately reaching a saturation limit at  $\beta \sim 10^{-3}$ . In general, the dependence on the target mass  $A$  is not strong, and the effects have nearly saturated around  $A \sim 50$ . This is the reason that the heaviest nucleus under consideration at ELIC is  $^{40}\text{Ca}$ .

The Drell-Yan process (a quark-antiquark annihilation process) has been used to study the sea quark

distribution in nuclei. No significant nuclear modification has been found in the region of  $x \approx 0.1$ , which remains one of the interesting puzzles of nuclear physics. If the nuclear force is considered to be predominantly mediated by pions, why do we not find any signature for them? What then is the cause for the enhancement found in the regular nuclear structure function ratio at  $x \approx 0.1$ ?

Our current understanding of hadron structure indicates that, at low  $x$ , the proton is overwhelmingly comprised of gluons. This fact was earlier applied to constrain the gluon distributions at low  $Q^2$  from measurements of  $F_L$ . In the nuclear medium, knowledge on gluon distributions is non-existent. This simply reflects the lack of data constraining gluons in the nucleus, with only marginal indirect constraints from the  $Q^2$  evolution of the precise nuclear structure function ratios of  $Sn$  and  $C$  measured by the New Muon Collaboration at CERN. Model calculations indeed show an impressive variety, ranging from a ratio of gluons in deuterium to  $^{40}\text{Ca}$ ,  $R_g^{\text{Ca}}$ , from 0.5 to unity. This presents a unique opportunity for ELIC to, for the first time, map the gluon distributions in nuclei. This can be done precisely, again from measurements of  $F_L$ , as illustrated in Fig. 7.

Given the large amount of gluons found at small values of  $x$  in the proton, one may approach the limit where the gluons are packed so densely that they start annihilating each other. In such a regime, where the gluon field strengths approach the maximum possible, their dynamics is non-linear, and the underlying physics of gluon interactions may become universal across hadrons and nuclei. In nuclei, such effects may be amplified by the simple reasoning that at a given  $x$ , one can find more of such gluons “in bulk”. Studies of the properties of gluons and the accompanying sea quarks in regimes where the gluons are abundant, across a wide range of nuclei, have the potential to fundamentally impact our understanding of QCD at high energies, and confirm the onset of the physics of gluon saturation.



Various model calculations are also shown and vary widely for this ratio, illustrative for our present lack of knowledge of the modification of the gluon distribution in the nuclear medium.

As referred to earlier, HERA/DESY data surprisingly discovered that for some 15% of the hard electron-proton collisions the entire proton was found to remain intact, reminiscent of a diffractive

process rather than a hard electron-quark scattering process. There has been growing speculation to link the experimental results found for these diffractive processes with the onset of saturation models. This can be unambiguously settled at an EIC, since one of the most striking predictions of the onset of such saturation physics is that for heavy nuclei this ratio can grow to nearly 40%, approaching the unitarity limit of 50%. For  $^{40}\text{Ca}$ , the heaviest nucleus considered at ELIC, this ratio is already some 35%, at  $\gamma = 10^3$  and  $Q^2 = 1 \text{ GeV}^2$ , well within range of ELIC.

The nuclear medium can alternatively be used as an arena to shed more light on fundamental QCD *processes*, ultimately aimed at gaining knowledge how quarks and gluons propagate through nuclear matter and form hadronic final-states. A hard e-A interaction with  $\gamma > 0.1$  produces a single quark of known energy  $\gamma$ . The quark propagation in the nuclear environment involves processes like rescattering with the surrounding medium, and induced gluon radiation, resulting in energy loss of the quark. In the end, due to the phenomenon of confinement, final-state hadrons have to be formed from the vehemently struck quark, through the process of fragmentation.

If the final hadron is formed inside the nucleus, the hadron can interact via the relevant hadronic interaction cross section, causing a reduction of the hadron yield. This is called nuclear attenuation. It has been experimentally shown that for high quark energies ( $\gamma > 50 \text{ GeV}$ ) such nuclear attenuation effects are small. For such energies hadrons are predominantly formed outside the nucleus in which the hard scattering occurred. Hence, this is the region where one can concentrate on the effect the nuclear medium has on the fragmentation process itself, likely due to a combination of energy loss and rescattering of quarks and gluons.

A modern view of the hard interaction above identifies two time scales. The first, the production time, is the characteristic time over which the struck quark remains deconfined. During this time, the quark retains color charge and emits gluons. The second time scale is that of the formation time, during which time the non-perturbative condensation of the hadron's color field occurs, producing a fully-formed hadron from a nascent color-singlet pre-hadron. It is during this formation time, believed to be several times longer than the production time, that the bare quarks of the pre-hadron become dressed and the hadron acquires its full mass.

Quark energy loss results primarily from radiative gluon emission, and to a much less extent, from collisional losses. The radiative emission is predicted to exhibit a rich coherence behavior analogous to the Landau-Pomeranchuk-Migdal effect in QED, where the interplay between the mean free path, coherence length, and medium size creates a coherent effect suppressing photon bremsstrahlung. In the QCD case of gluon emission, the analogous interplay implies a quark energy loss that has a novel quadratic dependence on the medium thickness below a critical length, and a linear dependence above the critical length. Ultimately, at asymptotically high energies, the coherence is complete and the quark is unable to transfer any energy to a medium of finite length. The critical length and the corresponding critical energy are experimentally unknown. The approach to the asymptotic condition at high energies and the interplay between the medium length and quark energy can be studied in detail to test the concepts of the underlying coherence behavior.

High-quality data exist from HERMES/DESY, and from JLab (at 5 GeV). Additional measurements are planned at the 12-GeV Upgrade at JLab. However, these experiments all reside in a region of  $\gamma > 50 \text{ GeV}$ , and focus on nuclear attenuation, allowing a broad program of extracting hadron formation lengths, and on understanding quark energy loss at low energies.

ELIC will allow a systematic investigation of the energy and quark-mass dependence of the energy loss. In addition, the narrowing or collimation of high-energy jets has been predicted, but has never been observed. The ideal environment for such measurements is at high e-A energies. Using a lepton probe limits the distortions due to initial-state interactions, whereas the high energy will render a sufficiently large number of particles in a jet to allow for a precision measurement of the jet width. Such measurements at ELIC would provide direct benefits as a baseline for experiments with hot QCD systems at RHIC and LHC, and test predictions for the fundamental QCD process of medium-stimulated gluon emission.

## 1.4 Summary of Luminosity Requirements

The final design luminosity of ELIC, at a center-of-mass energy of 65 GeV, corresponds to an integrated luminosity of up to 8,000 (pb)<sup>-1</sup> per day. For inclusive electron scattering experiments (only the scattered electron is detected), significant results can already be obtained for an integrated luminosity of 200 (pb)<sup>-1</sup>. This is *e.g.* illustrated in Figs. 1 and 2, which represent such inclusive-type measurements and are not statistics-limited. Here, a luminosity of order  $1 \times 10^{32}$  typically suffices.

For semi-inclusive measurements, required for a quark flavor separation of nucleon structure or the study of fragmentation, the detection of an additional hadron is essential. Figs. 3, 5 and 7 are typical examples for such cases, with detection of at least one hadron in combination with the scattered electron. Such measurements require a luminosity of order  $1 \times 10^{33}$  or higher.

The highest luminosity will finally be used for precision tests in QCD, such as the determination of the Bjorken Sum Rule, allowing a final attack to reduce the experimental uncertainties in this fundamental measurement (Fig. 4). A more direct application, however, of the highest luminosity is to access the correlations between spin and orbital motion within the nucleon. An example is given in Fig. 6, illustrating the access to transverse spin effects. Alternatively, this very high luminosity allows for unprecedented measurements of deep exclusive reactions (reactions where one puts a lot of energy transfer into the nuclear system, but still detects all fragments) over a large range of  $\eta$ . Here, results with similar statistical precision require an integrated luminosity typically a factor of 1,000 larger than for inclusive scattering, well within range of the final design luminosity.

## II General Description of ELIC at CEBAF

### Contents

- 2.1 *Nuclear physics requirements*
- 2.2 *Basic constituents and beam parameters*
- 2.3 *ELIC luminosity concepts*
- 2.4 *Electron facility*
- 2.5 *Positron source*
- 2.6 *Ion facility*
- 2.7 *Electron cooling*
- 2.8 *Interaction region*
- 2.9 *Polarization*

## 2.1 Nuclear physics requirements

The nuclear physics program outlined in the previous chapter sets the basic requirements for the electron-light-ion collider at CEBAF as follows:

### 1. Energy

The center-of-mass (CM) energy should be between 20 GeV to 65 GeV with ion-to-electron energy asymmetry of 10-20. The colliding beam energies would therefore range from 3 GeV electrons on 30 GeV/u ions to 7 GeV electrons on 150 GeV/u ions.

### 2. Luminosity

CW luminosity should be in the range of  $10^{33}$  to  $10^{35} \text{ cm}^{-2}\text{sec}^{-1}$  per interaction point.

### 3. Ion species

Ion species of interest include polarized protons, deuterons, and  $^3\text{He}$ . Light to medium ions, up to calcium, are desirable but do not have to be polarized.

### 4. Polarization

Longitudinal polarization for both electron and ion beams at the interaction region should be greater than 70%. Transverse polarization of the ions and spin-flip of both beams are extremely desirable. High precision (1-2%) ion polarimetry is required.

### 5. Positrons

Polarized CW positron beams colliding with ions are desirable.

An additional goal of the design is to have four interaction points.

## 2.2 ELIC layout, major constituents, and beam parameters

ELIC is envisioned as a future upgrade of CEBAF, beyond the planned 12 GeV Upgrade for fixed target experiments. The CEBAF accelerator with the existing polarized electron source will be used as a full energy injector into an electron storage ring, capable of delivering the required electron beam

energy, current, and polarization. The addition of a positron source to the CEBAF injector, will allow for CW positron beam to be accelerated in CEBAF, accumulated and polarized in the electron storage ring, and used in collisions with ions (and possibly electrons), with luminosity similar as for electron/ion collisions. Longitudinal polarization of the positrons up to 90% is expected to be maintained for the duration of the store. An ion complex with a green-field design optimized to directly address the science program of ELIC, will be used to generate, accelerate, and store polarized and unpolarized light to medium ions, and will be a major addition to the CEBAF facility.

Figure 3.2.1 displays the conceptual layout of ELIC at CEBAF. The three major constituents of ELIC are: the electron/positron complex, the ion complex with electron cooling, and the four interaction regions.

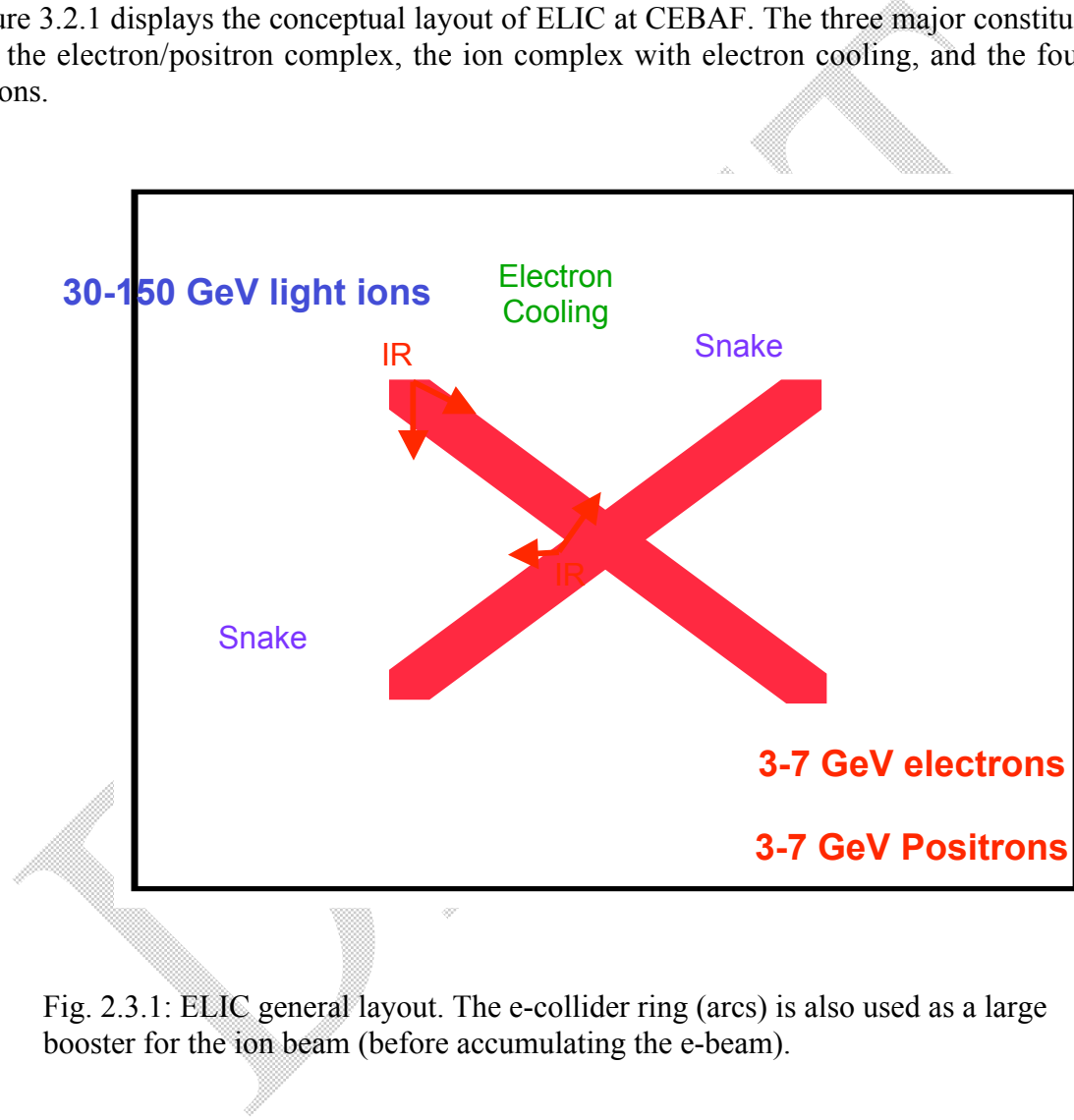


Fig. 2.3.1: ELIC general layout. The e-collider ring (arcs) is also used as a large booster for the ion beam (before accumulating the e-beam).

The electron/positron complex is designed to deliver electron beam of energy in the range of 3 GeV to 7 GeV, average beam current for collisions between 1A to 3A, and longitudinal polarization at the IP's of  $\sim 80\%$ . This electron/positron complex comprises two major facilities: the CEBAF accelerator upgraded to 12 GeV and an electron storage ring which will have to be constructed. CEBAF is a superconducting RF recirculating linac operating at the RF frequency of 1500 MHz. The 12 GeV Upgrade of CEBAF will allow energy gain of 11 GeV in 5 recirculations. Longitudinally polarized electrons are generated from CEBAF's polarized DC photo-injector and accelerated to the desired top energy of 3 to 7 GeV in a single or multiple recirculations through CEBAF. They are then injected

into a figure-8 shaped electron storage ring, where they are accumulated using stacking by synchrotron radiation damping. To accumulate the average electron current of 3 A in the storage ring, 3000 macropulses, of 1 mA CW current and 5  $\mu$ s duration each (corresponding to the ring circumference), separated by the radiation damping time of 4 ms at 7 GeV, are injected into the ring. In this scheme the accumulation time for 3 A of electron current is approximately 15 seconds. Alternatively, accumulation of such current can be completed in less than 1.5 seconds (at 7 GeV), if the macropulse duration is increased to about 50  $\mu$ s corresponding to 10 times the ring circumference and multi-turn injection (300 injections).

The ion complex is designed to deliver 30 to 150 GeV/u light to medium ions, with average current of 0.3 to 1 A. It consists of polarized ion sources, a 200 MeV to 400 MeV linac, a pre-booster up to 3 GeV/c, and a 150 GeV, 1 A storage ring. The ion source is designed to produce a variety of polarized light ion species: p, d,  $^3$ He and Li, and unpolarized light to medium ion species up to  $^{40}$ Ca. The pre-booster also serves for stacking of 2 mA bunch train from the ion sources to form the 1 A of ion beam. The electron ring (arcs) is used as the main, 15 to 30 GeV/u booster for the ion beam. The ion storage ring serves as the collider ring with four interaction regions.

As depicted in Figure 3.2.1, the electron and ion storage rings are designed as figure-8 shaped double rings and are housed in the same tunnel, with the ion ring below the electron ring. The figure-8 rings consist of two identical arcs connected by two crossing straight beam line sections. The choice of figure-8 shape eliminates the issue of spin maintenance at acceleration and allows one to easily arrange the desired spin orientation and flipping for all the ion species at all energies. Further, longitudinal polarization is guaranteed for protons,  $^3$ He, electrons, and positrons in all four IR's simultaneously, while deuterons can be longitudinally polarized in up to two IR's simultaneously.

A critical component of the ion complex is a 15 MeV to 75 MeV ERL-based continuous electron cooling facility, which is anticipated to provide low emittance and simultaneously very short ion bunches. The short ion bunches have two critical advantages: 1) they allow for extremely strong beam focusing at the collision points, and 2) they allow the use of crab crossing of the colliding beams. Together these advantages make head-on collisions at the maximum collision frequency (up to the RF frequency of 1.5 GHz) possible, while eliminating parasitic beam-beam interactions, for maximum attainable luminosity.

The interaction region of ELIC is designed to accommodate up to four detectors simultaneously, at four collision points located symmetrically around the centers of the figure-8 colliders, along each of the two crossing straights. After beam stacking and accumulation is complete, the two storage rings are switched to the collider mode, where electron bunches are bent vertically to collide with the ion bunches.

Table 3.2.1 below summarizes the basic parameters for the ring-ring version of the electron-light-ion collider at CEBAF. We show here three typical energy scenarios, from lowest 3 on 30 GeV to highest 7 on 150 GeV. The maximum attainable luminosity for ELIC is expected to be  $7.7 \times 10^{34} \text{ cm}^{-2} \text{s}^{-1}$  per interaction point for 150 GeV protons. ELIC is designed to be compatible with simultaneous operation of the 12 GeV CEBAF for fixed target program, and its potential extension to 24 GeV.

Table 2.2.1 Basic parameters for ELIC

Parameter	Unit	Value	Value	Value
Beam Energy	GeV	150/7	100/5	30/3
Cooling beam energy	MeV	75	50	15
Bunch collision rate	GHz	1.5	1.5	1.5
Number of particles/bunch	$10^{10}$	0.4/1.0	0.4/1.1	0.12/1.7
Beam current	A	1 / 2.4	1/2.7	0.3/4.1
Cooling beam current	A	2	2	2
Energy spread, rms	$10^{-4}$	3	3	3
Bunch length, rms	mm	5	5	5
Beta-star	mm	5	5	5
Horizontal emit. norm.	$\mu\text{m}$	1/100	.7/70	0.2/43
Vertical emit., norm.	$\mu\text{m}$	0.04/4	0.06/6	0.2/43
Number of IPs		4	4	4
Beam-beam tune shift (vertical) per IP		0.01/0.086	0.01/0.073	0.01/0.007
Space charge tune shift in p-beam		.015	.03	.06
Luminosity per IP, $10^{34}$	$\text{cm}^{-2}\text{s}^{-1}$	7.7	5.6	0.8
Core & luminosity. IBS lifetime	hrs	24	24	>24
Lifetime due to background scattering	hrs	200	>200	>200

## 2.3 ELIC Luminosity Concepts

The concept of ELIC ultra high luminosity is based on the advantages of the CEBAF SRF recirculator accelerator facility, advances in beam physics researches and cutting-edge accelerator technologies. It was resulted from thorough considerations of beam-beam interaction, space charge, intrabeam scattering and electron cooling effects in the ELIC conceptual design.

The ELIC ultra high luminosity is achieved through following two unique design optimizations: ultra high collision frequency and extremely small transverse beam spot sizes at collisions. These two optimizations are enabled and supported by several other technologies, among them are short colliding bunches, strong final focusing, electron cooling and crab crossing beams.

The ultra high collision frequency of the ELIC is derived from the CEBAF facility. Since the electron beam stored in the electron ring of the ELIC is 1.5 GHz CW beam from the 12 GeV CEBAF, the conceptual design of ELIC ion complex also calls for accumulation and storing of ion beams with same high repetition frequency. Thus the collision frequency of the CEBAF is 1.5 GHz at ELIC maximum operation condition.

The small transverse beam spot sizes at collisions relay on mainly the continuous electron cooling of the ion beams at the colliding ring. Since the normalized emittances of a stored beam are dictated by beam equilibrium inside storage rings, small transverse spot sizes are achieved by very short beta-stars, hence a very strong final focusing at collision points. Electron cooling, by suppressing emittance growth due to intrabeam scatterings and other space charge effects, can reduce emittances

of ion beams in all directions. On one hand, reduction of the transverse emittance by electron cooling allows one to increase the beam extension in the final focusing magnet, hence, reach a lower beta-star, On the other hand, electron cooling in cooperation with bunching SRF cavities provide very short ion bunches (5 mm or less), thus making allowing the design of a short beta-star. Short bunches make possible to implement the crab-crossing scheme for colliding beams that eliminates parasitic beam-beam interactions without the need to bend the beam near the detector area, while approaching the highest possible collision rate.

Beam-beam interactions at collisions are the usually the leading limiting factor of the collider's luminosity. Its characteristic parameters, beam-beam betatron tune shifts, pose strong constraint on colliding bunches' sizes and charges. ELIC found an optimal solution of relative small bunch charges, very large crossing angles and continuous electron cooling of ion beams in the collider ring. Reduction of charge per bunch increases beam stability against microwave interactions, in particularly, electron clouds. A large synchrotron tune (exceeding the beam-beam tune shift) eliminates the synchro-betatron non-linear resonances in the beam-beam interaction, thus allowing one to reach a large beam-beam tune shift. Flat beams (by lowering the x-y coupling at fixed beam area) lead to reduction of IBS rate against electron cooling. Equidistant fraction phase advance between four IPs of ELIC effectively reduces the critical beam-beam tune shift to a value normalized to one IP.

## 2.4 Electron Facility

The conceptual design of the ELIC calls employing of the upgraded 12 GeV CEBAF as electron accelerator with no major upgrades. The polarized photo-electron source, DC injector and SRF recirculating linac of the 12 GeV CEBAF are either already sufficient or with minor changes for providing required 1 mA CW electron beam with 80% spin polarization. A storage ring is the only addition.

### *Polarized electron source*

The polarized photo-emission electron source at CEBAF employ negative electron affinity photocathodes prepared on GaAs or similar semiconductors. Under illumination by circularly polarized light of wavelength close to the minimum direct bandgap, polarized electrons are emitted. Ordinary GaAs gives an electron polarization theoretically limited by degeneracy in the valence band to 50%, and in practice no better than about 40%. The very best polarized photocathodes used to date have provided polarization somewhat above 80% and maximum quantum efficiency of about 0.2% at the operating wavelength. At CEBAF, CW beams with average currents as high as 270  $\mu$ A have been delivered from a 100 kV DC gun at bunch repetition rates between 499 and 1497 MHz, corresponding to a fraction of a picocoulomb per bunch.

It has proven difficult to achieve long photocathode operational lifetimes in polarized sources, particularly at high average current. The cathode life of the CEBAF photo-cathode is limited only by ion back bombardment. The ions are produced on the residual gas in the cathode-anode gap. It is thus more reasonable to express the cathode life in terms of the number of coulombs delivered per unit

illuminated area, rather than in clock hours. Presently, the CEBAF polarized source has demonstrated cathode lifetimes in excess of  $2 \times 10^5$  coulombs/cm<sup>2</sup>. The only practical way to increase this number is to reduce the vacuum pressure. This is a challenging task, as the pressure in typical polarized guns is already below about  $10^{-11}$  mbar (and difficult to measure with precision).

### **DC Injector**

Figure 2.2.2 shows the layout of the 12 GeV CEBAF DC photo-injector. This energy upgraded injector is capable of delivering simultaneously three CW electron beams of different currents at 123 MeV injection energy to CEBAF SRF Linac. The injector starts with two 100 keV DC photocathodes (only one gun is in use at any given time), ends at the injection chicane (not shown) and consists of various element groups for acceleration, transverse emittance preservation, longitudinal bunching, and beam diagnostic and control. Electron energy after the DC gun is boosted, respectively, by a capture RF cavity to 500 KeV, a two-cell 1/4-SRF module to 5 MeV and two eight-cell full SRF modules to 123 MeV. The bunch lengths are regulated by a 3-way chopper and two-stage RF bunching by prebuncher and main buncher RF cavities. The transverse beam sizes and emittances are contained by magnetic elements and apertures. Previous measurements with typical beam currents (up to 0.2 mA in total) have shown a final bunch length of less than 0.3 mm (1 ps) and fractional energy spread of less than  $10^{-4}$ .

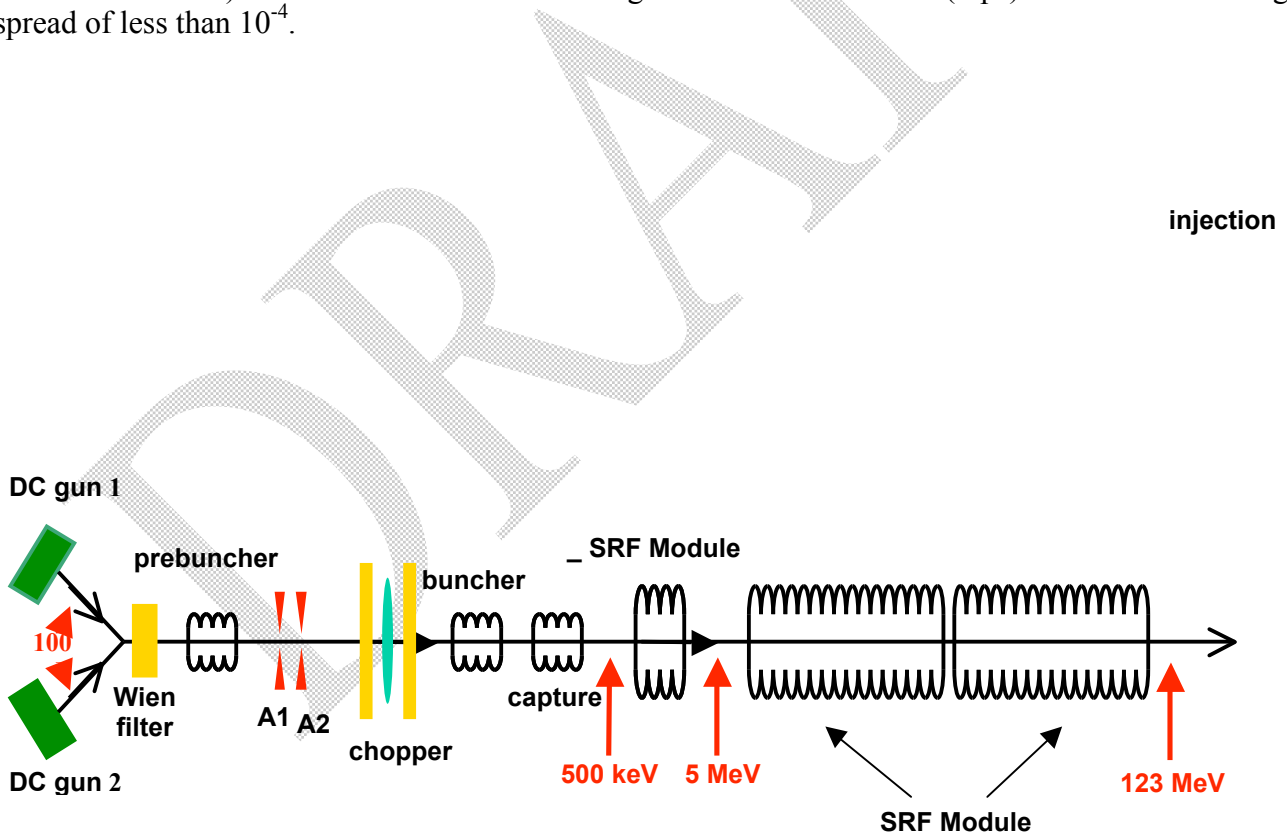


Figure 3.2.2 Schematic layout of the DC injector of the 12 GeV CEBAF Upgrade

## ***CEBAF SRF Recirculator Linac***

CEBAF at the Jefferson Lab is the only superconducting RF recirculator electron linac at or above GeV energy. It consists of two identical SRF linacs connected by a total of vertically separated 180 degree arcs on both ends of the racetrack. Presently, this 5-pass recirculating system delivers simultaneously three 1497 MHz CW electron beams up to 5.5 GeV energy to three experiment halls. The combined beam currents at three end stations is 0.2 mA. An energy upgrade of the CEBAF to 12 GeV has been planned and the supporting R&D is current underway. In the ELIC conceptual design, the 12 GeV energy upgraded CEBAF accelerator will assume the responsibility of accelerating electron beams for ELIC with a full energy injection into the electron storage ring of ELIC.

The 12 GeV energy upgrade of CEBAF consists of three major parts on the accelerator facility side, in addition to upgrade of detectors and construction of a fourth experiment hall. These three major parts are addition of a tenth arc to provide 12 GeV in the new experimental hall, upgrade of SRF linacs from 550 MeV to 1.09 GeV and increase of capacity of the central liquid helium refrigeration facility.

Upgrade of two CEBAF SRF linacs will be achieved as follows: in each linac, six existing 5-cell SRF modules will be refurbished to boost the cavity field gradients from 6 MV/m to 10 MV/m; the five current vacant slots will be filled with five new 7-cell SRF modules of high field gradients at 12.2 MV/m. The old modules will then provide 620 MeV and the new 500 MeV in each linac, totalling 1120 MeV versus 1090 MeV needed. Continued refurbishment at a rate of two per year will eventually provide 10% headroom. The magnets in spreaders, recombinars and arcs will be also upgraded to accommodate electron beams with higher energy. After completion of the 12 GeV CEBAF energy upgrade, the three existing experimental halls will receive beams up to 11 GeV in 5 passes of the racetrack while the new hall located on the other end of the racetrack will receive beams up to highest energy of 12 GeV in 5.5 passes.

There are several important points in the CEBAF 12 GeV upgrade plan, namely, the maximum recirculating beam current will be 0.425 mA; the beam spot sizes should be no large than five times of that at 4 GeV and energy spread should be under three times of that at 4 GeV; flexibility of adjusting beam energy at end stations should be preserved; technical choices of upgrade should be made that do not preclude the further upgrade of CEBAF to 24 GeV.

It is anticipated that there is no major technical challenges to use 12 GeV upgraded CEBAF for accelerating ELIC electron beams of 1 mA average beam current up to 7 GeV. With an appropriate setup, an ELIC electron beam gains 7 GeV energy either in three and half passes of the recirculating CEBAF at its top cavity field gradient or five passes when the cavity field gradient is at a low level. The higher ELIC beam current may requires higher power klystrons and higher HOM dampings. Nevertheless, all are within the technical achievable range.

## ***Electron Storage Ring***

A 1.5 GHz CW polarized electron beam of 1 mA current, accelerated to 3 to 7 GeV in CEBAF SRF linac, can be used for injecting and stacking full energy polarized beam in an electron storage ring by use of synchrotron radiation damping. The storage ring has circumference of about 1.5 km and is

designed in a “figure-8” shape for easy spin manipulation. The synchrotron damping time for this ring is about 50ms at 3 GeV and is reduced to 4 ms at 7 GeV. At stacking, a single pulse current of a duration about 50  $\mu$ s will add up to about 10 mA in the storage ring (10 times the ring circumference multi-turn injection). The accumulation time for 3 A stored current (300 injections) at 7 GeV is then about 1.5 s. An alternative regime might be a continuous low current injection to compensate for beam loss in the ring.

The storage ring is designed to provide necessary small transverse beam emittance (low dispersion in bends) to meet the ELIC luminosity requirements.

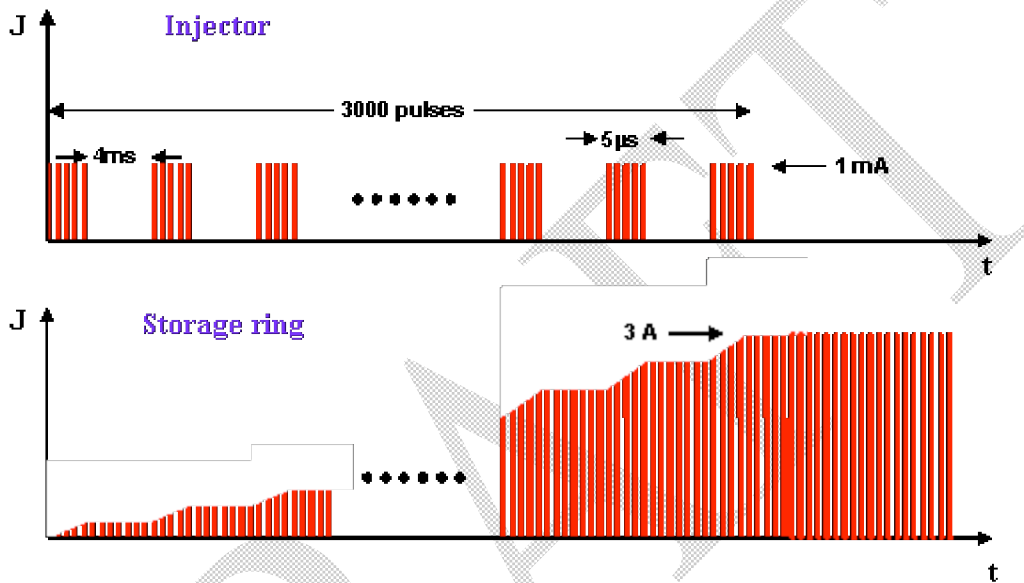


Figure 2.4.1 Stacking of a 3 A polarized electron beam in the storage ring.

## 2.5 Positron Source

A positron beam in ELIC at CEBAF would extend the electron-ion collider capabilities to include positron-ion ( $e+i$ ) collisions and possibly electron-positron ( $e^+e^-$ ) or positron-positron ( $e^+e^+$ ) collisions. A positron source is the only required addition to the ELIC electron facility, and this limited upgrade offers great benefits of including much richer physics to the ELIC project. In the energy range of electron beam 100-200 MeV, modern design converters can be accounted for stacking positron beam with rate about 0.1 A/min [ ], therefore, we conservatively plan to have 50 mA/min stacking rate, so it will take about one hour to accumulate 3 A of positron current in the ELIC. Figure 3.4.1 illustrates one scheme for producing non-polarized positrons based on the 12 GeV CEBAF DC electron injector. In order to generate positrons, the injector will work at 1.5% d.f. regime with 100 mA peak current accelerated to 123 MeV and sent to a converter to produce positrons. Total yield of positrons of 0.005 per incident electron from which a very small, but sufficient fraction of 0.001, is captured by the transverse and longitudinal emittance filters, with average energy of 30 MeV, and then redirected back to two full SRF modules of the CEBAF DC injector for acceleration to 123 MeV. These positrons are injected back into CEBAF for acceleration to 7 GeV and sent to the

same "electron" storage ring for stacking and accumulation. Polarization of the stored positrons will be achieved in the storage ring via the Sokolov-Ternov mechanism.

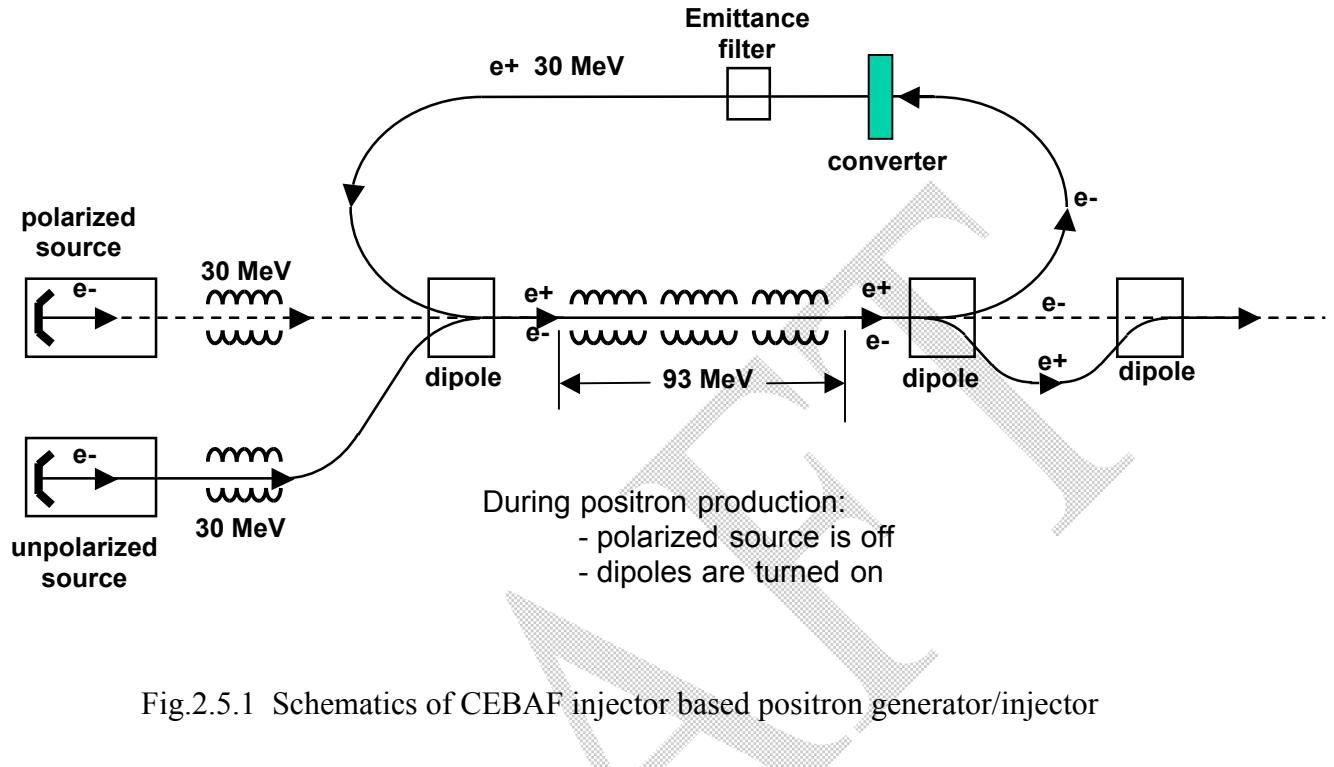
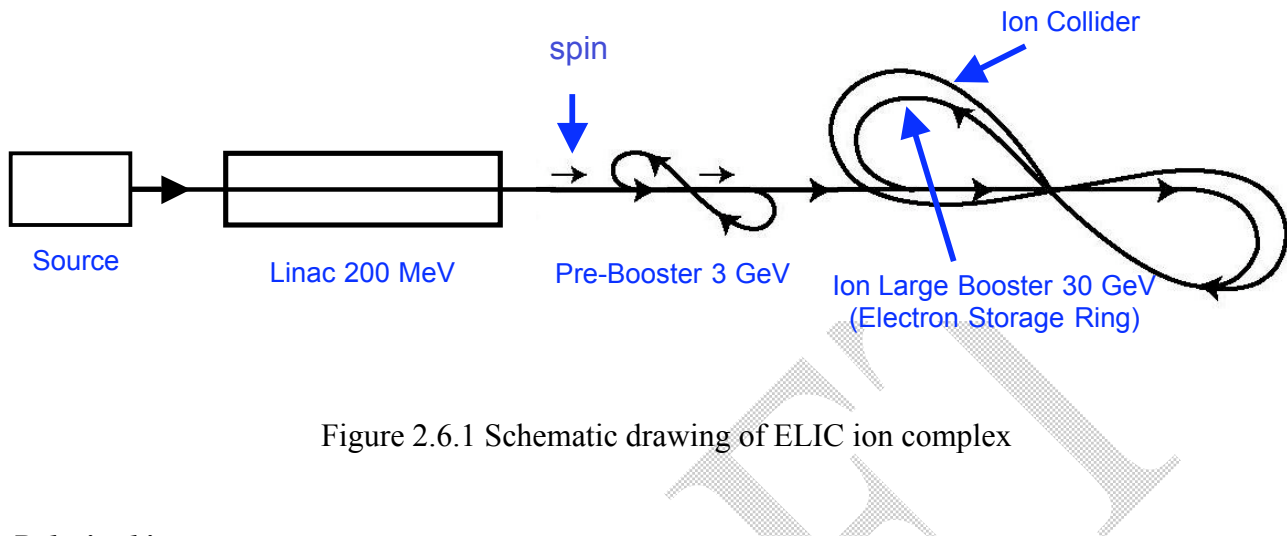


Fig.2.5.1 Schematics of CEBAF injector based positron generator/injector

## 2.6 Ion Facility

The ELIC ion facility is a green-field design that provides a unique opportunity to utilize new and emerging technologies as well as new schemes to deliver a high polarized and high quality ion beam for collisions. As shown in Figure 3.5.1, the ELIC ion complex consists of a polarized proton or light ion source, a 200 MeV RF linac, a 3 GeV stacking pre-booster synchrotron, a 15 to 30 GeV/u large booster synchrotron and a 75 to 150 GeV/u superconducting collider storage ring. A 75 MeV electron cooler for ion beam is also an essential part of the ion complex. All ion species are injected longitudinally polarized and accelerated in the RF Linac, then injected, stacked and accelerated in the pre-booster, etc. The "Figure-8" boosters and storage ring are used for the ions for their zero spin tune, thus intrinsic spin resonances are removed and spin resonance-crossing at beam acceleration is avoided. The longitudinal and transverse polarization at 2 or 4 interaction points in the collider then can be provided for all ion species at all energies avoiding spin rotators around the interaction points (for detail of spin manipulation and maintenance, see parts 3.5.6 and 6.7).

Also, for the purpose of providing accumulation of high current and high quality beams (level of 1 A) from *positive ion sources* (polarized  $^3\text{He}$ ,  $^6\text{Li}$  and unpolarized medium and heavy ions), we envision introducing an *accumulator-cooler ring with 200 KeV DC electron cooling*, to be installed after the linac and before the pre-booster.



### Polarized ion sources

#### Polarized *p* and *d* beams

Modern state of art of polarized ion sources provides 1 mA long pulse 80-90 % nuclei polarized negative hydrogen and deuterium ions.

Claimed future potential of positive and negative polarized hydrogen and deuterium sources: 20-40 mA, 90% polarization, 0.3  $\mu$ M normalized emittance current in pulse.

#### Polarized $^3\text{He}$ beam

There are in development options of polarized *positive* helium source  $^3\text{He}^{++}$ ;

1) Optically Pumped Spin Exchange method [ ]

- Polarization of 50% - 70% expected.
- $2 \times 10^{11}$  particles/pulse

2) Resonant Charge Exchange of Polarized Atoms with  $^4\text{He}^{++}$  [ ]

- Polarization of 70% - 80%.
- > 1mA beam current

#### Polarized Li beam

Existing techniques offer a few hundred nA's of *negative* ions.

The alternate technique such as to be developed polarized helium is able to deliver 1 mA fully stripped  $6\text{Li}^{+++}$  beam with high polarization.

### Linac, prebooster and large booster

Technical design of an advanced *SRF ion linac* has been developed at Argonne National Laboratory by RIA group [ ]. This 50 m long linac is very effective in accelerating a wide variety of polarized and unpolarized ions from  $\text{H}^-$  (200 MeV) to  $^{36}\text{Ar}^{17+}$  (100 MeV/u) and can be modified for a reasonable cost increase to accommodate also very heavy ions (completely stripped to the end of acceleration).

After linac, the ions will be injected and accelerated in a small booster, or *pre-booster* to reach an energy range of a few GeV/u. Polarized proton and deuteron beams can be stacked in pre-booster at injection energy by using the *stripping injection* of negative ions ( $H^-$  and  $D^-$ ) accelerated in the linac. As known, the intensity of a stacked beam is limited by the space charge effect. To diminish this limitation, an innovative technique of *beam painting in round mode optics* will be used at stacking. This concept has been developed and is supposed to be simulated and tested in collaboration with the SNS group of ORNL [ ]. The

Stacking of ions from a *positive source* (polarized  $^3He$ , Li and unpolarized medium and heavy ions stripped in source and in linac) is supposed to be realized in special *accumulator ring* with *non-relativistic electron cooling*. Such method has been successfully used for accumulating of polarized proton beam in Proton Cooler Ring of IUCF [ ]. To approach even higher current at stacking, a similar round mode beam optics technique as mentioned above can be implemented to the ring with electron cooling. After stacking, the positive high current beam will be injected and accelerated in pre-booster.

Next, the *electron collider-storage ring* will be used as a *large* or *main booster* for the ion beam, before accumulating the electron or positron beam in the ring (electron and ion beam pipes can be separated in sections with RF stations). This ring has the same circumference as the ion collider ring but a relatively low magnetic field to drive electrons: about .35 T warm dipoles for 7 GeV electron beam. Apparently, the ring is able to accommodate the ion beam after pre-booster for acceleration from a few GeV to 15-30 GeV/u and extraction to the collider ring. It is important, in particular, that maximum ion energy/u in the large booster (30 GeV) also appears significantly below its *transition energy* (50 GeV), thank to low dispersion design for low radiation of e-beam.

### ***Collider ring***

Similar to the electron collider-storage ring (which serves as the large booster for the ion beam), the figure 8 ion collider ring will have two  $240^\circ$ ,  $R=100$  m arcs (bend radius 70 M, dipole field 7.5 T for 150 GeV proton beam) connected by two  $60^\circ$  crossing straights each 340 m long. The straights will be long enough to accommodate 2 interaction regions (including long beam extension sections) with 2 detectors in each, electron cooling, RF and SRF stations and injection-ejection sections. Introduction of two Siberian Snakes in the arcs, technically much less challenging than the snakes presently used in RHIC (shorter and of smaller aperture), will be used for proton and helium spin control and stabilization, and will extend the total length of the straight sections around the ring by about 60 m. An additional similar snake in one of the two crossing straights will be used for proton and helium spin stabilization, and solenoids for deuteron spin. The transition energy of the ring is designed below the minimum injection energy/u (15 GeV/u for deuteron beam).

### ***Beam clocking***

Synchronization between electron and ion bunches is a common constraint of any electron-ion collider (ELIC) design. The synchronization condition is expressed by a relationship,  $f = q_e f_e = q_i f_i$ , between the RF frequency  $f$  and the revolution frequencies  $f_e = v_e / C_e$ ,  $f_i = v_i / C_i$ , where  $v_e$ ,  $v_i$  and  $C_e$ ,  $C_i$

are the beam velocities and orbit circumferences respectively, and  $q_e$  and  $q_i$  are integers. The constraint is due to the ion velocity change by a factor of about  $10^{-3}$  in the energy range of an EIC. It would be very difficult to compensate the related change of ion beam revolution frequency by changing the ion orbit length with energy. In the ELIC design where the ion beams are driven by RF of very high  $q_i$  (about 7500 at  $f = 1.5$  GHz), a possible solution consists of varying the integer  $q_i$  yet admitting “residual” change of the ion path length in the arcs up to one bunch spacing (about 20 cm, corresponding to  $\pm 12$  mm orbit displacement in the arcs). Ion acceleration in the collider ring can be performed using normal conducting cavities of variable frequency, and after that one can switch (via beam re-bunching) to high voltage superconducting cavities.

## 2.7 Electron cooling

*Electron cooling* (EC) of heavy particle beams in synchrotrons was invented by G. Budker in 1966 [ ] and introduced in the accelerator physics and technology in 1974 [ ]. In this method, an electron beam accompanying a hadron (proton, antiproton) beam along straight section of the synchrotron, serves like a thermostat for the hadron beam via collisions between electron and hadron particles. Today, EC is widely used in low energy storage rings to produce the high quality hadron beams for research and applications. (Cooling at Fermilab, R&D at BNL for RHIC)

Electron cooling of the ion beam is an inevitable component of an electron-ion collider. Cooling of an ion beam injected into the collider ring increases the initial luminosity and extends the luminosity lifetime. Continuous cooling of proton or ion beam during an experiment is required in order to compensate for beam size increase due to the intrabeam scattering, noise and other heating effects. Shortening the bunch length via cooling, in particular, is critical for the high luminosity of ELIC, since it allows one to realize two important advances: an extreme colliding beams focus and implementation of crab crossing at the collision points for achieving the highest bunch collision rate (up to 1.5 GHz).

To realize an efficient EC for 150 GeV proton beam of EIC, one needs a high current (2-3 A) relativistic (80 MeV) electron beam. Such parameter requirements for the electron beam presents a serious challenge. Despite this issue, EC is considered as a prominent candidate for cooling of intense ion beam for EIC. Other methods such as stochastic cooling or optical stochastic cooling at the present state of technical maturity present serious technical challenges and are not capable of providing the required cooling rate for the intense bunched proton or light ion beam of EIC.

Realization of EC at high energies requires the use of a high current SRF ERL. After quite a long period of pre-conceptual studies of the ERL-based high energy EC by the international accelerator community [ ], the Brookhaven National Laboratory started a profound R&D work on realization of high current 55 MeV ERL for electron cooling for luminosity upgrade of heavy ion colliding beams (110 GeV/nucleon) in RHIC [ ].

Similar to electron cooling for RHIC, EC design for ELIC is based on use of SRF ERL as solution in principle to operate 75 MeV, 3 A electron beam and recover its energy. However, that high current presents a very serious challenge. In order to alleviate the constraint of that high CW current, the EC concept for ELIC includes the use of a circulator-cooler ring, where the electron beam injected from

the ERL will circulate during about one hundred revolutions before the quality of the beam is disrupted by the heating processes. Such design allows one to reduce the average current from the source by a factor of 100, thus utilizing a source and ERL with average current of a level 30-100 mA, while the light ion beam is continuously cooled by electron current of a few Amps.

A general electron cooling layout is shown in Figure 2.7.1. The characteristic set of EC parameters for ELIC is presented in Table .

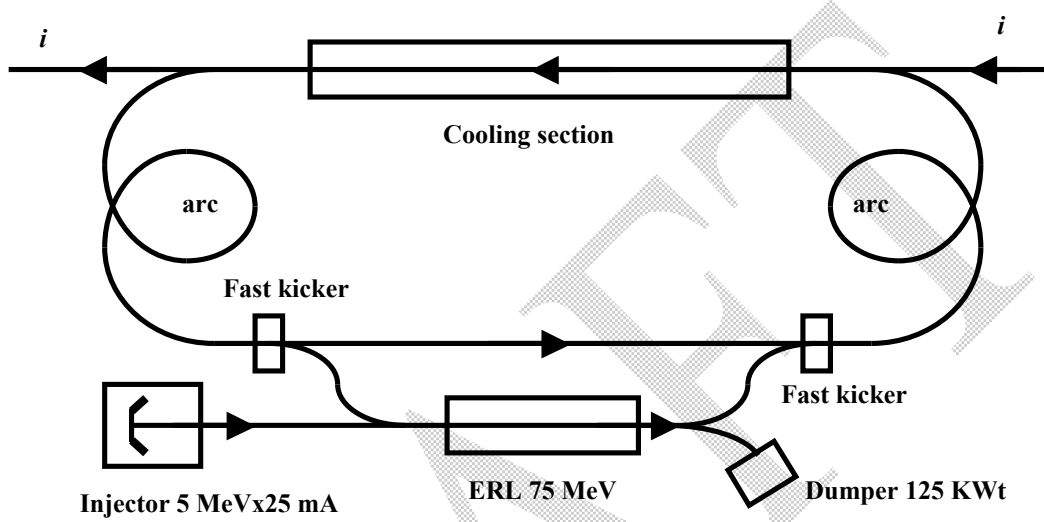


Figure 2.7.1 Schematic of electron cooling for ELIC.

Description of the EC facility, operation and cooling scenario in detail are presented in Part VIII. Here, we underline the following important features of the ERL-based EC conceptual design for ELIC:

- 1) Use of an electron circulator-cooler ring, to reduce drastically (by a factor 100) a necessary average current from electron source
- 2) Implementation of a *staged* EC (i.e. starting cooling after injecting the ion beam in the collider ring and continuing cooling along and after acceleration to energy of an experiment), as a way to minimize the cooling time required for approaching the start luminosity
- 3) Cooling with flat beams (both electron and ion), to minimize the intra-beam scattering impact on luminosity

It should be noted, that EC parameters are designed under the requirement of sufficiently low initial emittance of the high current ion beam in the collider ring. To satisfy this requirement, we develop a specific concept of stacking ion beam in the booster that allows one to significantly reduce the space charge impact on beam emittance (see Part VI.4).

Another challenge of high energy EC is the design of electron beam transport system compatible with efficient acceleration and beam alignment. In cooperation with Cooling Team of BNL, we explore two concepts of cooling beam transports: a classical scheme with magnetized DC e-gun but discontinuous solenoid (recently successfully implemented in Fermilab's cooler of 8 GeV antiproton

beam [9]) and an SRF gun based scheme with non-magnetized, space charge dominated beam [7] (in both schemes the source is photo-cathode based).

Table x: Electron Cooling Parameters for ELIC

Parameter	Unit		
Beam energy	GeV/MeV	30/15	150/75
Length of cooling section	M	30	30
Particles per bunch	$10^{10}$	.4/1	.4/1
$I_{ave}$ in ERL	mA	2x25	2x25
$I_{circulating}$	A	1/2.5	1/2.5
Proton emit., norm (injected)	$\mu\text{m}$	4x4	
Proton emit., norm (equilibrium)	$\mu\text{m}$	1x1	1x.04
Initial cooling time	min	15	10
Cooling time at equilibrium	min	.3	1

At equilibrium in collider mode, the cooling beam area frequently exceeds the ion beam area. The lifetime of the ion beam core and luminosity shown in Table 1 has been estimated by taking into account the Touscheck scattering of particles beyond the edge of the cooling beam [3].

Electron cooling, in cooperation with strong SRF fields in ion storage rings, will allow one to obtain small transverse size, short ion bunches, then allowing one to realize an extremely tight beam focusing at the collision point. Short bunches also make feasible the *crab crossing colliding beams*, that allows one to remove the parasitic beam-beam interactions and maximize the bunch to bunch collision rate.

## 2.8 Interaction Region

The ELIC interaction region is designed to accommodate up to four detectors for different nuclear physics experiments simultaneously at four collision points located symmetrically on the two straight sections of the beam line around the center of the figure-8 collider ring (see Fig. 3.2.1). To attain the highest luminosity, the beams have to be focused at the collision points as tightly as possible. The focusing principle for colliding beams is similar to focusing of light beams in optical microscopes and electron beams in electron microscopes. The scheme generally includes a relatively long section of beam transverse extension and final focusing lenses (quadrupole doublet or triplet magnets). These lenses transform the large beam size (obtained after the extension) to a maximum beam angle divergence and, correspondently, a minimum size at the *collision point*. In addition to the final focusing principle, other considerations of the IR design include detector instrumentation, beam separation after the collisions, synchrotron radiation at the IPs, beam polarization.

### **Interaction region geometry**

The electron and ion storage rings of ELIC are stacked vertically in the same tunnel with the electron ring on top. While the ion ring lies entirely within a horizontal plane, the electron beam emerging from the arcs is bent vertically near the first IP to collide with the ion beam, then is bent back

vertically to cross the second IP before entering the next arc of the electron ring. The distance between the two IPs on the straight section of the beam line is 60 meters. Due to the very close bunch spacing (20 cm) for both colliding beams, a relatively large crossing angle, 0.1 rad or 5.8 degrees, will be used in order to avoid parasitic collisions. Such a large crossing angle eliminates the need for separation dipoles required in conventional IPs with small crossing angles and thus makes the design of ELIC IP's greatly simplified. The present design makes provision for a 4 meter (with the possibility of extension to 6 m) free space around each interaction point for physics detectors.

### **Electron cooling, short bunch and crab crossing**

Electron cooling is the essential part of the ion complex of ELIC at CEBAF. Under a two stage *continuous* cooling of ion beams at the large booster and at the collider ring, the intrabeam scattering induced ion bunch emittance growth is effectively suppressed, and the ion bunches shrink in all dimensions. The shrinkage at the longitudinal direction is especially large such that it could lead to an equilibrium ion bunch size as short as 5 mm. The electron bunches can also be managed to that short or even shorter. One advantage of short colliding bunches is to utilize a very tight beam transverse focusing at the collision point. Such an extreme focusing requires a necessary large beam transverse extension in area of the final focusing quadrupoles. This constraint relaxes of a low transverse emittance under the electron cooling, again. Short bunches also allow one to realize the crab-crossing colliding beams, in order to approach a highest head-on bunch to bunch collision rate (up to 1.5 GHz) while eliminating the parasitic beam-beam interaction. Crab-crossing beams seem to be an effective alternative to a conventional IP design based on introduction of dipole magnetic field in a vicinity of the IP in detector for merging the electron and ion colliding beams.

### **Final focusing and beam sizes at IPs**

The final focusing of colliding beams in ELIC is achieved by two sets of quadrupole triplets? as shown in Figure 3.6.1. The ion beams are focused by a superconducting quadrupole doublet located 2 m from the IP. The first quadrupole (counted from the IP) of this doublet focuses the ion beam vertically while the second quadrupole does focusing in the horizontal direction. These two quadrupoles are 1.2 m and 3 m long with a peak field of 6.2 T and 4.3 T, respectively. A similar set of quadrupole doublet for electron low beta-star is arranged further away from the IP, with 0.6 m and 0.7 m lengths and 1.6 T and 1.9 T peak magnetic fields respectively. The beta-star for both beams can be achieved to 5 mm in both directions. With such small values of beta-stars, the vertical and horizontal RMS sizes of both beams are about 6 \_m and 1.2 \_m. After two IPs in a straight section, a symmetrically identical lattice then returns the beam to its normal sizes in arcs, providing in this way the succeeding transport of a normal beam and multi-turn use of the beam for collisions.

As shown in Figure 3.6.1, two sets of crab cavities, one set for ions, the other set for electrons, are placed outside of final focusing elements. Each set consists of two crab cavities, one for tilting bunch upward or downward by a half of crossing angle and the cavity on the other side of IP restoring the beam back to the original shape after collision.

### **Synchrotron radiation**

Since there are no dipoles in the detector vicinity (the vertical bends of the electron transport are sufficiently far away), synchrotron radiation in this area is mostly generated in quadrupoles. For a well-steered beam, the core of the beam where the majority of the electrons are located experiences relatively low magnetic fields and therefore generates soft photons. A small number of electrons in the transverse tail of the bunch (at amplitude of  $20\sigma$ ) experience magnetic fields as strong as 2 T and thus generate photons of 65 keV energy. The overall radiation power generated by these electrons however is relatively weak due to the small fraction of electrons at these amplitudes, and can be easily collimated upstream of the detector to protect it from high energy photons. These collimators will be placed where the horizontal beam size is small while the radiation fan is wide, ensuring sufficient free aperture for the beam.

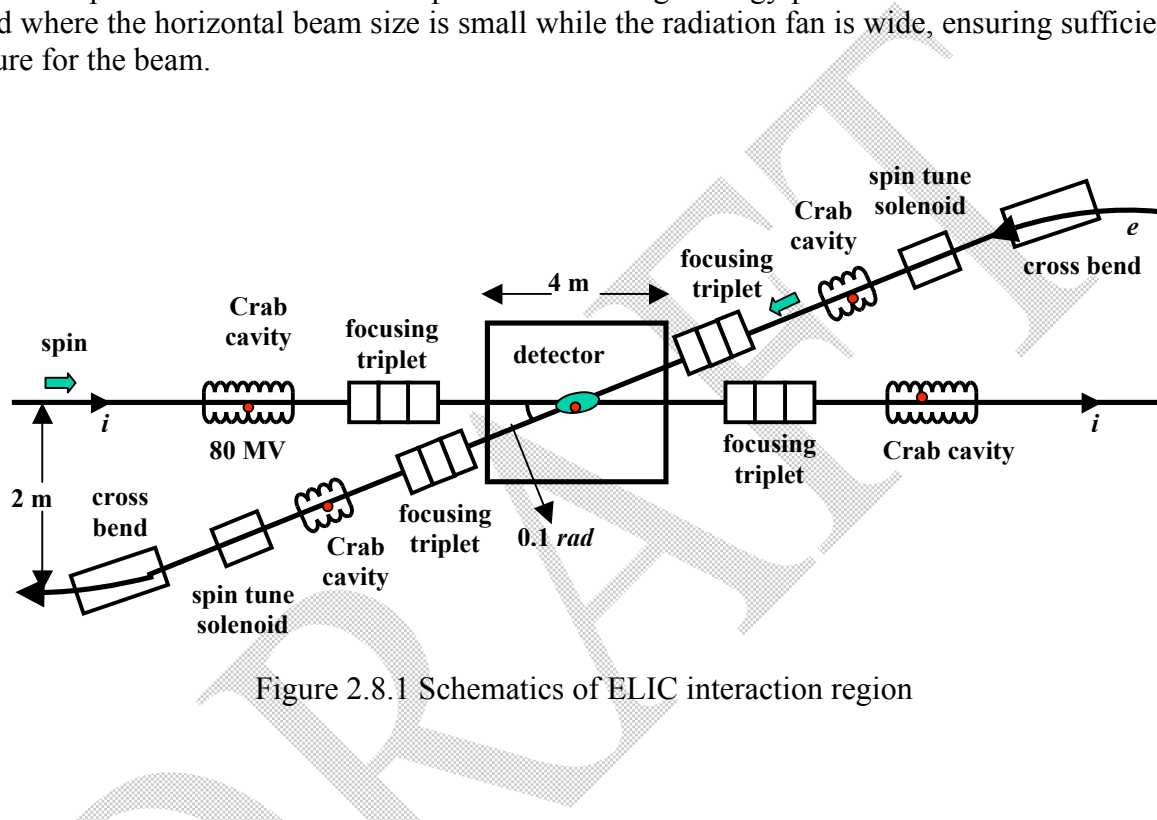


Figure 2.8.1 Schematics of ELIC interaction region

## 2.9 Polarization

### Polarized ions

The “figure-8” rings in ELIC have been proposed to advance the spin features of the collider. There are two important advantages of the “figure-8” rings: first, spin is easily maintained during beam acceleration in the boosters, and second, it is possible to create the desired spin polarization, longitudinal or transverse, at the collision points, and manipulate it for all particle species at any beam energy in the collider ring.

The ion beam spin transport in ELIC evolves as follows: After longitudinally polarized protons or ions traverse the linac, they are injected into the straight section of the figure-8 pre-booster with stable longitudinal spin, accelerated to a few GeV, injected in a similar way to the large figure-8 booster (the electron collider ring), accelerated to an energy of 15-30 GeV and injected to the figure-8 collider ring where acceleration can be continued. To stabilize the spin near the longitudinal direction in the collider ring, warm or superconducting solenoid can be used for light ions, and superconducting Siberian Snake (i.e. snake conserving the longitudinal spin) can be used for proton and helium beam.

This way, longitudinal spin can be delivered from the source to the collision points of the figure-8 collider ring.

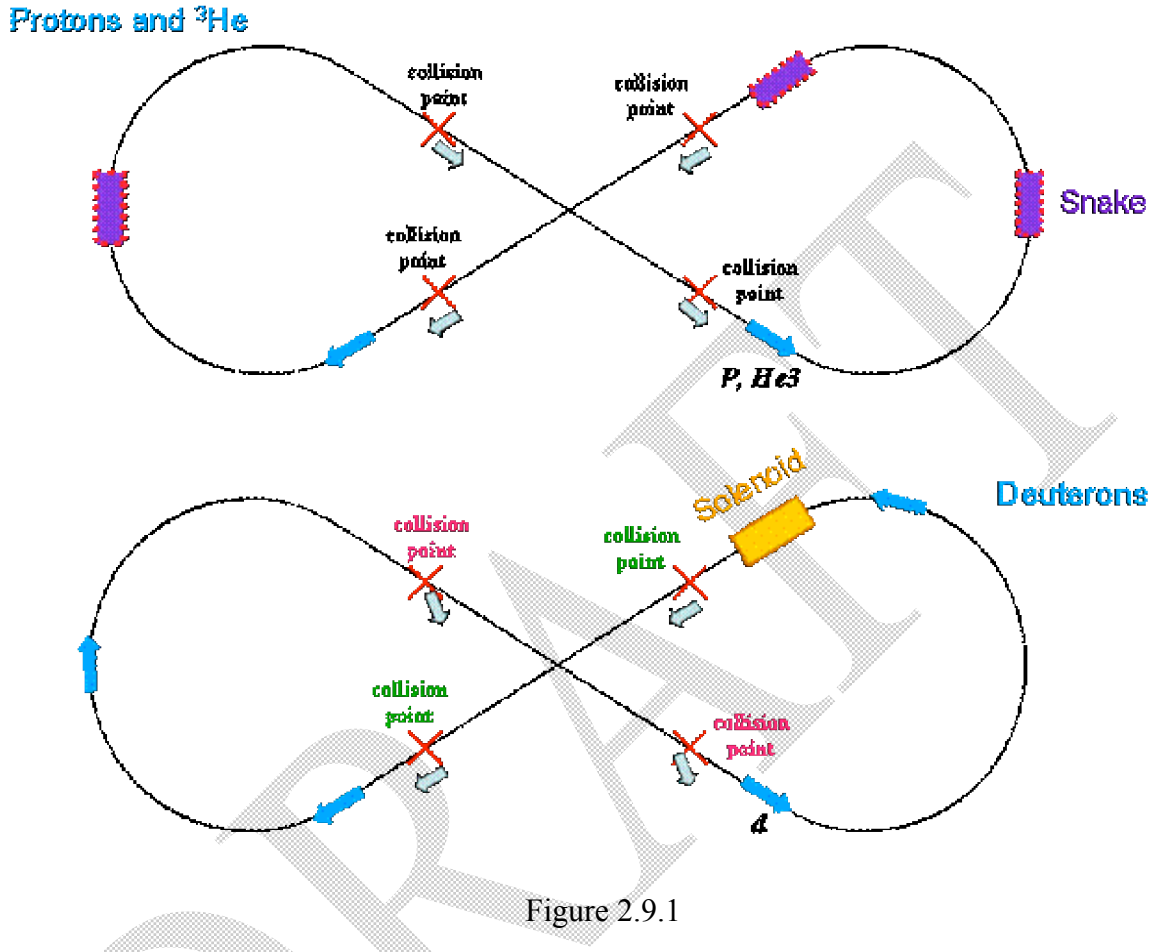


Figure 2.9.1

Furthermore, for protons and  $^3\text{He}$  two interaction points (along the straight section) with simultaneous longitudinal polarization are guaranteed in the absence of any snakes, while two Siberian Snakes in the arcs are required to ensure longitudinal polarization at 4 IP's simultaneously, as shown in Fig. xxx. For deuterons, two IP's with simultaneous longitudinal polarization are guaranteed with no snakes (can be switched between two cross-straight). See Fig. xxx.

### **Spin steering and flipping**

*Transverse spin* required for experiments on CP violation can be obtained (after the beam has been accelerated to the energy required for the experiment) by turning the stable spin from the longitudinal to the horizontal direction, by adiabatically ramping several horizontal dipoles distributed in a proper way around the figure-8 ring. The strength of the stabilizing solenoid or the longitudinal snake should then be turned down to zero or a different optimum value. Here, one has to account for the related orbit excursions. Steering technique also could be used in order to switch the stable spin, either longitudinal or transverse, between two intersecting straights.

Several techniques can potentially be used to alternate the ion polarization during the beam pulse: it can either be done at the source [7] or by developing and applying an RF-induced flipping technique that has been established for low energy beams [8]. Alternatively, one may consider using the steering technique described above to periodically reverse the stable ion spin. An additional possibility for each turn flipping of the transverse proton spin might be the *RF trapped flipping spin* technique [9]. This could work in cooperation with the full longitudinal snake that has to be introduced to one of the two intersecting straights of the figure-8 ring in order to make the spin tune in the ring equal to \_.

### Polarized electrons

Electrons are emitted from the CEBAF polarized DC photocathode source longitudinally polarized at the 80% level. The Wien filter, located in the CEBAF injector, is used to rotate their spin to the vertical direction in the arcs of the figure-8 storage ring. A special spin rotation scheme has been developed to transform the electron spin from vertical in the arcs to longitudinal in the IPs over a wide energy range (5 to 10 GeV or wider) at constant orbit. The scheme, shown schematically in Fig. xxx, is based on the combination of the energy-dependent spin rotation caused by the beam crossing bend (associated with the crab crossing) and a complementary rotation introduced by spin rotators in the arc and after the arc. The spin rotators consist of two SC solenoids with a bend in between to ensure energy-independent orbit. Spin-stabilizing solenoids are introduced around each IP in order to provide (ultimate) the  $\chi$  value of the global spin tune in the ring. This removes spin resonances and makes polarization insensitive to energy. Self-polarization in the arcs supports the injected polarization of the electron beam.

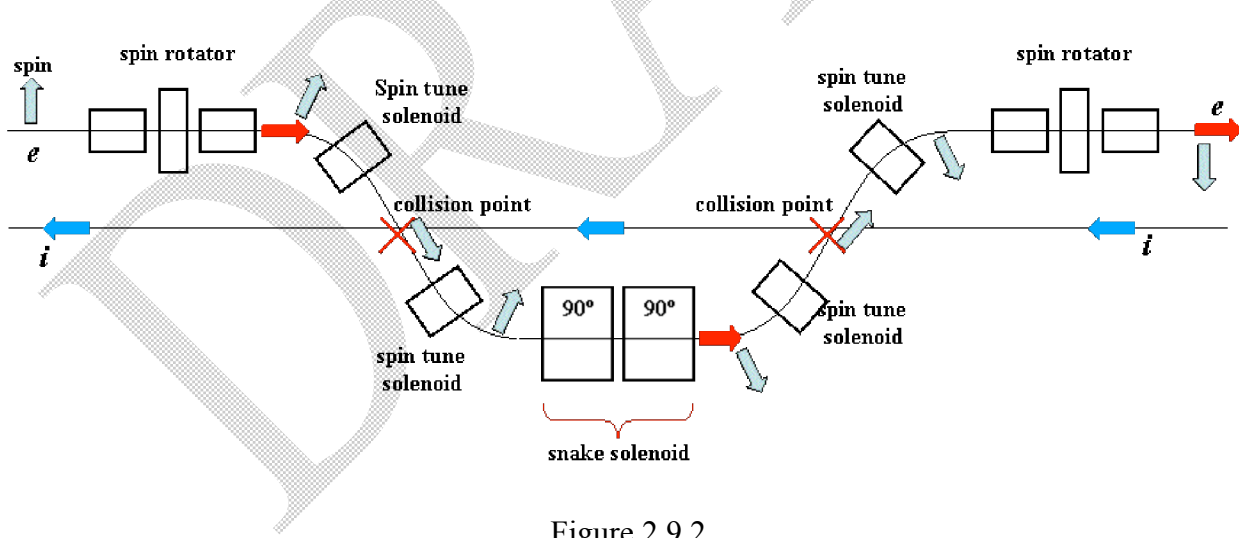


Figure 2.9.2

### Polarized positrons

Positrons are accumulated unpolarized in the storage ring, and can be polarized by the Sokolov-Ternov (S-T) mechanism. The self-polarization time is 2 hours at 7 GeV and can be accelerated with the introduction of damping wigglers. The spin is vertical in the arcs, along the S-T equilibrium, and is reversed (from one arc to the other) using  $180^\circ$  solenoids in the crossing straights between IP's, (see

Figure xxx) thus ensuring four IP's with simultaneous longitudinal polarization. The ideal maximum equilibrium polarization is expected to be 92.4%, however quantum depolarization in spin rotators degrades this value to approximately 88%.

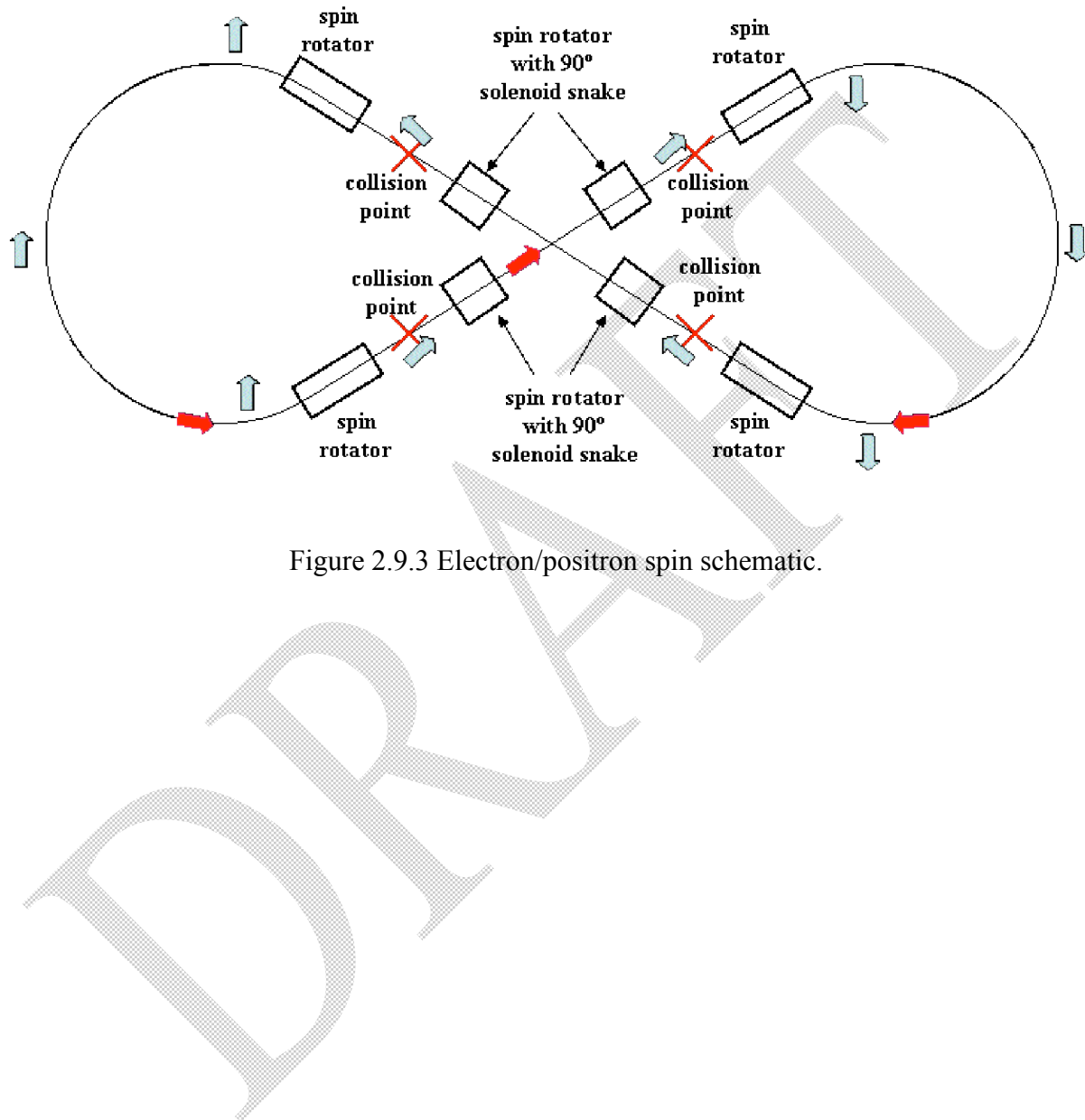


Figure 2.9.3 Electron/positron spin schematic.

## **III Forming and Operating Electron/Positron Beams**

### **Contents:**

- 3.1 General Description**
- 3.2 Polarized Electron Source And Injector**
- 3.3 12 Gev Upgrade CEBAF**
- 3.4 Positron Source At CEBAF**
- 3.5 Collider-Storage Ring**
  - 3.5.1 Layout And Basic Parameters**
  - 3.5.2 Lattice Design And Beam Emittances**
  - 3.5.3 Synchrotron Radiation**
- 3.6 Polarized Electrons And Positrons In Storage Ring**
- 3.7 Polarimetry**
- 3.8 Beam Stability And Lifetime**

### **3.1 General description**

### **3.2 Polarized electron source and injector**

The CEBAF photo-injector [1] provides highly polarized electrons to three end-stations simultaneously, each with independently controlled beam current that can span 6 decades, from 100 pA to 200  $\mu$ A. All of the electrons originate from a single GaAs photocathode within a 100kV DC high voltage photogun and for many years, beam polarization has exceeded 70%. Today's CEBAF photogun exhibits exceptional operating lifetime, with uninterrupted beam delivery for months. The charge lifetime, defined as the amount of charge that can be extracted before QE falls to 1/e of the initial value, is typically 100 to 200C and the charge density lifetime can be as high as  $2 \times 10^5$  C/cm<sup>2</sup>. CEBAF employs synchronous photoinjection (as would ELIC), where lasers emit RF-pulsed light synchronized to the accelerator frequency (1497 MHz).

The Ring-Ring scenario requires average beam current approximately five times greater than demonstrated at CEBAF and extrapolation to this higher value appears to be very reasonable as a result of two recent technological developments. In particular, strained layer superlattice photocathode material has become commercially available [ref], providing experimenters beam polarization >85%, the highest polarization ever measured at Jefferson Lab, and with initial quantum efficiency of ~0.5% at 780 nm, a factor of five enhancement over conventional photocathode material used previously. In addition, this photocathode material can be used with new fiber-based laser technology that was developed for the telecommunications industry [2]. The fiber-based laser provides RF-pulsed light that is easily locked to the accelerator with average power ~ 2W, roughly a factor of four improvement over lasers used previously. Together, these developments (higher QE and laser power) greatly reduce the degree of difficulty associated with the ELIC Ring-Ring electron beam requirements however, routine operation at high polarization with milliAmpere currents has not

yet been demonstrated. An experiment is underway at Jefferson Lab using an improved CEBAF load locked photogun to explore photocathode lifetime at high polarization and average current >1 mA [3].

Despite the optimistic comments stated above, it is prudent to consider potential stumbling blocks related to high current polarized beam operation imposed by the Ring-Ring scenario. One of the most serious obstacles associated with high current operation is ion backbombardment, where residual gas within the cathode/anode gap is ionized by the extracted electron beam and accelerated toward the photocathode surface. These ions damage the photocathode crystal or sputter away the chemicals used to create the negative electron affinity condition. A photocathode subjected to ion backbombardment will exhibit a surface charge limit effect, where photo-excited electrons become trapped near the photocathode surface, creating a retarding potential that reduces the QE of the photocathode. This effect has been mitigated to a large extent using photocathodes with heavily doped surface layers [4] however, repeated heat and reactivation cycles have shown that dopant diffuses throughout the material limiting the utility of a single photocathode to a relatively short time period. Moreover, surface charge limit studies to date have primarily focused on high bunch charge operation with long optical pulses and large laser spots rather than conditions appropriate for ELIC. The stacking scheme of the Ring-Ring scenario requires a relatively low bunch charge of 0.67 pC, but over a short laser pulse (50 ps) and small laser spot size (~1 mm), producing a peak current density of ~10 mA/mm<sup>2</sup>, a regime where surface charge limit effects will likely play a role.

Laser induced photocathode heating is a mild concern for high current operation at Ring-Ring specifications. Heating the photocathode will “boil-off” the chemicals applied to the photocathode surface, reducing the quantum efficiency at the location of photoemission. Also important for high brightness photo-injectors is degradation of the transverse emittance as the thermal temperature of the photocathode is increased. Generally, photocathode heating is more of a concern for photoinjectors operating in the 10 to 100 mA regime, where average power of many Watts is required. In the case of the Ring-Ring scenario, a modest laser power of ~1 W should suffice and laser heating effects will be relatively small and manageable by implementing modest design modifications to existing guns.

### 3.3 12 GeV upgrade CEBAF

### 3.4 Positron source at CEBAF

The experiments with ELIC positron beam include a top luminosity  $e^+e^-$  factory, DVCS and quark Compton scattering accessible via interference between an electron and a target quark radiation. The positron beam at CEBAF will also permit highly desirable experiments with positron beam on fixed target at very large luminosity.

#### Basic parameters

- Beam energy for stacking is 7 GeV.
- Accumulated beam current  $J_{ELIC}$  is 3A.

- Standard CEBAF beam emittance is  $1 \text{ mm} = 1 \text{ mm} \times \text{mrad}$ .
  - Period of beam turn  $T_{\text{rev}}$  is of 5 ms.
  - Beam damping time  $t_{\text{rad}}$  is of 3 ms.
  - Injection rate  $n_{\text{injection}}$  is of 300 Hz.
  - Total time of beam accumulation  $T_{\text{accum}}$  is of one hour.
  - Number of turns in a single train  $N_{\text{turns}}$  is 10.
- Instantaneous current from CEBAF  $J_{\text{injection}}$  is of 300 nA.  
Duty factor of injection:  $10 \text{ turns} \times 5 \text{ ms} \times 300 \text{ Hz} \Rightarrow \text{d.f.} \sim 1.5\%$

### ***Emittance of the positron beam for 123 MeV electron beam and 30 MeV positron beam after 0.5 mm tungsten converter***

Transverse size of the incident electron beam on the converter is  $s_x = 20 \text{ mm}$  (tighter focus doesn't help, however it requires a very large raster frequency due to high power heat power density in converter) for 0.5 mm thickness of the converter and 30 MeV positron beam energy leads to the positron beam source transverse size of  $s_x = 25 \text{ mm}$  (a thickness of the radiator – 0.5 mm product with a positron typical angle –  $q_x \sim 0.03 \text{ rad}$  and 20 mm electron beam spot size). Emittance is  $e^{n(\text{normalized})} = s_x q_x g_{\text{beam}} = 45 \text{ mm}$ . After acceleration in the injector linac to 123 MeV positrons injected to the North linac, where  $b_x$  up to 60 m. The size  $s_x$  will be up to 3 mm. Such size is bit too large, however the value of  $s_x$  likely drops to 2 mm, when acceleration on the way through the linac taken into account. After acceleration in the first linac the beam has energy of 800 MeV and the  $s_x$  in the arc 1 is 1.5 mm (in some places the value of  $b_x$  is 70 m).

Conclusion: 300 nA positron beam intensity doesn't require major additional facility.

## **3.5 Electron/positron storage ring**

### **3.5.1 Layout and basic parameters**

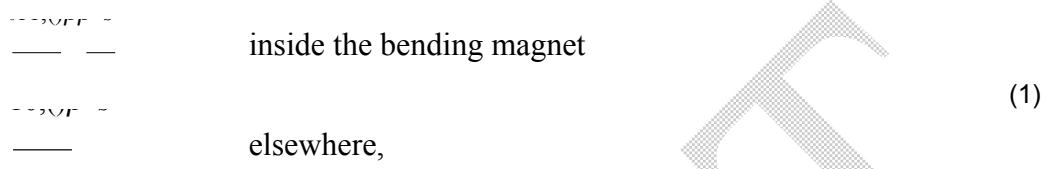
### **3.5.2 Lattice design and beam emittances**

#### ***Natural Equilibrium Emittance***

Synchrotron radiation effects are of paramount importance for the motion of electrons in a storage ring. Each time a quantum is emitted the energy of the electron suffers a small discontinuity. Sudden emissions of individual photons excite various oscillations; the resulting energy 'drop' disturbs the trajectory of the electron causing their amplitudes to grow. However, for the ultra-relativistic electrons the radiation is emitted primarily along the direction of motion within a narrow  $1/\gamma$  cone, therefore the resulting momentum change is opposite to the direction of motion. This radiation reaction force is to be balanced by the action of the RF system.

In a storage ring the electron beam reaches the state of equilibrium when the quantum emission excitations of both transverse and longitudinal oscillations are balanced by the radiation damping originating from the action of the RF system. Because of the statistical nature of the quantum emission the equilibrium is characterized by a Gaussian distribution. Details of single particle dynamics were given by M. Sands; here are some major results [1]

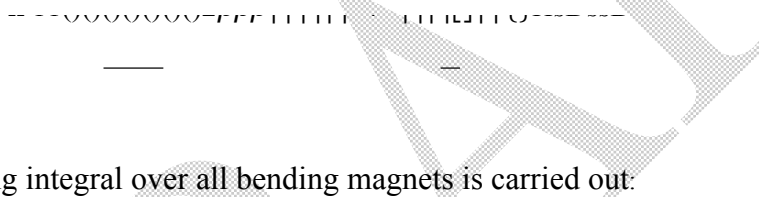
Assuming the isomagnetic guide field, defined as follows:



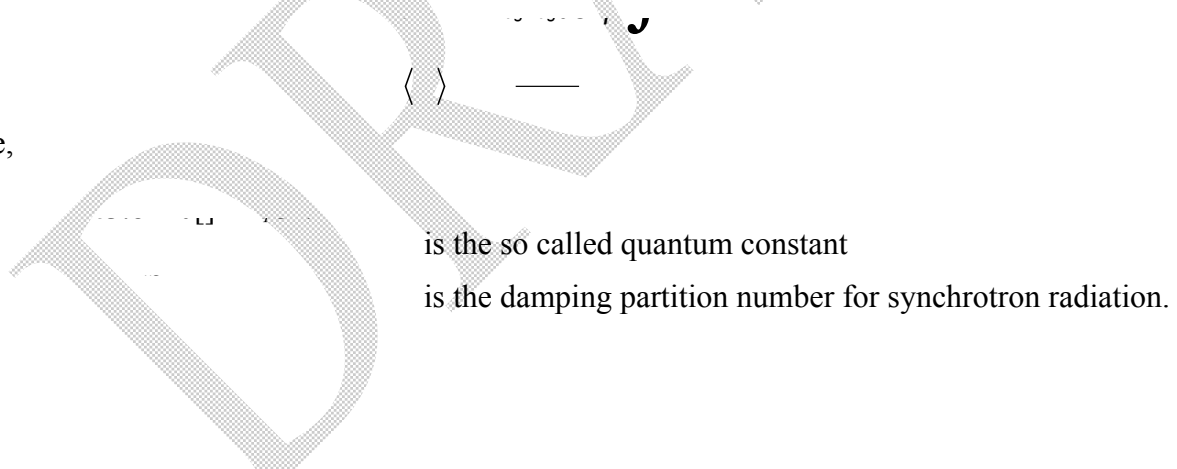
the natural beam emittance is given by the following expression

$$\langle \langle \dots \rangle \rangle \quad (2)$$

where



and the following integral over all bending magnets is carried out:



### **Small Equilibrium Emittance Lattices**

By careful lattice design one can appropriately ‘tailor’ Twiss functions and their derivatives in the bending magnets, so that the value of  $\langle \langle \dots \rangle \rangle$  is minimized. The H-function can be expressed analytically [2] for various types of lattices; then the equilibrium emittance can be written in the following compact form:

$$\langle \langle \dots \rangle \rangle = \frac{1}{\lambda} \int \frac{d\lambda}{\lambda} \quad (3)$$

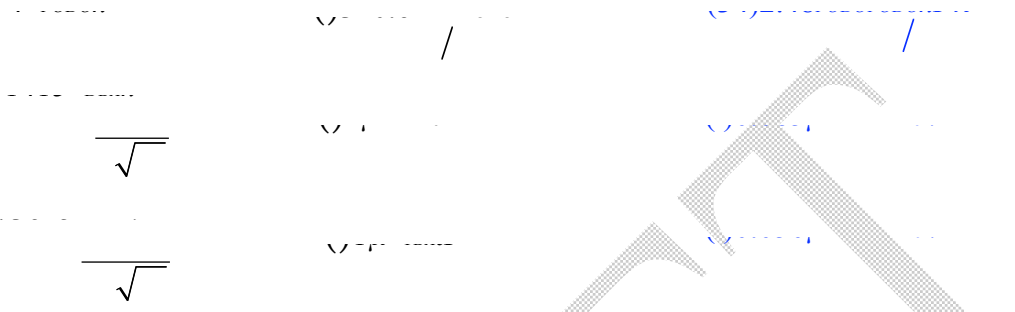
where

is a single dipole bend angle and the factors

depend only on the type of lattice structure.

Here we considered three styles of cells: the FODO, the Double Bend Achromat and the Triple Bend Achromat – the corresponding

factors are summarized below [2]:



As shown in [2] for the FODO optics the above F-factor depends on the phase advance per cell,  $\mu_c$  having a shallow minimum at  $3\pi/4$  (135 deg.). All three styles of low emittance cells (based on the same bend angle magnet) are illustrated in terms of Twiss functions in Figure 1.

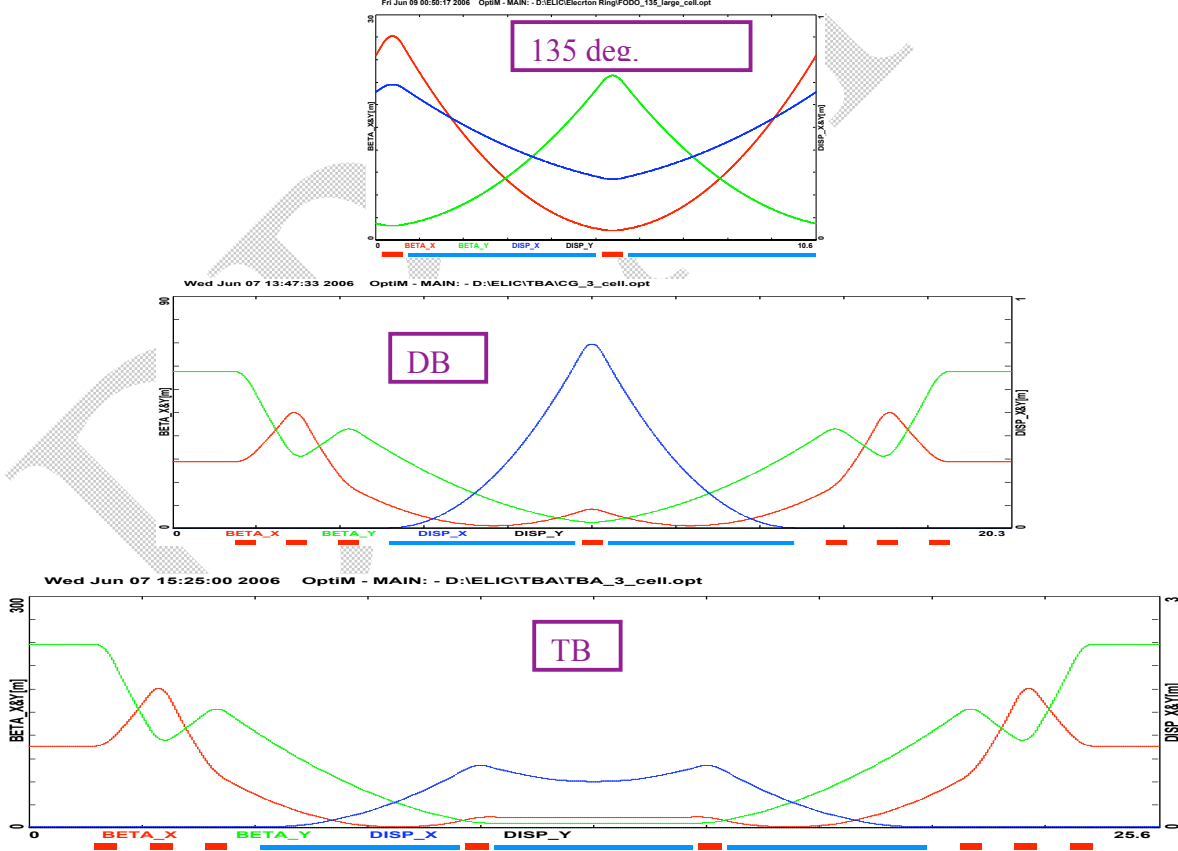


Figure 1 Low equilibrium emittance lattices: FODO, DBA and TBA periodic cells

As one can see from Figure 1, the FODO structure offers great lattice compactness compare to the DBA and TBA cells (roughly factor of 2 longer then the FODO), while the DBA and TBA based rings excel in minimizing the equilibrium emittance (about factor of 40 down from the FODO). Naturally, one would use the achromat cells (DBA or TBA) to build a high brilliance synchrotron light source where there is a great need for even distribution of the RF throughout the ring, since each cell offers a dispersion free straight suitable to host RF cavities. On the other hand, for a compact collider ring with the RF confined to one or two long straights, the FODO based lattice seems more suitable. One can still maintain appropriately small equilibrium emittance driven by the collider luminosity consideration while taking advantage of uniform focusing and superior lattice compactness.

### **Figure-8 Collider Ring Architecture**

To maintain high polarization of the electron beam in a collider ring there is a great advantage of the Figure-8 configuration vs. a conventional 360 deg. ring. Here we will present linear optics design for such lattice topology based on the previously described 135 deg. FODO structure.

First, one needs to design an achromat super-period out of 135 deg. FODO cells. Starting with zero dispersion and its derivative at the beginning of the achromat one needs to advance the betatron phase by a multiple of  $2\pi$  to create a periodic dispersion wave (zero dispersion and its derivative at the end). This can be accomplished by putting together minimum of eight 135 deg FODO cells as shown by a simple numerology:  $8 \cdot 3\pi/4 = 3 \cdot 2\pi$ . The resulting achromat super-period (a sequence of eight 135 deg. FODO cells) is illustrated in Figure 2.

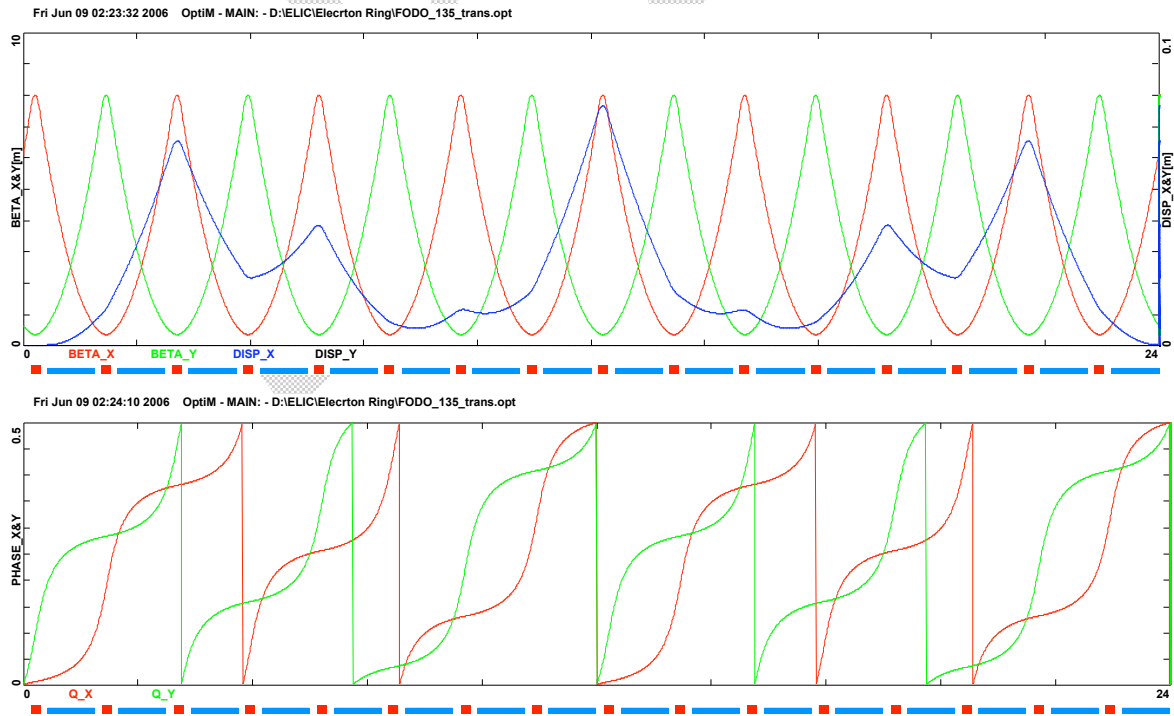


Figure 2 Achromat super-period – Twiss functions (top) and betatron phase advance in units of  $2\pi$  (bottom)

The above periodic module will be used as a building block to construct bending parts ‘loops’ of the Figure-8 ring. The Achromat super-period is also naturally matched to individual 135 deg. FODO cells with removed dipoles – the so called ‘empty’ cells. The empty cells will be used to construct the straight sections of the Figure-8 ring.

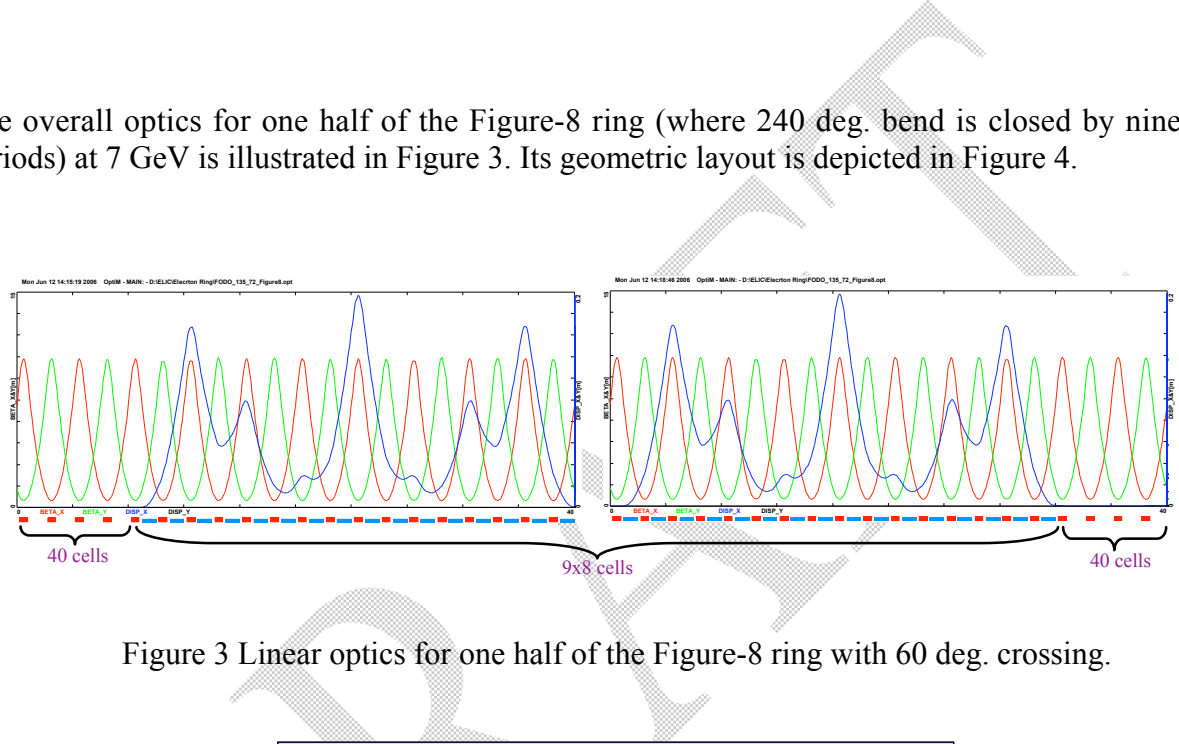


Figure 3 Linear optics for one half of the Figure-8 ring with 60 deg. crossing.

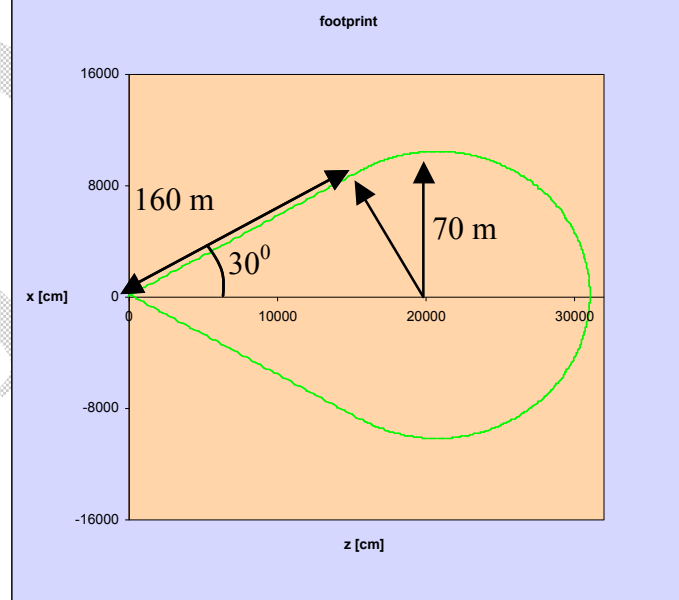


Figure 4 Layout of one half of the Figure-8 ring with 60 deg. crossing.

The long dispersion free straights (2\_160 m each) will accommodate the RF as well as four interaction regions (IR). The FODO structure of the straights is quite flexible to ‘launch’ matching inserts around the IRs.

### ***Equilibrium Emittance of the Figure-8 Ring***

The equilibrium emittance for the above Figure-8 lattice can be evaluated numerically from Eq. (2) modified for the new ‘topology’ – full closing of the Figure-8 ring requires 480 deg. of net bending rather than usual 360 deg. in the conventional circular layout. The resulting modified formula acquires a factor of 4/3 (480/360) as expressed below

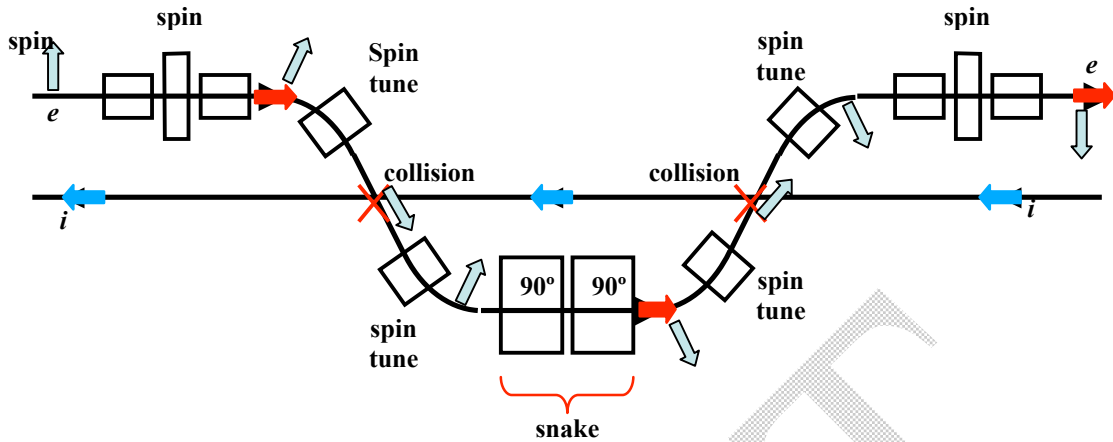
(4)

The above formula was evaluated numerically for two lattice varieties fitting in the layout illustrated in Figure 4: the ‘small emittance’ lattice with fewer longer dipoles (240 deg loop closed with 9 super periods – total of 9\_8\_2 = 144 ‘long’ dipoles) and the ‘very small emittance’ lattice with larger number of shorter dipoles (240 deg loop closed with 19 super periods – total of 18\_8\_2 = 304 ‘short’ dipoles). Both results are summarized below including the equilibrium emittance evaluated from the lattice H-functions as calculated numerically by OptiM [3] (linear optics program):

Lattice variety	‘small emit. lattice’	‘very small emit. attice’
number of bends	288	608
Dipole bend angle [mrad]	29.08	13.77
Dipole length [cm]	50	100
Dipole field [kGauss]	6.44	6.79
equilibrium emittance (analytic) [nm rad]	5.87	0.623
equilibrium emittance (OptiM) [nm rad]	5.97	0.635

### ***3.5.3 Synchrotron radiation issue***

### ***3.6 Polarized electrons and positrons in storage ring***



Rotation of spin from vertical in arcs to longitudinal at IP:

- Beam crossing bend causing energy-dependent spin rotation, together with Energy-independent orbit spin rotators [two SC solenoids with bend in the middle] in the arc and after the arc.

### **Spin matching in storage ring**

Matching at vertical spin in arcs (5-10 GeV)

#### **Matching of the vertical spin with the cross bend**

Rotation of electron spin from vertical direction in arcs to the longitudinal direction at IP: The beam cross bend (angle  $\alpha$ ) causes an energy-dependent spin rotation by angle

$$\varphi = \gamma G \alpha,$$

one radian of order of value, but changes with energy if one keeps the orbit fixed, as usual. Assume  $\alpha \approx 0.07$  rad, then at 10 GeV,  $\varphi = \pi / 2$ , and

$$\varphi = \frac{\pi}{2} \frac{E_{GeV}}{10}; \quad \Delta\varphi = \frac{\pi}{2} \frac{\Delta E}{10}; \quad \Delta E \equiv E_{max} - E$$

Spin rotation to compensate for  $\Delta\varphi$ :

SC solenoid in arc before the end orbit horizontal bend by angle  $\alpha$ , to rotate spin around beam direction by angle  $\varphi_1$ :

$$\sin \varphi_1 = \operatorname{ctg}(\gamma G \alpha) = \operatorname{tg}\left(\frac{\pi}{2} \frac{\Delta E}{10}\right)$$

SC solenoid after arc to rotate spin angle  $\varphi_2$ :

$$\operatorname{tg} \varphi_2 = -\operatorname{tg} \varphi_1 \cdot \cos(\gamma G \alpha) = -\operatorname{tg} \varphi_1 \cdot \sin\left(\frac{\pi}{2} \frac{\Delta E}{10}\right)$$

$$E_{min} = \frac{1}{2} E_{max} = 5 \text{ GeV}; \quad \varphi_{1max} = 90^\circ = -\varphi_{2max};$$

$$(B_s l)_{max} \approx 52.5 \text{ TM}$$

## Spin stabilization

In order to stabilize the spin near the periodic motion around the ring, one can install solenoids, two the short ones around each IP, where the polarization is longitudinal. The maximum integrated precession of spin deviated from the longitudinal direction, is 180 degrees; that gives 22.5 degrees each solenoid. Assuming 6T field at 10 GeV, it requires a single solenoid near 2m as long.

## Matched spin injection

Spin injected being parallel to the periodic polarization vector at the place of injection – by use of the Wien filter

Table 2: Polarized e-beam run

Parameter	Unit				
Energy	GeV	3	5	7	10
Beam cross bend at IP	mrad	70			
Radiation damping time	Ms	50	12	4	1.5
Accumulation time	S	15	3.6	1	.4
Self-polarization time <sup>*)</sup>	H	20	10	2	.33
Equilibrium polarization, max <sup>**)</sup>	%	92	91.5	90	88
Beam run time	H	lifetime	lifetime	lifetime	lifetime

<sup>\*)</sup> One exponent. The time can be shortened by use of high field wigglers

<sup>\*\*) The ideal maximum of equilibrium polarization 92.4 %. Degradation is due to radiation in the spin rotators</sup>

Sokolov-Ternov polarization for positrons:

a possibility for polarized  $e^+ i^-$  and  $e^+ e^-$  collider

Energy region 5-10 GeV

Vertical spin in arcs (reversing with field by use of 180 degrees solenoids between arcs)

4 IP with longitudinal spin

Polarization exponent time 20 min at 10 GeV, changes with energy

as  $E^{-5}$  (can be accelerated by introduction of high field wigglers)

### Quantum depolarization in the IP bends:

Here, spin is transverse to the bend field, then

$$\Lambda_{dep} = \Lambda_p [1 + \frac{11}{54}(\gamma G \alpha)^2] \frac{l_{cb}}{C}$$

- Balance equation:

$$\frac{d\xi}{dt} = \frac{8}{5\sqrt{3}} \Lambda_p - \left\{ 1 + \frac{3\alpha}{\pi} [1 + \frac{11}{54}(\gamma G \alpha)^2] \right\} \Lambda_p \xi$$

## Equilibrium polarization: $\leq 89\%$

### $e^+e^-$ colliding beams (longitudinally polarized)

- Same spin transport for both beams as for positrons in the  $e^+i$  collider
- Electrons can be injected from polarized source
- Crab crossing beams separated by SRF dipoles (?)
- An option: build two lepton rings (before ion complex), then three polarized colliders : $e^+e^-$ ,  $e^-e^-$  and  $e^+e^+$  become possible (all crab-crossing beams!)

Parameter	Unit	3	5	7
Energy	GeV	3	5	7
Beam cross bend at IP	mrad	70		
Radiation damping time	ms	50	12	4
Accumulation time	s	15	3.6	1
Self-polarization time	h	20	10	2
Equilibrium polarization, max	%	92	91.5	90
Beam run time	h		Lifetime	

\*One e-folding. Time can be shortened using high field wigglers.

\*\*Ideal max equilibrium polarization is 92.4%. Degradation is due to radiation in spin rotators.

## 3.7 Polarimetry

## 3.8 Beam stability and lifetime

### Stability of Electron Beam in ELIC

Here are some results of the stability studies for the collective effects in the electron storage ring in ELIC using the following parameters:

Energy :  $E = 7 \text{ GeV}$

Number of electrons per bunch :  $N_e = 10^{10}$

RF acceptance :  $\frac{\dot{A}p_{rf}}{p} = 1.4\%$

Momentum compaction :  $\alpha = 4 \times 10^{-3}$

Harmonic number :  $h_{rf} = 7500$ ;

Bunch length :  $\sigma_z = 5 \text{ mm}$

Normalized emittance :  $\epsilon_{nx} = 100 \mu\text{m}$ ,  $\epsilon_{ny} = 1 \mu\text{m}$

Average beta function in the ring :  $\beta_x = 5 \text{ m}$ ,  $\beta_y = 5 \text{ m}$

momentum spread :  $\delta_p = 3 \times 10^{-4}$

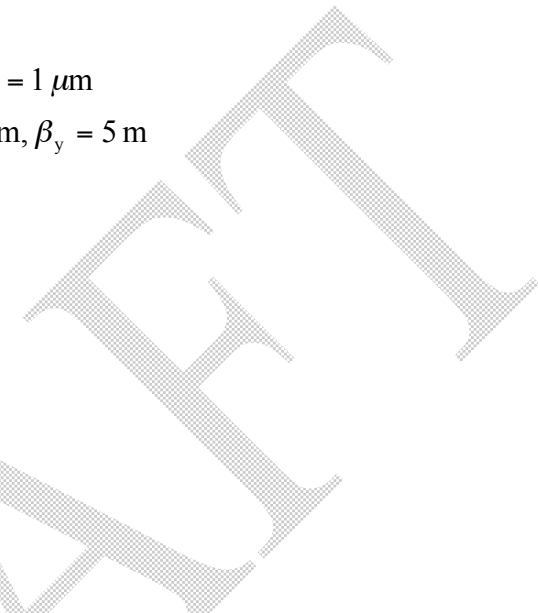
Betatron tune :  $\nu_x \approx \nu_y = 15$

Bending radius :  $\rho = 100 \text{ m}$

Circumference :  $C = 1.5 \text{ km}$

Beam pipe radius :  $b = 1.74 \text{ m}$

Synchrotron tune :  $\nu_s = 0.25$



### 3.8.1 Incoherent Effect

- Touschek Effect

$$\frac{1}{\tau} = \frac{r_e^2 c N_e}{8\pi\gamma^2 \sigma_x \sigma_y \sigma_z (\Delta p_{rf} / p)^3} D(\xi)$$

and

$$D(\xi) = \sqrt{\xi} \left( -\frac{3}{2} e^{-\xi} + \frac{\xi}{2} \int_{\xi}^{\infty} \frac{\ln u}{u} e^{-u} du + \frac{1}{2} (3\xi - \xi \ln(\xi) + 2) \int_{\xi}^{\infty} \frac{e^{-u}}{u} du \right)$$

For the ELIC electron ring parameters, the Touschek lifetime is  $\tau = 20 \text{ hr}$ .

- Intrabeam Scattering (IBS)

(assume  $\log_c = 10$ )

$$\frac{1}{\tau_s} = \frac{e^4 N_e \log_c}{8m_e^2 c^3 \beta^3 \gamma^3 \sigma_z \epsilon_x^{3/2} \sigma_p^2} \sqrt{\frac{\nu_x}{R}}$$

$$\frac{1}{\tau_x} = \frac{e^4 N_e \log_c}{16m_e^2 c^3 \beta^3 \gamma^3 \sigma_z \epsilon_x^{5/2}} \sqrt{\frac{R}{\nu_x}} \left( \frac{2}{\nu_x^2} - \frac{1}{\gamma^2} \right)$$

For  $\epsilon_x$  being geometric horizontal emittance, the IBS growth time is

$\tau_s = 96 \text{ sec}$  and  $\tau_x = 55 \text{ sec}$ .

- Incoherent Space Charge Tune Shift

$$\Delta Q_y = \frac{r_e R}{\sqrt{2\pi}\gamma^3} \frac{\beta_y N_e}{\sigma_y(\sigma_x + \sigma_y)\sigma_z}$$

The estimation of  $\Delta Q_y$  is 0.00026.

- Incoherent Synchrotron Radiation (ISR)

$$P = \frac{2e^2 c}{3\rho^2} \gamma^4$$

Single bunch power loss due to ISR is 1.62kW. The total power loss by nb=7500 bunches in the ring is 12 MW.

### 3.8.2 Single Bunch Instabilities

- Longitudinal Microwave Instability Threshold

$$\frac{Z}{n} = \frac{2\pi\eta E_e (\sigma_p)^2}{I_{peak}} = 0.41 \Omega$$

The electron beam should be safe from this instability for  $Z/n \leq 0.41 \Omega$ .

- CSR Microbunching Instability

CSR is shielded for wavelength

$$\lambda_{sh} \geq \frac{b^{3/2}}{\sqrt{\rho}} = 0.2 \text{ mm} .$$

Microbunching may develop for  $\sigma_z \geq 0.5\rho\Lambda^{-3/2}$  for  $\Lambda = \frac{1}{\eta\gamma} \left( \frac{I_{peak}}{I_A} \right) \left( \frac{\rho}{R} \right)$ , when

$$I_{peak} \geq \frac{\eta\gamma\sigma_p^2 I_A R}{\rho} \left( \frac{\rho}{2\sigma_z} \right)^{2/3}.$$

Here the threshold for peak current is 92A, which is bigger than the design peak current of  $I_{peak}=38A$ . Moreover, this CSR instability is suppressed because

$$\lambda_{sh} \leq \sigma_z .$$

- Transverse Mode Coupling Instability

$$\text{Im } Z \leq \frac{2\pi(E/e)v_s}{\sqrt{\pi}I_b R < \beta >} =$$

This design should be safe from the transverse mode coupling instability for  $\text{Im } Z \leq 57 \text{ M}\Omega/\text{m}$ .

- Transverse Microwave Instability

$$Z_\perp \leq \frac{\pi\gamma\eta R\sigma_p\sigma_z}{3N_e r_e < \beta > b} Z_0$$

This design should be safe from the transverse microwave instability for  $Z_\perp \leq 3 \text{ M}\Omega/\text{m}$ .

- Power Loss Due to Coherent Synchrotron Radiation

Power loss due to CSR for each bunch

$$P_{coh} = \frac{N_e^2 e^2 2^{4/3} 3^{1/6} [\Gamma(2/3)]^2 c}{\rho^{2/3} \sigma_z^{4/3} 2\pi} = 332 \text{ W}$$

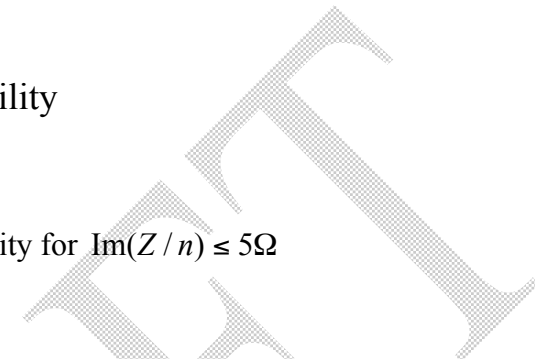
Total power loss by nb=7500 bunches is Ptot=2.4MW.

### 3.8.3 Coupled Bunch Instabilities

- Longitudinal Coupled Bunch Instability

$$\text{Im}\left(\frac{Z}{n}\right) \leq \frac{\pi \eta^2 (E/e) h^2 \beta^2 \sigma_p^2}{4 I_b v_s^2} \approx 5.3 \Omega$$

The design should be safe for this instability for  $\text{Im}(Z/n) \leq 5\Omega$



### 3.8.4 Two Stream Instabilities

- Fast Beam-Ion Instabilities (linear model)

Assuming ionization cross section  $\sigma_{ion} = 42 \text{ Mb}$ , gas density  $d_{gas} = 5.1 \times 10^{13} \text{ m}^{-3}$ , A=1;

$$\frac{1}{\tau} = \frac{4 d_{gas} \sigma_{ion} \beta_y N_e^{3/2} n_b^2 r_e \sqrt{r_p} \sqrt{L_{sep}} c}{3\sqrt{3} \sigma_y^{3/2} \gamma (\sigma_x + \sigma_y)^{3/2} A^{1/2}}$$

The growth time is  $\tau = 0.2 \text{ msec}$

- Electron-Cloud Induced Single Bunch head-tail Instability

For a positron-proton colliding scheme, the threshold for the electron-cloud density due to head-tail instability is

$$\rho_{th} = \frac{\gamma v_s}{\pi^2 r_e R \langle \beta \rangle} = 1.0 \times 10^{14} \text{ m}^{-3}$$

## IV Forming and operating ion beam

### Contents

- 4.1 General description of ELIC ion facility**
- 4.2 Polarized light ion and heavy ion sources**
- 4.3 Linear accelerator**
- 4.4 Pre-booster**
- 4.5 Stacking ions**
- 4.6 Large booster**
- 4.7 Collider ring**
- 4.8 Cooling of ion beam**
- 4.9 Transport, maintenance and manipulation of ion spin**
- 4.10 Collective effects and beam stability**

### 4.1 General description of ELIC Ion Facility

#### *Ion complex layout and basic parameters*

The ELIC ion facility is a green-field design that provides us a unique opportunity to utilize new and emerging technologies as well as new schemes to deliver a high polarized and high quality ion beam for collisions. As shown in Figure 3.5.1, the ELIC ion complex consists of a polarized proton or light ion source, a 200 MeV RF linac, a 3 GeV stacking pre-booster synchrotron, a 20 GeV large booster synchrotron and a 150 GeV superconducting collider storage ring. A 75 MeV electron cooler for ion beam is also essential part of the ion complex. All ion species are injected longitudinally polarized and accelerated in the RF Linac, then injected, stacked and accelerated in the pre-booster, etc. The “Figure-8” boosters and storage ring are used for the ions for their zero spin tune, thus intrinsic spin resonances are removed and spin resonance-crossing at beam acceleration is avoided. The longitudinal and transverse polarization at 2 or 4 interaction points in the collider then can be provided for all ion species at all energies avoiding spin rotators around the interaction points (for detail of spin manipulation and maintenance, see parts 3.5.6 and 6.7). Table presents main the ion facility and beam parameters

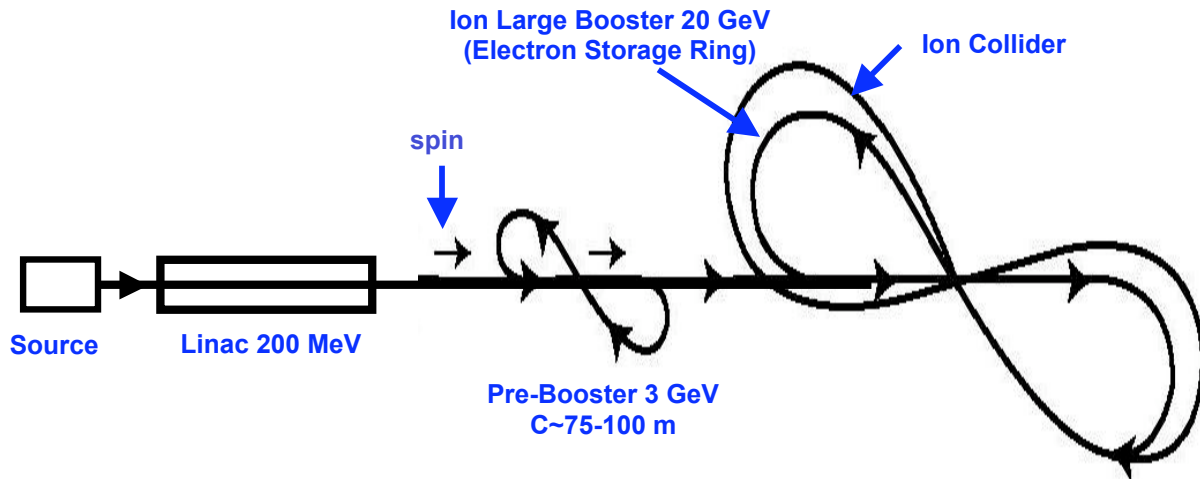


Figure 4.5.1 Schematic drawing of ELIC ion complex

Also, with the purpose to provide accumulation of high current and quality beams (level of 1 A) from *positive ion sources* (polarized  $^3\text{He}$ ,  $^6\text{Li}$  and unpolarized medium and heavy ions), we are envisioning introduction of an *accumulator-cooler ring with 200 KeV DC electron cooling*, to be installed after linac before pre-booster.

Technical design of an advanced SRF *ion linac* has been developed at Argonne National Laboratory by RIA group [ ]. This 50 m as long linac is very effective in acceleration of a wide variety of polarized and unpolarized ions from  $\text{H}^-$  (200 MeV) to  $^{36}\text{Ar}^{17+}$  (100 MeV/u) and can be modified for a reasonable cost increase to accommodate also very heavy ions (completely stripped to the end of acceleration).

After linac, the ions will be injected and accelerated in small booster, or *pre-booster* to reach energy range of a few GeV/u. Polarized proton and deuteron beams can be stacked in pre-booster at injection energy by using the *stripping injection* of negative ions ( $\text{H}^-$  and  $\text{D}^-$ ) accelerated in the linac. As known, the intensity of a stacked beam is limited by the space charge effect. To diminish this limitation, an innovative technique of *beam painting in round mode optics* will be used at stacking. This concept has been developed and is supposed to be simulated and tested in collaboration with the SNS group of ORNL [ ].

Stacking of ions from *positive source* (polarized  $^3\text{He}$ ,  $\text{Li}$  and unpolarized medium and heavy ions stripped in source and in linac) is supposed to be realized in special *accumulator ring* with *non-relativistic electron cooling*. Such method has been successfully used for accumulating of polarized proton beam in Proton Cooler Ring of IUCF [ ]. To approach even higher current at stacking, a similar round mode beam optics technique as mentioned above can be implemented to the ring with electron cooling. After stacking, the positive high current beam will be injected and accelerated in pre-booster.

Next, the *electron collider-storage ring* is supposed to be used as *large* or *main booster* for ion beam, before accumulating the electron or positron beam in the ring (electron and ion beam pipes can be separated in sections with RF stations). This ring has the same circumference as the ion collider ring but a relatively low magnetic field to drive electrons: about 3.5 T warm dipoles for 7 GeV electron

beam. Apparently, the ring is able to accommodate the ion beam after pre-booster for acceleration from a few GeV to 15-30 GeV/u and extraction to the collider ring. It is important, in particular, that maximum ion energy/u in large booster (30 GeV) appears significantly below of its *transition energy* (50 GeV).

### ***Collider ring***

#### ***Basic parameters***

Similar to the electron collider-storage ring (which serves as the large booster for ion beam), the figure 8 ion collider ring will have two  $240^\circ$ ,  $R=100$  M arcs (bend radius 70 M, dipole field 7.5 T for 150 GeV proton beam) connected by two  $60^\circ$  crossing straights each 340 M as long. The straights will be long enough to accommodate 2 interaction regions (including long beam extension sections) with 2 detectors in each, electron cooling, RF and SRF stations and injection-ejection sections. Introduction of 2 easy Siberian snakes to arcs for proton and helium spin control and stabilization will extend the total straight section length by about of 60 m. Additional spin stabilization elements in crossing straights would be the third snake for proton and helium spin and solenoids for deuteron spin. The transition energy of the ring is designed below the minimum injection energy/u (15 GeV/u for deuteron beam).

## **4.2 Polarized light ion sources and heavy ion sources**

#### ***Polarized ion sources [ ]***

##### ***Polarized p and d beams***

Modern state of art of polarized ion sources provides 1mA long pulse 80-90 % nuclei polarized negative hydrogen and deuterium ions [ ].

Claimed future potential of positive and negative polarized hydrogen and deuterium sources: 20-40 mA, 90% polarization, 0.3  $\mu$ M normalized emittance current in pulse [ ].

##### ***Polarized $^3\text{He}$ beam***

There are in development options of polarized *positive helium source*  $^3\text{He}^{++}$ ;

- 1) Optically Pumped Spin Exchange method [ ]
  - Polarization of 50% - 70% expected.
  - $2 \times 10^{11}$  particles/pulse
- 2) Resonant Charge Exchange of Polarized Atoms with  $^4\text{He}^{++}$  [ ]
  - Polarization of 70% - 80%.
  - $> 1\text{mA}$  beam current

##### ***Polarized Li beam***

Existing techniques offer a few hundred nA's of *negative* ions.

The alternate technique such as to be developed polarized helium is able to deliver 1 mA fully stripped  $^6\text{Li}^{+++}$  beam with high polarization.

## Potential H<sup>+</sup>/H<sup>-</sup> Source Parameters

Techniques:

- Atomic Beam Source with Resonant Charge Exchange Ionizer, eg., IUCF/INR CIPIOS with improvements.
- Optically Pumped Polarized Ion Source, eg., BNL OPPIS

Claimed Future Potential\*:

ABS/RX Source:

$$\begin{aligned} \mathbf{H}^- &\sim 10 \text{ mA}, 1.2 \pi \cdot \text{mm} \cdot \text{mrad} (90\%), P_z = 85\% \\ \mathbf{H}^+ &> 20 \text{ mA}, 1.2 \pi \cdot \text{mm} \cdot \text{mrad} (90\%), P_z = 85\% \end{aligned}$$

OPPIS

$$\begin{aligned} \mathbf{H}^- &\sim 40 \text{ mA}, 2.0 \pi \cdot \text{mm} \cdot \text{mrad} (90\%), P_z = 85\% \\ \mathbf{H}^+ &\sim 40 \text{ mA}, 2.0 \pi \cdot \text{mm} \cdot \text{mrad} (90\%), P_z = 85\% \end{aligned}$$

- Estimates are based on projections of existing source parameters. These characteristics seem feasible but must be proven.

## Potential D<sup>+</sup>/D<sup>-</sup> Source Parameters

Techniques:

- Atomic Beam Source with Resonant Charge Exchange Ionizer, eg., IUCF/INR CIPIOS with improvements.
- Optically Pumped Polarized Ion Source, eg., KEK OPPIS

Claimed Future Potential\*:

ABS/RX Source:

$$\begin{aligned} \mathbf{D}^- &\sim 10 \text{ mA}, 1.3 \pi \cdot \text{mm} \cdot \text{mrad} (90\%), P_z = 90\%, P_{zz}=90\% \\ \mathbf{D}^+ &> 20 \text{ mA}, 1.3 \pi \cdot \text{mm} \cdot \text{mrad} (90\%), P_z = 90\%, P_{zz}=90\% \end{aligned}$$

OPPIS

$$\begin{aligned} \mathbf{D}^- &\sim 40 \text{ mA}, 2.0 \pi \cdot \text{mm} \cdot \text{mrad} (90\%), P_z = 55\%, P_{zz}=? \\ \mathbf{D}^+ &> 40 \text{ mA}, 2.0 \pi \cdot \text{mm} \cdot \text{mrad} (90\%), P_z = 55\%, P_{zz}=? \end{aligned}$$

\* Estimates are based on projections of existing source parameters. These characteristics seem feasible but must be proven.

Existing Source Parameters

OPPIS/BNL, H <sup>-</sup> only (In operation)	Pulse Width	500 $\mu\text{s}$ (up to DC?)
	Peak Intensity	>1.6 mA
	Max Pz	85% of nominal
	Emittance (90%)	2.0 $\pi \cdot \text{mm} \cdot \text{mrad}$
IUCF/INR CIPIOS: (Shutdown 8/02)	Pulse Width	Up to 500 $\mu\text{s}$
	Peak Intensity H <sup>-</sup> /D <sup>-</sup>	2.0 mA/2.2 mA
	Max Pz/Pzz	85% to > 90%
	Emittance (90%)	1.2 $\pi \cdot \text{mm} \cdot \text{mrad}$
INR Moscow: (Test Bed Only)	Pulse Width	> 100 $\mu\text{s}$
	Peak Intensity H <sup>+</sup> /H <sup>-</sup>	11 mA/2.5 mA
	Max Pz	80%/85%
	Emittance (90)%	1.0 $\pi \cdot \text{mm} \cdot \text{mrad}$ / 1.8 $\pi \cdot \text{mm} \cdot \text{mrad}$

## Polarized $^3\text{He}^{++}$ Options

### Spin Exchange in Optically Pumped Rb with EBIS Ionizer (Zelenski)

- Polarization of 50% - 70% expected.
- $2 \times 10^{11}$  particles/pulse, small emittance.

### Resonant Charge Exchange of Polarized Atoms with $^4\text{He}^{++}$ (Belov)

- Polarization of 70% - 80%.
- $> 1\text{mA}$  beam current with  $1 \pi\cdot\text{mm}\cdot\text{mrad}$ .

Note: No existing high current polarized  $^3\text{He}^{++}$  source using these techniques exists.

## Polarized $^6\text{Li}^{+++}$ Options

### Existing Technology:

- Create a beam of polarized atoms using ABS.
- Ionize atoms using surface ionization on an 1800 K Tungsten foil – singly charged Li of a few 10's of  $\mu\text{A}$
- Accelerate to 5 keV and transport through a Cs cell to produce negative ions. Results in a few hundred nA's of negative ions.

Investigate alternate processes such as EBIS ionizer proposal or ECR ionizer. Should be possible to get 1 mA? fully stripped beam with high polarization.

Properties of  $^6\text{Li}$ :  $B_c = 8.2 \text{ mT}$ ,  $m/m_N = 0.82205$ ,  $I = 1$

$B_c$  = critical field,  $m/m_N$  = magnetic moment,  $I$  = Nuclear spin

## 4.3 Linear accelerator

Technical design of an advanced *SRF ion linac* has been developed at Argonne National Laboratory by RIA group [ ]. This 50 m long linac is very effective in accelerating a wide variety of polarized and unpolarized ions from  $\text{H}^-$  (200 MeV) to  $^{36}\text{Ar}^{17+}$  (100 MeV/u) and can be modified for a reasonable cost increase to accommodate also very heavy ions (completely stripped to the end of acceleration).

The linac includes room temperature RFQ and interdigital IH structure operating at fixed velocity profile. These two structures are very effective up to  $\sim 4$  MeV/u especially for pulsed machines. At 7.5 MeV/u the argon beam must be stripped to charge state 17+. ECR source can provide charge state 9+ with pulsed current up to several millamps.

After stripping some dog leg system should clean unwanted charge states. Based on the RIA the cost of such linac will be  $\sim \$50\text{M}$ . Should be some difference in the cost due to the pulsed mode of operation – the cryogenic load should be much smaller than for the RIA cavities.

Total length	120 m
Output energy for $^{36}\text{Ar}^{17+}$	95 MeV/u
Output energy for protons (H-minus)	200 MeV/u
Fundamental frequency	115 MHz
Number of 115 MHz QWR (RIA type)	68
$E_{\text{peak}}$	20 MV/m
Voltage	1.58 MV
$\beta_G$	0.15
Number of 345 MHz DSR (RIA type)	63
$E_{\text{peak}}$	20 MV/m
Voltage	2.28 MV
$\beta_G$	0.394

Element	Ar beam charge	Ar beam energy, MeV/u	Proton energy, MeV	Length, m	# of cryostats
115 MHz RFQ	$^{36}\text{Ar}^{9+}$	1.0	1.0	3.0	-
115 MHz Room Temperature IH structure	$^{36}\text{Ar}^{9+}$	4.0	4.0	6.0	-
115 MHz QWR	$^{36}\text{Ar}^{9+}$	7.5	20.7	10.0	2
115 MHz QWR	$^{36}\text{Ar}^{17+}$	40.4	78.3	40.6	7
345 MHz DSR	$^{36}\text{Ar}^{17+}$	94.5	199.8	51.3	9

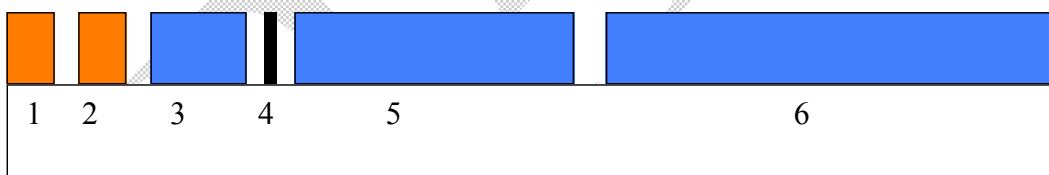


Fig.1. Layout of the linac. 1-RFQ, 2- RT IH structure

3 and 5 - QWR, 115 MHz

4 – stripper for Argon beam,

6 – 345 MHz double-spoke resonators.

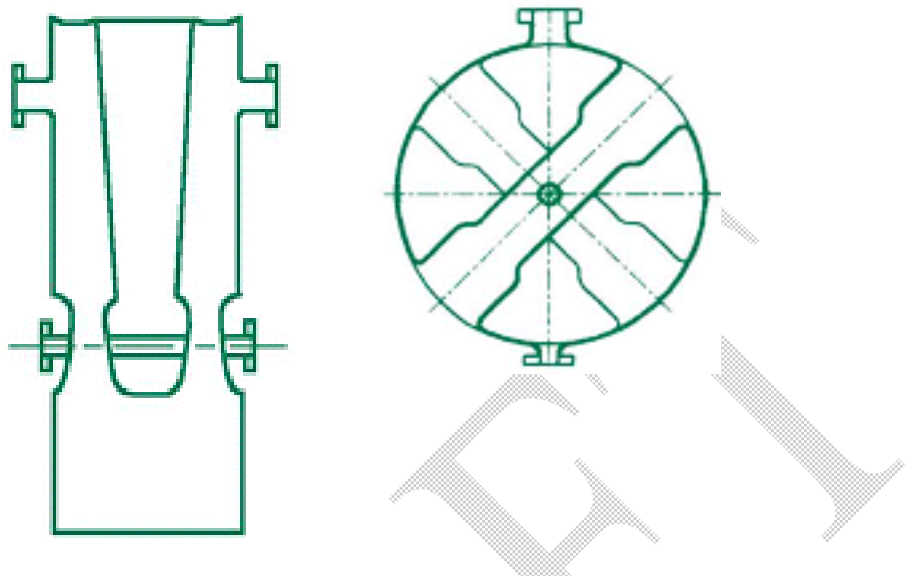


Fig. 2. 115 MHz QWR, beta=0.15 and 2-spoke cavity, 345 MHz, beta=0.4

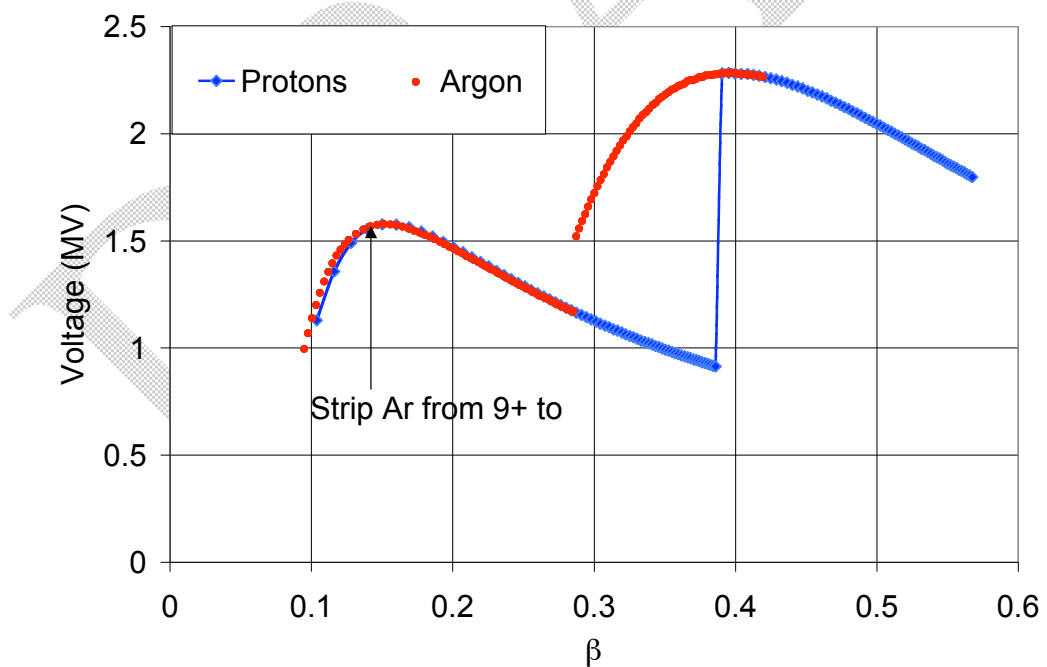


Fig. 3. Voltage gain per resonator as a function of ion velocity.

*Accelerated beam parameters:*

Transverse emittance ( $5\text{-rms}$ )  $\sim 1 \pi \cdot \text{mm} \cdot \text{mrad}$

Longitudinal emittance ( $5\text{-rms}$ )  $< 10 \pi \cdot \text{keV/u} \cdot \text{nsec}$

Momentum spread can be controlled by the rebuncher and can be as low as  $\sim 0.05\%$ .

## 4.4 Pre-booster

The small booster synchrotron, or pre-booster, will be designed to accelerate ion beams after linac to maximum momentum between 2-4 (GeV/c)/u. Before accelerating, the low current beam (1-2 mA polarized beam, 10-30 mA heavy ion beam) accelerated in linac will be stacked to a high (up to 1 A) current. Stacking of negatively charged polarized ions ( $H^-$  and  $D^-$ ) will be performed by use of stripping injection. Stacking of fully stripped positive polarized and unpolarized ions requires use of cooling techniques, namely electron cooling in the accumulator ring installed between linac and pre-booster.

The pre-booster and accumulator-cooling ring designs are under way.

Table of basic parameters of the Small Booster

Parameter	Unit	Value
Circumference	m	150
Arc radius	m	10
Crossing straights length	m	2x34
Maximum momentum	GeV/c	3.7
Transition Lorentz-factor		5
Acceleration time	s	0.1
Injected current	mA	2
Injected pulse duration	ms	0.4
Stacked current	A	1

## 4.5 Stacking ions

### *Stripping injection of beams from negative ion source*

To minimize the space charge impact on transverse emittance, the *circular painting* technique can be used at stacking. Such technique was originally proposed for stacking proton beam in SNS [7]. In this concept, optics of booster ring is designed strong coupled in order to realize circular (rotating) betatron eigen modes of two opposite helicities. During injection, only one of two circular modes is filled with the injected beam. This mode grows in size (emittance) while the other mode is not changed. The beam sizes after stacking, hence, tune shifts for both modes are then determined by the radius of the filled mode. Thus, reduction of tune shift by a factor of  $k$  (at a given accumulated current) will be paid by increase of the 4D emittance by the same factor, but not  $k^2$ .

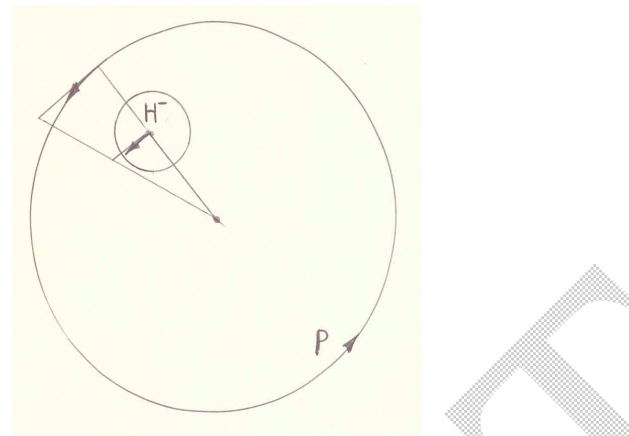


Figure 1 : Circular painting principle: transverse velocity of injected beam is in correlation with vortex of a circular mode at stripping foil

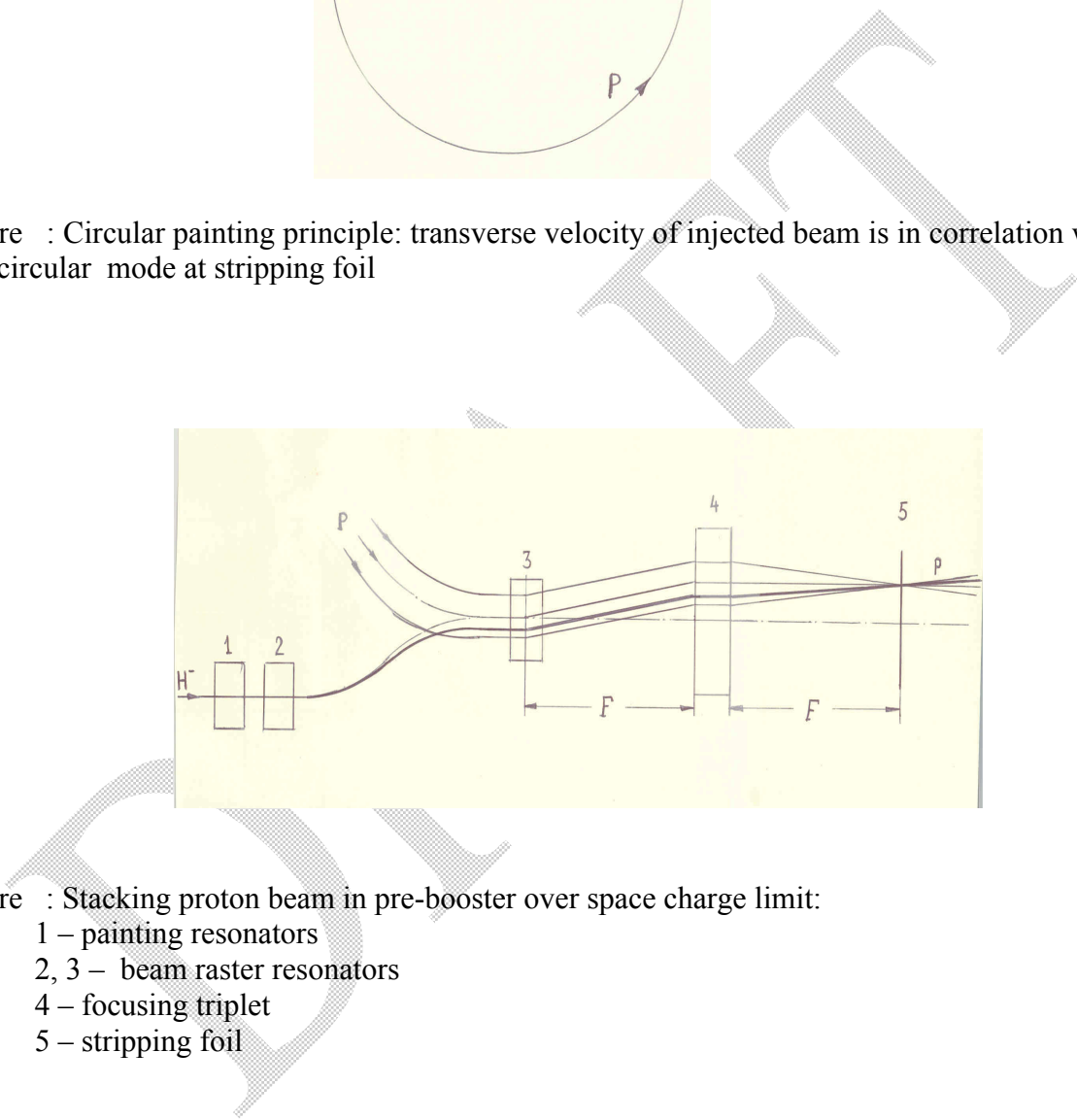


Figure 1 : Stacking proton beam in pre-booster over space charge limit:

- 1 – painting resonators
- 2, 3 – beam raster resonators
- 4 – focusing triplet
- 5 – stripping foil

*This reduction of the 4D emittance growth at stacking 1-3 Amps of light ions is critical for effective use of electron cooling in collider ring.*

Table : Parameters of beam stacking in pre-booster

Stacking parameters	Unit	Value
Beam energy	MeV	200
H- current	mA	2
Transverse emittance in linac	_m	.3
Beta-function at foil	cm	4
Focal parameter	m	1
Beam size at foil before/after stacking	mm	.1/.7
Beam radius in focusing magnet after stacking	cm	2.5
Beam raster radius at foil	cm	1
Increase of foil temperature	oK	<100
Proton beam in pre-booster after stacking		
Accumulated number of protons		2 x10 <sup>12</sup>
Increase of transverse temperature by scattering	%	10
Small/large circular emittance value	_m	.3/15
Regular beam size around the ring	cm	1
Space charge tune shift of a coasting beam		.02

### ***Stacking positive ions by use of Accumulator-cooler ring***

Stacking of positive fully stripped polarized ( ${}^3\text{He}^{++}$ ,  ${}^6\text{Li}^{+++}$ ) and unpolarized ions can be realized in the accumulator-cooler ring (ACR) with electron cooling. A classical system of electron cooling with 100-200 KeV DC electron beam can be used for this purpose. The ion beam of pulse duration about a number of beam revolutions in the ring is injected from linac and experience damping and cooling with characteristic time about .01 s, then next pulse injected and cooled, etc. Accumulation of about 1A ion beam will require about 3-10 s. After that, the beam is injected to the pre-booster for acceleration and injection to the large booster. Characteristic parameters of ACR are shown in Table .

Such method has been successfully used for accumulating of polarized proton beam in Proton Cooler Ring of IUCF [ ]. To approach even higher current while diminishing the space charge impact on beam quality, a similar round mode beam optics technique as mentioned above for stripping injection can be implemented to the ring with electron cooling. After stacking, the positive high current beam will be injected and accelerated in pre-booster.

This ring can be designed as figure 8, as well, though it seems interesting to consider a race-track or a “quadrant” type of design with strong solenoids along straights that can be used to transport electron and ion beam. The solenoids also could be used to stabilize the horizontal spin for all polarized (positive) ion species.

Implementation of the ACR in beam injection system requires a profound simulation efforts and experimental study.

Table . Estimated parameters of the Accumulator-Cooler Ring

Parameter	Unit	Value
Circumference	m	50
Arc radius	m	3
Crossing straights length	m	2 x 15
Energy/u	GeV	.02 -.04
Electron current	A	1
Electron energy	KeV	100-200
Cooling time for protons	ms	10
Stacked ion current	A	1
Large norm.emittance after stacking (required)	μm	16

- Table of basic parameters
- Cooler design advances
- Issues /space charge limitations, ejection//

## 4.6 Large booster

Table of basic parameters

Parameter	Unit	Value
Circumference	m	1560
Arc radius	m	100
Crossing straights length	m	2x360
Injection momentum	GeV/c	3.7
Maximum energy	GeV/c	30
Maximum field	T	1.4
Transition Lorentz-factor		50
Acceleration time	s	0.1
Stacked current	A	1.4
Norm.emittance		

## 4.7 Collider ring

### 4.7.1 General description

Table of basic parameters

Parameter	Unit	Value
Circumference	m	1560
Arc radius	m	100
Crossing straights length	m	2x360

Injection energy	GeV	30
Maximum energy	GeV	150
Transition Lorentz-factor		10
Acceleration time	Min	2
Stacked current	A	1.2
Norm.emittance		

## 4.7.2 Lattice design

**Figure-8 Ion Ring – Minimum Emittance Lattice**

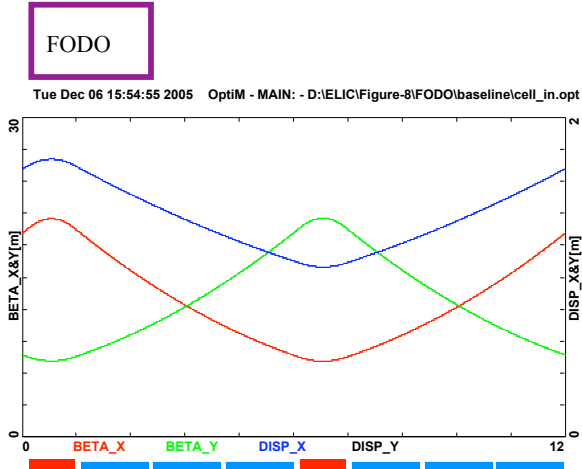
To maintain high polarization of the colliding beams it is advantageous to use a Figure-8 configuration rather than a conventional circular collider ring. In the Figure-8 ring one needs to implement dispersion free straights to accommodate up to four Interaction Regions (IR), while maintaining minimum dispersion in the arcs. Two styles of focusing (FODO and Triplet) were considered as a base for building such a lattice. The FODO structure was chosen based on factor of three weaker quad strengths required for the same betatron phase advance (as for the Triplet) and much better separation of the horizontal and vertical beta functions to facilitate more effective chromaticity control. Here we will design the minimum dispersion optics for the Figure-8 lattice topology based on the 60 deg. FODO structure.

### FODO vs. Triplet Focusing

Both the FODO and Triplet focusing styles are commonly used to build highly periodic lattices. The requirement of uniform focusing throughout the entire ring imposes consistent use of one of the styles for all lattice segments. Specific features (advantages and disadvantages) of these two focusing styles are summarized in Figure 1.

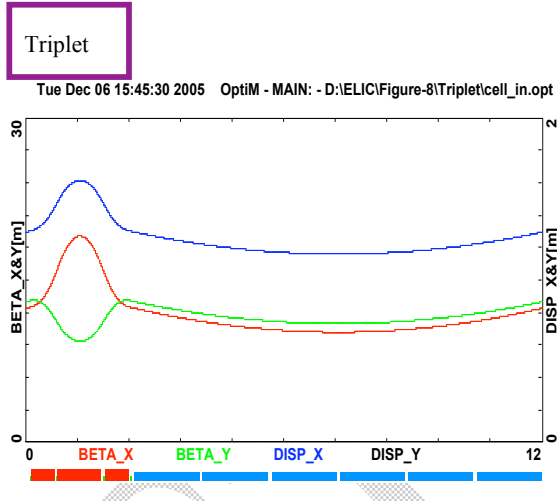
For a high energy collider ring ( $\sim 150$  GeV) the required quadrupole strength may become a limiting factor. Therefore the virtue of FODO focusing (factor of three weaker quads required for the same betatron phase advance per cell) makes this style more feasible. Furthermore, better separation of the horizontal and vertical beta functions in case of the FODO cell facilitates more effective chromaticity correction for the ring. Both advantages, strongly favor the FODO structure as a base for building the collider lattice.

In the next section, we will present a complete lattice design of the Figure-8 ring based on the FODO focusing.



Advantages:

- much weaker quads (~3 times)
- shorter quads (total)
- easier chromaticity correction



Advantages:

- longer straight sections
- smaller vertical beta-function
- uniform variation of betas and disp.

Figure 1 FODO vs. Triplet focusing – Comparison of two periodic cells of the same length and the same phase advance per cell ( $\Delta\phi_x = 60^\circ = \Delta\phi_y$ )

## Figure-8 Ring – Minimum Dispersion Lattice

The natural chromaticity of a high energy collider ring needs to be compensated and controlled through appropriately distributed families of sextupole magnets. Independent control of chromaticities in both the horizontal and vertical planes requires minimum of three families of sextupoles. Their effectiveness in a periodic lattice is highly enhanced by choosing 60 deg. betatron phase advance per cell in both planes [1]. Here we will present linear optics design for the Figure-8 lattice topology based on the previously described 60 deg. FODO cell.

First, one needs to construct the bending ‘loops’ of the Figure-8 ring, so that entire loop is horizontally achromatic and it is naturally matched to individual 60 deg. FODO cells with removed dipoles – the so called ‘empty’ cells. The empty cells will be used to construct the straight sections of the Figure-8 ring. The achromat could be configured as super-period of 6 cells. Starting with zero dispersion and its derivative at the beginning of the achromat the betatron phase will advance by  $2\pi$  (as given by a simple numerology:  $6\pi/3 = 2\pi$ ). This in turn will create a periodic dispersion wave across the achromat (zero dispersion and its derivative at the achromat end). The resulting achromat super-period is illustrated in Figure 2.

Thu Dec 21 22:39:09 2006 Optim - MAIN: - D:\ELIC\Figure-8\FODO\baseline\spr1\_in.opt

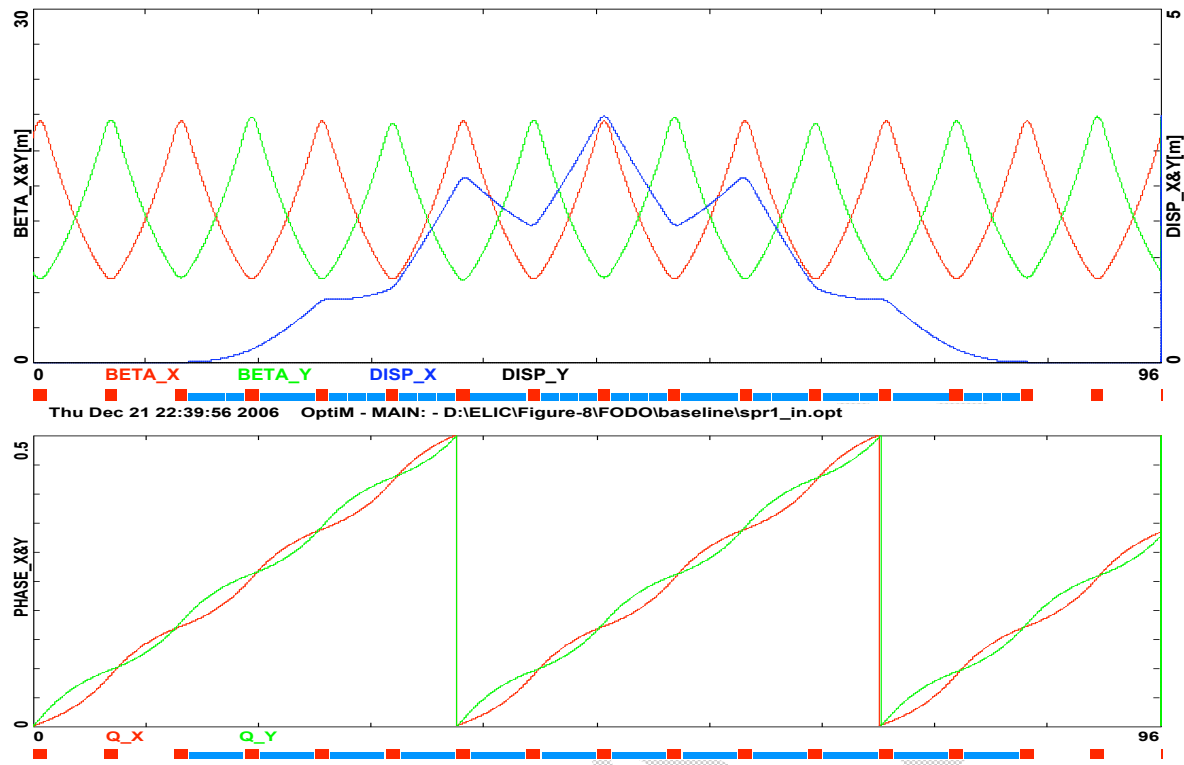


Figure 2 Achromat super-period – Twiss functions (top) and betatron phase advance in units of  $2\pi$  (bottom)

In principle, one could build the entire arc as a sequence of the above achromat superperiods, which are inherently matched to the straight sections (sequence of empty cells). However, his solution would end up with rather large average dispersion and large momentum compaction. One may observe that the minimum dispersion is reached for a periodic solution as illustrated in Figure 1. Therefore, to minimize the average dispersion in the ring it would be beneficial to build the Figure-8 bends out of periodic FODO cells and then suppress the dispersion at the transitions to the straight sections. This can be accomplished by removing specific dipoles from the transition cells. The process of dispersion suppression based on pure geometry is illustrated in a sequence of lattices with removed dipoles (evolutionary pattern) as shown in Figure 3.

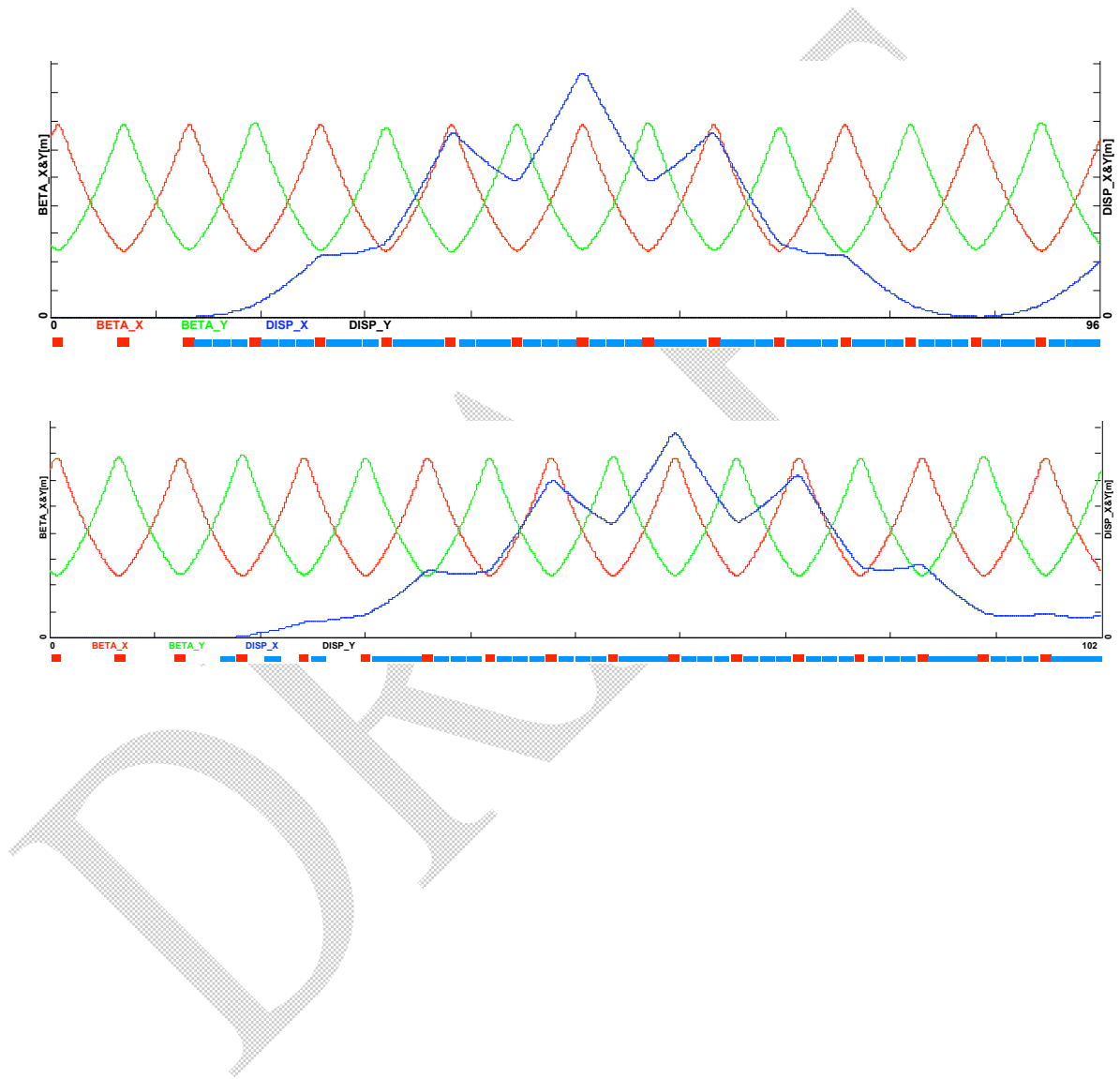


Figure 3 Minimizing the average dispersion in the ring by removing specific dipoles from the transition cells.

The bottom picture in Figure 3 illustrates the desired minimum dispersion solution for the Figure-8 loop. One can see the unperturbed periodicity of the beta functions across the dispersion suppression region, which makes this solution even more attractive.

The overall optics for one half of the Figure-8 ring (where 240 deg. bend is closed by 24 periodic FODO cells) is illustrated in Figure 4. Its geometric layout is depicted in Figure 5.

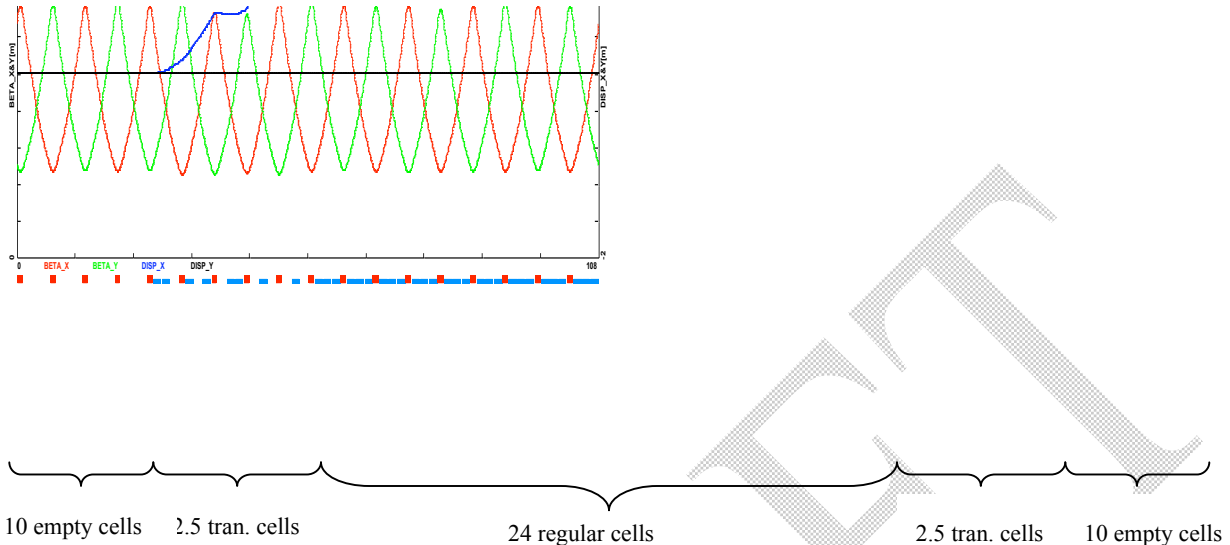


Figure 4 Linear optics at 150 GeV for one half of the Figure-8 ring with 60 deg. crossing.

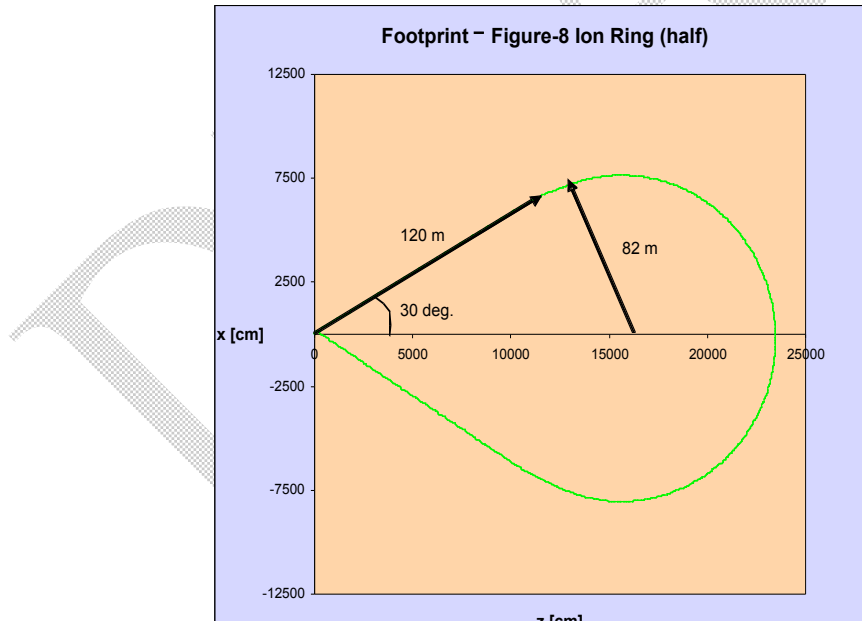


Figure 5 Layout of one half of the Figure-8 ring with 60 deg. crossing.

The long dispersion free straights (2\_120 m each) will accommodate as many as four interaction regions (IR). The FODO structure of the straights is quite flexible to ‘launch’ matching inserts around the IRs.

## Summary

To maintain high polarization of the colliding beams it is advantageous to use a Figure-8 configuration rather than a conventional circular collider ring. In the Figure-8 ring one needs to implement dispersion free straights to accommodate the Interaction Regions (IR), while maintaining minimum dispersion in the arcs. Two styles of focusing (FODO and Triplet) were considered as a base for building such lattice. The FODO structure was chosen based on factor of three weaker quad strengths required for the same betatron phase advance (as for the Triplet) and much better separation of the horizontal and vertical beta functions to facilitate more effective chromaticity control. To minimize the average dispersion in the ring it is beneficial to build the Figure-8 bends out of periodic FODO cells and then suppress the dispersion at the transitions to the straight sections. This was accomplished by removing specific dipoles from the transition cells making the dispersion suppression purely geometrical.

Complete lattice design at 150 GeV for the Figure-8 collider topology based on the 60 deg. FODO structure was presented. The key parameters of the Figure-8 ring, computed via OptiM [2], are summarized in the Table below [2]:

Figure-8 Ion Ring – Small Dispersion Lattice	
circumference, C [m]	1200
arc bending radius, R [m]	82
dipole bending radius, $\rho$ [m]	59
Average betas ( $h/v$ ) [m]	12.5/12.5
Average dispersion, $D_x$ [cm]	168
betatron tunes ( $h/v$ )	16.69/16.69
chromaticities ( $h/v$ )	-17.85/-18.01
[cm]	1420
momentum compaction, $\alpha = M_{56}/C$	$1.2 \cdot 10^{-2}$
transition gamma,	9

## References

1. Andrew Hutton, private communication
2. <http://www-bdnew.fnal.gov/pbar/organizationalchart/lebedev/OptiM/optim.htm>

### 4.7.3 The beam clocking

Synchronization between electron and ion bunches is a common constraint of EIC design. It condition is expressed by a relationship,  $f = q_e f_e = q_i f_i$ , between RF frequency  $f$  and revolution frequencies  $f_e = v_e/C_e$ ,  $f_i = v_i/C_i$ , where  $v_e$ ,  $v_i$  and  $C_e$ ,  $C_i$  are the beam velocities and orbit circumferences respectively,  $q_e$  and  $q_i$  are integers. The constraint is due to the ion velocity change by a factor of about  $10^{-3}$  in the energy range of an EIC. It would be very difficult to compensate the related change of ion beam revolution frequency by changing of the ion orbit length with energy. In the ELIC design

where the ion beams are driven by RF of very high  $q_i$  (about 7500 at  $f = 1.5$  GHz), a possible solution consists of varying the integer  $q_i$  yet admitting “residual” change of ion path length in arcs up to one bunch spacing (about 20 cm, corresponding to  $\pm 12$  mm orbit displacement in the arcs). Ion acceleration in the collider ring can be performed using warm resonators of changeable frequency, after that one can switch (via beam re-bunching) to high voltage superconducting resonators.

## 4.8 Cooling of ion beam in collider ring

### *Staged cooling*

Electron cooling time grows with beam energy in the first or second power and with normalized beam emittances - the third power. Therefore, it seems critically important to organize the cooling process in collider ring in two stages: cool the ion beam initially at injection energy (see Table 5, same electron current is assumed as in Table 3) after stacking it in collider ring (in parallel or after re-bunching), and continue the cooling during and after acceleration to a high energy. Note, that the staged cooling appears as a natural possibility with the ERL-based EC. The electron beam area could be then varied with time in an optimum way to minimize the time of beam shrinkage to equilibrium and maximize the lifetime as above discussed.

Table 4 ERL-based EC with circulator ring

Parameter	Unit	Value
Max/min energy of e-beam	MeV	75/10
Electrons/bunch	$10^{10}$	1
Number of bunch revolutions in CR	100	1
Current in CR/current in ERL	A	2.5/0.025
Bunch rep. rate in CR	GHz	1.5
CR circumference	M	60
Cooling section length	M	15
Circulation duration	$\mu$ s	20
Bunch length	Cm	1
Energy spread	$10^{-4}$	3-5
Solenoid field in cooling section	T	2
Beam radius in solenoid	mm	1
Cyclotron beta-function	M	0.6
Thermal cyclotron radius	$\mu$ m	2
Beam radius at cathode	mm	3
Solenoid field at cathode	KG	2
Laslett's tune shift in CR at 10 MeV		0.03
Time of longitudinal inter/intrabeam heating	$\mu$ s	200

Table 5: Initial electron cooling (p/e)

Parameter	Unit	Value
Energy	GeV/MeV	20/10

Cooling length/ circumference	%	1
Particles/bunch	$10^{10}$	0.2/1
Energy spread*	$10^{-4}$	3/1
Bunch length*	cm	20/3
Proton emittance, norm*	$\mu\text{m}$	4
Cooling time	min	10
Equilibrium emittance, **	$\mu\text{m}$	1
Equilibrium bunch length**	cm	2
Laslett's tune shift		0.1

\* max.amplitude

\*\* norm.,rms

## 4.9 Transport and manipulation of ion spin

Proton polarization could be realized by mean of dipole Siberian Snakes and spin rotators in collider ring and techniques of adiabatic overcoming depolarizing spin resonances in booster. The adiabatic techniques also could be used in order to preserve the polarization of light ions at acceleration and obtain the longitudinal spin in narrow energy regions near the integer or half-integer (RF introduced) spin resonances.

An alternative to these techniques might be the twisted spin, or figure 8 EIC (Fig.6 and 7), with basic features as follows: spin precession in vertical field is compensated, i.e. the fundamental spin tune is zero; intrinsic spin resonances stay away; there is no crossing spin resonances. Using the degeneration of spin motion on ideal plane orbit, one can easily control spin direction (including flipping the spin) for all particle species at all energies in booster and collider ring by introducing solenoids in straights or horizontal dipoles along the arcs. Spin rotators around the interaction points would not be needed. Compact full snakes with longitudinal axis of spin rotation can be introduced in order to stabilize the proton spin. Twisted orbit also can be used for electron circulator-collider; after all, the circulator (arcs) could also be used as booster for ion beam.

### Spin In Figure 8 Synchrotrons

In twisted rings the spin precession in one arc is cancelled by the reverse precession in the opposite arc, thus, the global spin tune does not change with energy being simply equal to zero. Spin motion on a plane twisted orbit is degenerated, i.e. unstable, but it is easily stabilized by a solenoid introduced in one of two intersecting straights of the orbit, then the spin tune is determined by the spin rotation in solenoid, and the longitudinal polarization in this straight appears the stable one. Spin rotation by solenoid must frequently exceed the spin deviation by the imperfection fields related to orbit excursions. The imperfection effect is proportional to the particle anomalous gyro-magnetic factor, g-2, therefore, spin control by solenoid is especially effective for particles with small g-2 value (d, He<sup>3</sup>). Such stabilization is similar in principle to Partial Siberian Snake used successfully at AGS to prevent proton beam depolarization due to crossing the imperfection spin resonances at acceleration [3]. At high energies, when the anomalous spin precession in arcs becomes large, the horizontal spin can be effectively stabilized by transverse magnetic fields associated with vertical excursions of the closed

orbit [1]. The intrinsic spin resonances, i.e. resonances between spin precession in vertical field and particle oscillation in focusing quadrupoles, stay away in twisted rings. Thus, the issue of preventing the depolarization due to the intrinsic spin resonances, that challenges operating the proton booster and light ion collider rings [3], disappears in the twisting design. Spin tune spread and high order spin resonances [4,5], or “snake resonances” [3], will be diminished with emittance decrease by electron cooling.

### **Spin steering**

*Transverse spin* for experiments on CP violation can be obtained (after beam acceleration to energy of the experiment) turning the stable spin in horizontal plane from longitudinal direction by adiabatic ramp of a few or several horizontal dipoles distributed in a proper way around the twisted ring. The strength of stabilizing solenoid or longitudinal snake then should slow down to zero or other optimum value. Here, one has to account for the related orbit excursions. Steering technique also could be used in order to switch the stable spin, either longitudinal or transverse, between two intersecting straights with 4 experiments being hold in total.

### **Proton beam in twisted ring with longitudinal snakes in arcs**

Two full longitudinal snakes installed at the middle of arcs will allow for arrangement of 4 simultaneously operated collision points all with the longitudinal or transverse polarization of proton beam stabilized in a way as above discussed. Note, that the helical longitudinal snakes are compact [6]: one snake would occupy a space not longer than 3 m.

### **Flipping the ion spin**

Besides the possibilities to alternate the ion polarization over beam pulses from source [7] or to develop and apply an RF-induced flipping technique established for low energy beams [8], one may consider the possibility to use the above described steering technique for periodical reverse of stable ion spin. An additional possibility for each turn flipping transverse proton spin might be the *RF trapped flipping spin* technique [9]. It could work in cooperation with the full longitudinal snake that has to be introduced to one of two intersecting straights of twisted ring in order to make the spin tune in the ring equal to  $\pm$ .

## **4.10 Collective effects and beam stability**

### **4.10.1**

There exist various collective modes which can become unstable for the beam in an ion storage ring which is currently being considered in our ELIC design. We have studied major beam stability problems most likely to affect beam in ELIC’s highest energy ion ring. In the following we summarize results for proton beam to be more specific.

#### **Longitudinal Microwave Instability Threshold:**

$$I_p = \frac{2\pi|\eta| \left( \frac{E}{e} \right) \beta^2 \sigma_\delta^2}{\left| \frac{Z}{n} \right|_{eff}} - \left| \frac{Z}{n} \right|_{eff} = 133\Omega$$

**Tune Spread due to Nonlinear RF Bucket:**

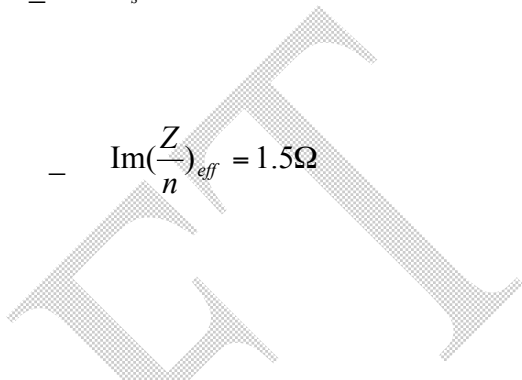
$$\Delta\nu_s = \frac{1}{8} \left( \frac{\sigma_z}{R} \right)^2 h_{rf}^2 \nu_s - \Delta\nu_s = 1.8 \times 10^{-4}$$

**Longitudinal Coupled Bunch Instability:**

$$I_p = \frac{\pi|\eta|^3 \left( \frac{E}{e} \right) h_{rf}^2 \beta^2 \sigma_\delta^4}{4 \operatorname{Im} \left( \frac{Z}{n} \right)_{eff} \nu_s^2} - \operatorname{Im} \left( \frac{Z}{n} \right)_{eff} = 1.5\Omega$$

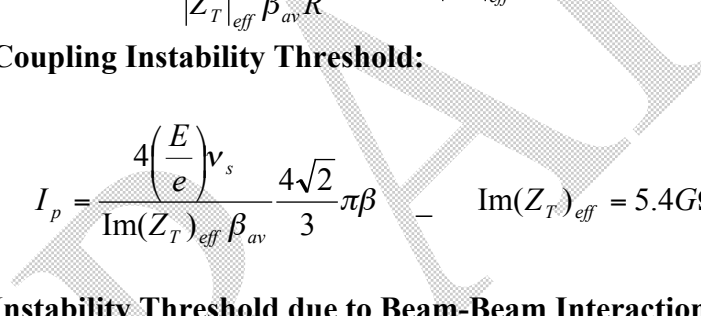
**Transverse Microwave Instability Threshold:**

$$I_b = \frac{4 \left( \frac{E}{e} \right) \nu_s b}{\left| Z_T \right|_{eff} \beta_{av} R} - \left| Z_T \right|_{eff} = 2.5G\Omega/m$$



**Transverse Mode Coupling Instability Threshold:**

$$I_p = \frac{4 \left( \frac{E}{e} \right) \nu_s}{\operatorname{Im} \left( Z_T \right)_{eff} \beta_{av}} - \frac{4\sqrt{2}}{3} \pi \beta - \operatorname{Im} \left( Z_T \right)_{eff} = 5.4G\Omega/m$$



**Strong Head-Tail Instability Threshold due to Beam-Beam Interaction:**

$$\xi_e \xi_p \leq \frac{\beta_e \nu_s}{\pi^2 \sigma_z} - \text{Safe}$$

**Head-Tail Instability Growth Rate due to Beam-Beam Interaction:**

$$\tau^{-1} = \frac{f_{rev} D_e D_p \sigma_{pz}}{16 \sigma_{ez}} - \tau = 195(12)\mu s \quad \text{About 50(3) turns - a big problem!}$$

**Intrabeam Scattering Growth Rates:**

( $\log_c = 10$  is assumed)

$$\tau_s^{-1} = \frac{e^4 N_p \log_c}{8m_p^2 c^3 \beta^3 \gamma^3 \sigma_z \varepsilon_x^{3/2} \sigma_\delta^2} \sqrt{\frac{\nu_x}{R}} - \tau_s = 180s$$

$$\tau_x^{-1} = \frac{e^4 N_p \log_c}{16m_p^2 c^3 \beta^3 \gamma^3 \sigma_z \varepsilon_x^{5/2}} \sqrt{\frac{R}{\nu_x}} \left( \frac{2}{\nu_x^2} - \frac{1}{\gamma^2} \right) - \tau_x = 2.3s \quad (\text{what does this mean?})$$

**Electron Cooling Times:**

( $\log_c = 2$  and  $\gamma = 0.01$  is assumed)

$$\tau_s = \frac{3m_p m_e c^3 \beta^3 \gamma^5}{16\pi n_e e^4 \eta \log_c} \left( 2\sigma_x^2 + 0.66 \left( \frac{\sigma_\delta^2}{\gamma^2} \right) + 1.6\sigma_{ex}^2 \right) \sqrt{\left( \frac{\sigma_\delta^2}{\gamma^2} \right) + 2.4\sigma_{ex}^2}$$

This is basically same as Derbenev's expression

$$\tau_s = \frac{8\gamma\Gamma}{r_p r_c N_e \eta \log_c} \frac{S_e}{S_{ion}} - N_e^{critical} = 6.7 \times 10^9 \text{ (assuming } \underline{\gamma} = 0.01 \text{ and } S_e/S_{ion} = 10)$$

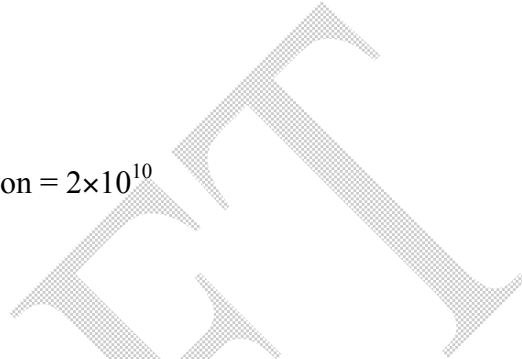
### Synchrotron Radiation:

*For Proton in Storage*

$P_s = 19 \text{ mW for } B = 5 \text{ Tesla } \underline{\gamma} \text{ negligible}$

Number of emitted photons per bunch per revolution =  $2 \times 10^{10}$

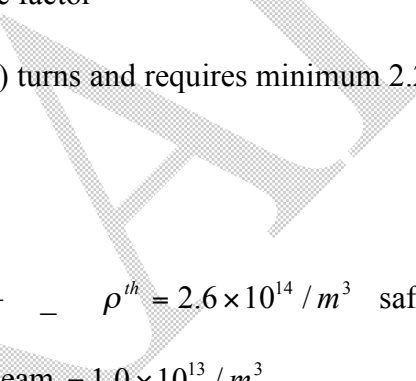
Mean energy of photons = 5 meV



*For Electron in Circulator Ring*

$P_s = 5.1 \text{ MW for } B = 2.34 \text{ kG } \underline{\gamma} \text{ a huge factor}$

Electron beam damps after 13000 (3500?) turns and requires minimum 2.2 MV just to keep electrons in the ring with no phase focusing at all.



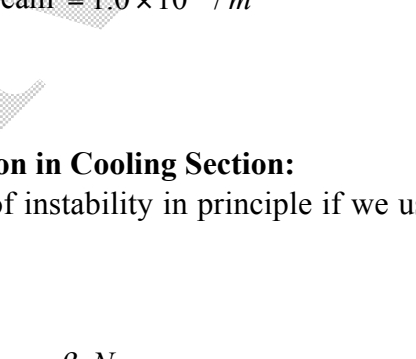
### Electron Cloud Instability:

Single bunch head-tail instability

$$\rho^{th} = \frac{\gamma Q_s}{\pi^2 r_p R \beta_{av}} - \rho^{th} = 2.6 \times 10^{14} / m^3 \text{ safe}$$

Average volume density of ELIC proton beam =  $1.0 \times 10^{13} / m^3$

Coupled bunch instability



### Instability due to Beam-Beam Interaction in Cooling Section:

Is this a problem? There is a possibility of instability in principle if we use a circulator ring concept for cooler.

### Incoherent Space Charge Tune Shift:

$$\Delta Q_y^L = \frac{r_p R}{\sqrt{2\pi} \beta \gamma_p^3} \frac{\beta_y N_B}{\sigma_y (\sigma_x + \sigma_y) \sigma_z} - \Delta Q_y^L = 0.017$$

We conclude that energy recovering linear collider has a potential for making high energy experiments demanding an extremely large luminosity possible.

### Appendix

A consistent set of ELIC design machine and beam parameters is presented in the Table below.

<b>A List of ELIC Parameters as of 2/23/04</b>	
$\gamma_p / \gamma_e$	160/13700
$\sigma_\delta \equiv \Delta\gamma / \gamma$	$3 \times 10^{-4}$ (relative energy spread)
$\varepsilon_{nx}^p / \varepsilon_{nx}^e$	1/86 $\mu\text{m}$ (normalized horizontal emittance)
$\varepsilon_{ny}^p / \varepsilon_{ny}^e$	0.01/0.86 $\mu\text{m}$ (normalized vertical emittance)
$\sigma_z^p / \sigma_z^e$	5/1 mm (bunch length)
$N_p / N_e$	$2 \times 10^9 / 10^{10}$
$\beta^*$	5 mm (beta at interaction point)
$\sigma_y^*$	0.56 $\mu\text{m}$ (vertical beam size at interaction point)
R	191 m (mean radius of ring)
$\nu_x, \nu_y$	15 (betatron tunes)
$\beta_{av}$	12.7 m (average beta in ring)
$\sigma_y$	$2.82 \times 10^{-5}$ m
$\theta_y$	$2.22 \times 10^{-6}$
$I_b$	0.08 mA (bunch current)
$I_p$	3.1 A (bunch peak current)
$I_{av}$	480 mA
M	6000 (number of bunches)
U	300 kJ (stored beam energy)
$V_{rf}$	$1.0 \times 10^8$ V
$h_{rf}$	6000 (harmonic number)
$f_{rev}$	0.25 MHz
$\eta$	$4 \times 10^{-3}$ (frequency slip parameter)
$\nu_s$	0.06 (synchrotron tune)
b	1.74 cm (beam pipe radius)
$c / 2\pi b$	2.75 GHz
$\xi_{ex} / \xi_{ey}$	0.0095/0.095 (tune shift per interaction)
$\xi_{px} / \xi_{py}$	0.0022/0.022 (tune shift per interaction)
$D_{ex} / D_{ey}$	0.12/1.2 (disruption per interaction)
$D_{px} / D_{py}$	0.0055/0.055 (disruption per interaction)
$r_e$	$2.818 \times 10^{-15}$ m
$r_p$	$1.535 \times 10^{-18}$ m (proton radius)

#### 4.10.2 SRF FOR BUNCHING ION BEAM

The proton ring will require the installation of a bunching system capable to providing 100 MV of voltage at 1.5 GHz, 90° out of phase with respect to a circulating beam current of 1 A. This

voltage could be provided by 5 m of superconducting cavities operating at 20 MV/m. The power dissipation at 2 K in those cavities would be about 200 W, assuming an R/Q per unit length of 1000  $\Omega/\text{m}$  and a  $Q_0$  of  $10^{10}$ . These assumptions are consistent with the design parameters of the JLab 12 GeV upgrade. Ideal optimization of the rf parameters (detuning  $\delta$  and coupling coefficient  $\kappa$ ) would occur at  $\delta = 2.5 \cdot 10^5$  and  $\kappa = 1$ , at which point only 200 W would need to be provided by the RF source. Larger amount of RF power would be needed to provide stabilization with respect to fluctuations in the time of arrival of the beam. For example, for the system to be stable with respect to fluctuations of the order of  $10^{-2}$  rad, then the RF source for the bunching cavities must be able to provide 1 MW.

## 4.11 ELECTRON CLOUD SIMULATIONS FOR ELIC

### ***Introduction***

Electron clouds are a performance limitation for high intensity beams with positive charge [1]. In hadron beams electron clouds can lead to vacuum pressure rise, instabilities, tune shifts, and incoherent emittance growth. In RHIC, dynamic pressure rises were the dominant electron cloud effect in the past. The large-scale installation of NEG coated beam pipes in the warm regions, and pre-pumping of the cold regions before cool-down have now largely eliminated these pressure rises [2]. Electron clouds have also been shown to reduce the stability threshold during transition crossing [3], and are likely to increase the transverse emittance of short proton bunches at injection [4].

Figure 1 shows the bunch intensity and bunch spacing of existing machines, and the planned electron-ion colliders ELIC and eRHIC. Generally, the electron cloud density is high for parameters in the lower right corner of the plot, and low for parameters in the upper left corner. With respect to electron clouds, ELIC and eRHIC operate in different parameter regimes. In ELIC, proton bunches of moderate intensity have a very small spacing. In RHIC and eRHIC, high intensity proton bunches have a relatively large spacing.

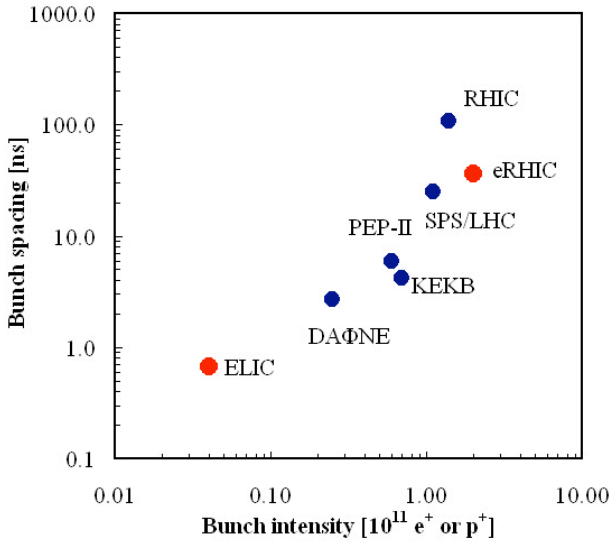


Figure 1: Bunch intensity and bunch spacing for existing machines, and the planned electron-ion colliders ELIC and eRHIC.

We use the code CSEC to simulate the electron cloud formation in ELIC [5]. CSEC can simulate cylindrically symmetric geometries without external magnetic fields. Because of the restriction to these cases, the code runs faster than the codes ECLOUD [6] and POSINST [7], which can treat more general cases including external magnetic fields. The fast turn around of CSEC is especially useful in parameter scans.

## ***simulation PARAMETERS***

We simulate the electron cloud built-up for proton beams only. Other ion beams will create the same electron cloud as protons, provided the charge per bunch is the same. We consider two cases: (1) a bunch intensity of  $0.4 \times 10^9$  and a bunch spacing of 0.67 ns, and (2) a bunch intensity of  $1.2 \times 10^9$  and a bunch spacing of 2.0 ns. The longer bunch spacing may be necessary due to detector technology limitations. For the longer bunch spacing we increased the bunch intensity to recover the lost luminosity.

For the surface parameters we consider stainless steel with a maximum secondary electron yield (SEY) up to  $\delta_{\max} = 2.5$ . Only untreated and unconditioned stainless steel surfaces would have such a large SEY. Beryllium, if not coated by a NEG layer, can have a  $\delta_{\max}$  larger than 2.5 [7]. Of the surface parameters, the electron cloud density is most sensitive to the maximum secondary electron yield  $\delta_{\max}$ , and the probability for the electron reflectivity at small energies  $P_0$ .

Table 1: Proton beam parameters in electron cloud simulation. See Refs. [5,8] for explanations of the electron generation and surface parameters.

Parameter	Unit	Value
<b>Bunch spacing, <math>t_b</math></b>	ns	<b>0.67, 2.0</b>
Beam offset	mm	0
Rms beam radius	mm	1.0
Pipe radius	mm	65
Electrons generated per bunch	...	100
Electron generation radius	mm	1.0
Rms bunch length	ns	0.1
Bunch shape parameter $n$	...	3
<b>Bunch intensity <math>N_b</math></b>	<b><math>10^9</math></b>	<b>4.0, 12.0</b>
Bunch charge	nC	0.64
Longitudinal slices	...	5000
Macroparticles, initially	...	2500
Smoothing length, $d$	mm	0.1
Electron line density $\lambda_{ce}$ , initial	pC/m	1.6
Reflection probability for small $E$ , $P_0$	...	0.4
Reflection probability for large $E$ , $P_\infty$	...	0.4
Exp. decay const. for reflection, $E_{\text{reflect}}$	eV	50
Probability of rediffusion, $P_{\text{rediffuse}}$	...	0.5
<b>Maximum SEY, <math>\delta_{\max}</math></b>	...	<b><math>\leq 2.5</math></b>
Energy at which SEY peaks, $E_{\max}$	eV	310
Half height, energy distrib., $E_{\text{secondary}}$	eV	8.9

Energy distribution parameter, $\alpha_\delta$	...	1.0
Angular distribution parameter, $\alpha_\theta$	...	1.0

All simulation parameters are listed in Table 1. The electron generation and surface parameters are explained in Refs. [5,8]. In Ref. [8] the sensitivity of the electron cloud with respect to all input parameters was tested for a RHIC case.

## results

For the beam and surface parameters listed above, and for both cases, no electron cloud formation is observed in the simulation. With the short bunch spacing in ELIC, the cloud formation is suppressed. The hadron beam is effectively a coasting beam.

With coasting beams, no electron clouds are created through multipacting but other problems can occur. Electrons are generated through rest gas ionization and beam loss. These electrons can accumulate in the hadron beam and lead to instabilities. Gaps in the hadron beam or clearing electrons may be needed to reduce the electron accumulation [10,11].

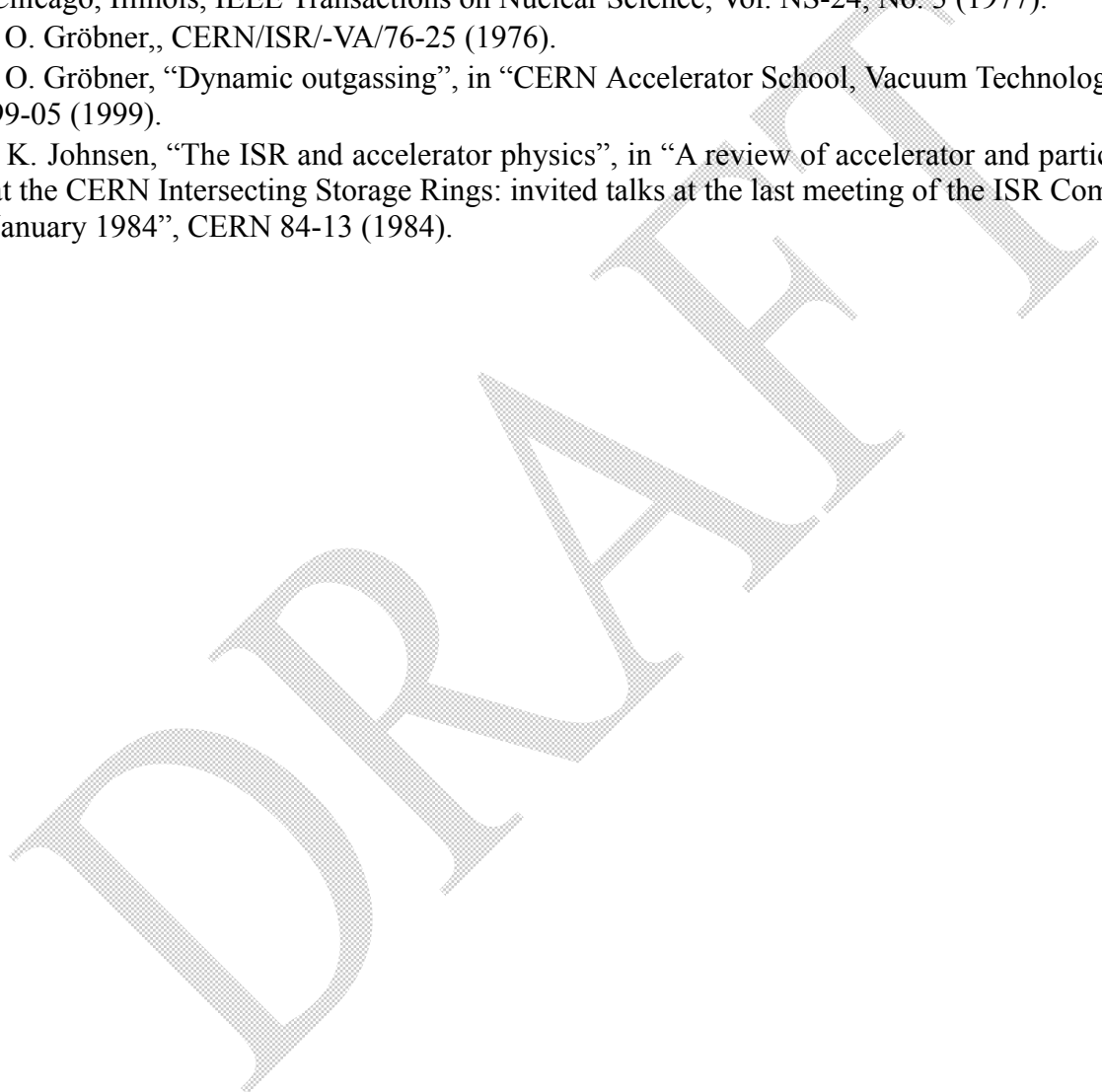
Coasting beams can also create pressure instabilities. In this case positive ions are created through rest gas ionization, and then accelerated in the beam potential. Upon hitting the beam pipe wall, desorb molecules. The newly released molecules can then be ionized, and so on. Such a pressure instability had been observed in the ISR [12,13].

With an anticipated current of about 1 A in ELIC, these coasting beam problems are likely to be manageable. The ISR had stored proton beams up to a current of 57 A [14].

## References

- [1] M. Furman, S. Henderson, and F. Zimmermann (editors), “Proceeding of ECLOUD’04”, Napa, California, CERN-2005-001, ISSN 0007-8328, ISBN 92-9083-241-X, LBNL-56372, CARE-Conf-04-010-HHH, SNS-104000000-TR0024-R00, BNL-72451-2004-CP (2004, 2005).
- [2] S.Y. Zhang, M. Bai, M. Blaskiewicz, P. Cameron, A. Drees, W. Fischer, D. Gassner, J. Gullotta, P. He, H.C. Hseuh, H. Huang, U. Iriso-Ariz, R. Lee, W.W. MacKay, B. Oerter, V. Ptitsyn, V. Ponnaiyan, T. Roser, T. Satogata, L. Smart, D. Trbojevic, and K. Zeno, “RHIC pressure rise and electron cloud”, proceedings of the 2003 Particle Accelerator Conference, Portland, Oregon (2003).
- [3] J. Wei, U. Iriso, M. Bai, M. Blaskiewicz, P. Cameron, R. Connolly, A. DellaPenna, W. Fischer, H. Huang, R. Lee, R. Michnoff, V. Ptitsyn, T. Roser, T. Satogata, S. Tepikian, L. Wang, S.Y. Zhang, “Observation of electron-ion effects at RHIC transition”, proceedings of the 2005 Particle Accelerator Conference, Knoxville, Tennessee (2005).
- [4] S.Y. Zhang and V. Ptitsyn, “Proton beam emittance growth in Run-5 and Run-6”, BNL C-AD/AP/257 (2006).
- [5] M. Blaskiewicz and U. Iriso, “How to use CSEC”, BNL C-A/AP/260 (2006).
- [6] G. Rumolo and F. Zimmermann, “Practical user guide for ECLOUD”, CERN-SL-Note-2002-016 (AP) (2003).
- [7] M.A Furman and M.T.F. Pivi, “Probabilistic model for the simulation of secondary electron emission”, Phys. Rev. ST Accel. Beams 5, 124404 (2002).

- [8] G. Rumolo and W. Fischer, "Observations on background in PHOBOS and related electron cloud simulations", BNL C-A/AP/146 (2004).
- [9] W. Fischer, J.M. Brennan, M. Blaskiewicz, and T. Satogata, "Electron cloud measurements and simulations for the Brookhaven Relativistic Heavy Ion Collider", Phys. Rev. ST Accel. Beams 5, 124401 (2005).
- [10] H.G. Hereward, "Coherent instability due to electrons in a coasting proton beam", CERN report 71-15 (1971).
- [11] O. Gröbner and P. Strubin, "ISR clearing current monitor system", proceedings of PAC77, Chicago, Illinois, IEEE Transactions on Nuclear Science, Vol. NS-24, No. 3 (1977).
- [12] O. Gröbner, CERN/ISR/-VA/76-25 (1976).
- [13] O. Gröbner, "Dynamic outgassing", in "CERN Accelerator School, Vacuum Technology", CERN 99-05 (1999).
- [14] K. Johnsen, "The ISR and accelerator physics", in "A review of accelerator and particle physics at the CERN Intersecting Storage Rings: invited talks at the last meeting of the ISR Committee, 27 January 1984", CERN 84-13 (1984).



# Chapter V Electron cooling for colliding beams

## Contents

- 5.1 *Introduction: EC principles and physics*
- 5.2 *Basic parameters and general concept of HEEC for EIC*
- 5.3 *ERL for HEEC*
- 5.4 *HEEC with circulator ring*
- 5.5 *Beam transport for HEEC*
  - 5.5.1 *DC gun with discontinuous solenoid*
  - 5.5.2 *Space charge dominated beam from SRF gun*
- 5.6 *Dispersive cooling*
- 5.7 *Flat beams cooling*

## References

## 5.1 Method of electron cooling (EC)

EC of heavy particle beams in synchrotrons was invented by G. Budker in 1966 [ ] and incepted in the accelerator physics and technology in 1974 [ ]. In this method, an electron beam accompanying a hadron (proton, antiproton) beam along straight section of the synchrotron, serves like a thermostat for hadron beam via collisions between electron and hadron particles. Today, EC is widely used in low energy storage rings to produce the high quality hadron beams for research and applications. Implementation of EC in projects of luminosity upgrade at high energy colliders was detained long years by the absence of an appropriate accelerating and transporting technique for the electron beam. The situation changed in recent years with appearance of ideas for matching and adapting optics for magnetized electron beam [1-3,13,15] and, especially, after the inception of superconducting energy recovering RF linear accelerators (ERL) [4]. Recently, cooling of 8 GeV antiproton beam for Tevatron at FNAL has been successfully realized being based on 4.5 MeV, 1A DC magnetized electron source and implementation of beam transport to cooling section with discontinuous solenoid [ ]. Realization of EC at higher energies requires use of high current SRF ERL. After quite a long period of pre-conceptual studies of the ERL-based high energy EC by the international accelerator community [ ], the Brookhaven National Laboratory started a profound R&D work on realization of high current 55 MeV ERL for electron cooling for luminosity upgrade of heavy ion colliding beams (110 GeV/nucleon) in RHIC [ ].

To realize an efficient EC for 150 GeV proton beam of EIC, one needs a high current (2-3 A) relativistic (75 MeV) electron beam. Such request on parameters of the electron beam presents a serious challenge. Despite this issue, EC is considered as a prominent candidate for cooling of intense ion beam in EIC. Other method – stochastic cooling – is not capable to provide the required cooling rate for the intense bunched proton or light ion beam of EIC.

Similar to electron cooling for RHIC, EC design for EIC is based on use of SRF ERL as solution in principle to operate 75 MeV, 3 A electron beam and recover its energy. However, that high current presents a very serious challenge. In order to alleviate the constraint of that high CW current, the EC concept for EIC includes use of a circulator-cooler ring, where the electron beam injected from ERL will circulate during about a hundred revolutions before the quality of the beam is disrupted by the

heating processes. Such design allows one to reduce the average current from the source by a factor 100, thus utilizing a source and ERL with average current of a level 30-100 mA, while the light ion beam is continuously cooled by electron current of a few Amps.

A general EC layout is shown in Figure . The characteristic set of EC parameters for ELIC is presented in Table .

Description of the EC facility, operation and cooling scenario in detail are presented in Part VIII. Here, we underline the following important features of the ERL-based EC conceptual design for ELIC:

- 1 Use of an electron circulator-cooler ring, to reduce drastically (by a factor 100) a necessary average current from electron source
- 2 Implementation of a *staged* EC (i.e. starting cooling after injecting the ion beam in the collider ring and continuing cooling along and after acceleration to energy of an experiment), as a way to minimize the cooling time required for approaching the start luminosity
- 3 Cooling with flat beams (both electron and ion), to minimize the intra-beam scattering impact on luminosity

It also should be noted, that EC parameters are designed under a requirement of a sufficiently low initial emittance of high current ion beam in the collider ring. To satisfy this requirement, we develop a specific concept of stacking ion beam in booster that allows one to significantly reduce the space charge impact on beam emittance (see Part VI.4).

Electron cooling, in cooperation with strong SRF fields in ion storage rings, will allow one to obtain small transverse size, short ion bunches, then allowing one to realize an extremely tight beam focusing at the collision point. Short bunches also make feasible the *crab crossing colliding beams*, that allows one to remove the parasitic beam-beam interactions and maximize the bunch to bunch collision rate.

## Beam transport with discontinuous solenoid

Since inception of electron cooling in accelerator technology at low energies, the electron beam immersed in solenoid (starting at the gun cathode) was recognized as a favorable transport solution for the cooling beam, since it resolves a contradiction between the requirements of strong focusing and low transverse temperature of the beam. To make this principle technically compatible with efficient acceleration at relativistic energies (especially when using superconducting resonators), it was proposed to cut the solenoid under conditions of optical matching (i.e. restoring the canonical cyclotron invariant) between magnetized gun and solenoid of cooling section [3]. This possibility has been proved in analysis and simulations and incorporated with medium and high energy electron cooling designs [13,15,8,17]. It should be noted that, thank to the magnetized cooling mechanism, the influence of a mismatch between solenoids, that may lead to excitation of relatively large transverse velocities of electrons in cooling section, is reduced to just to a decrease of the Coulomb logarithm value in cooling rate given by formula in (1). Also note that the cyclotron matching condition leaves a

freedom to transform from round to an elliptical beam between solenoids, applying adapting optics [2], and even matching between two solenoids of the opposite sign in cooling section [2,17].

## Beam alignment

In order to keep the electron cooling efficiency near a maximum, one has to control the relative position of two beams along the cooling section with accuracy better than the ion beam size (vertical one of a flat beam), using a multiple BPM technique for bunched beams. A simple analysis shows that an absolute precision,  $\Delta_y$ , provides a value of  $\ln(\sigma_y/\Delta_y)$  for the factor  $\log_e$  in the cooling time formula in equation (1) (considering  $\theta_e \gg \theta_i$ ,  $\Delta_y \gg r_c$ , where  $r_c$  is the thermal cyclotron radius of electrons in solenoid).

## ERL based EC

High energy electron cooling was earlier considered based on electron storage rings wherein the electron beam can be cooled (against heating by inter- and intra-beam scattering and quantum radiation) by the synchrotron radiation in wigglers. The transverse temperature of electron beam in solenoid can be reduced (to a level determined by the vertical emittance in arcs) by introducing *plane-vortex beam adapters* [2]; nevertheless, the storage ring approach is still challenging the designers with issue of large electron energy spread. Realization of energy recovery in superconducting RF accelerators [4] makes the linear approach advantageous with regard to the quality of electron beam, especially considering the longitudinal beam emittance. Other important advantage of ERL is the possibility of *staged cooling*, as discussed below.

## Cooling with circulator ring

The high beam current that is needed for high luminosity colliding beams requires a large average current in the electron cooler that might be difficult to attain with modern state of art electron sources. Acceleration and recovery of such high current might also be quite challenging. This issue can be relaxed drastically through use of an electron circulator-cooler ring, similar in basic concepts to the circulator-collider ring [1,11-14] but designed for an electron energy smaller than the ion energy by a factor of the mass ratio. Use of an electron circulator ring as a complementary to the accelerator line was earlier suggested as an option for beam transport for medium energy relativistic electron cooling [6]. Optical scheme of circulator ring matched with magnetized electron gun through an RF accelerator line has been developed in conceptual studies of electron cooling of a proton beam in PETRA for HERA [8]. Circulator-cooler ring can work in conjunction with ERL, as well; the only considerable addition to a CW single loop scheme would be fast kickers for switching the electron bunches between the ERL and the circulator. Gain in electron current, obviously, is equal to the number of bunch revolutions in the ring,  $q$ . Maximum  $q$  is limited by the electron longitudinal temperature lifetime due to inter- ( $\tau_{ei}$ ) and intra- ( $\tau_e$ ) beam scattering and synchrotron radiation. Scattering times can be expressed via the relationship with the IBS time in an ion beam at equilibrium (compare formula in (2)):

$$(\tau_e / \tau_i) \approx (N_i / N_e)(r_i / r_e)^2 (\theta_e \log_i / \theta_i \log_e), \quad (6)$$

$$(\tau_{ei}/\tau_i) \approx (r_i/Zr_e)^2 (C_e \log_i/l_c \log_c), \quad (7)$$

here  $C_e$  is the electron ring circumference, and  $Zr_e$  is an ion charge. The estimates indicate that, typically, electron bunches can stay in circulator during 100 revolutions, at least, before the dilution of beam longitudinal emittance due to the intra- and inter-beam scattering, quantum radiation or CSR leads to a significant reduction of cooling rates. Table 4 illustrates design parameters of electron cooler for the proposed electron-light ion collider at CEBAF (ELIC) [5,12].

## Staged cooling

Electron cooling time grows with beam energy in the first or second power and with normalized beam emittances - the third power. Therefore, it seems critically important to organize the cooling process in collider ring in two stages: cool the ion beam initially at injection energy (see Table 5, same electron current is assumed as in Table 3) after stacking it in collider ring (in parallel or after rebunching), and continue the cooling during and after acceleration to a high energy. Note, that the staged cooling appears as a natural possibility with the ERL-based EC. The electron beam area could be then varied with time in an optimum way to minimize the time of beam shrinkage to equilibrium and maximize the lifetime as above discussed.

Table 4 ERL-based EC with circulator ring

Parameter	Unit	Value
Max/min energy of e-beam	MeV	75/10
Electrons/bunch	$10^{10}$	1
Number of bunch revolutions in CR	100	1
Current in CR/current in ERL	A	2.5/0.025
Bunch rep. rate in CR	GHz	1.5
CR circumference	m	60
Cooling section length	m	15
Circulation duration	$\mu$ s	20
Bunch length	cm	1
Energy spread	$10^{-4}$	3-5
Solenoid field in cooling section	T	2
Beam radius in solenoid	mm	1
Cyclotron beta-function	m	0.6
Thermal cyclotron radius	$\mu$ m	2
Beam radius at cathode	mm	3
Solenoid field at cathode	KG	2
Laslett's tune shift in CR at 10 MeV		0.03
Time of longitudinal inter/intrabeam heating	$\mu$ s	200

Table 5: Initial electron cooling (p/e)

Parameter	Unit	Value
Energy	GeV/MeV	20/10
Cooling length/ circumference	%	1
Particles/bunch	$10^{10}$	0.2/1
Energy spread*	$10^{-4}$	3/1
Bunch length*	cm	20/3
Proton emittance, norm*	$\mu\text{m}$	4
Cooling time	min	10
Equilibrium emittance, **	$\mu\text{m}$	1
Equilibrium bunch length**	cm	2
Laslett's tune shift		0.1

\* max.amplitude

\*\* norm.,rms

The ERL-based high energy electron cooling seems quite promising in approaching a very high luminosity in colliders with hadron beams. The low longitudinal emittance of the electron beam and possibility of a staged cooling are the important advantages of ERL approach. To operate at a modest average beam current, the ERL accelerator should be complemented with electron circulator-cooler ring. Also, certain improvements in forming and transporting the hadron beams before injecting to collider ring might be required in order to reduce the time of initial electron cooling in the ring [9]. A comprehensive analysis, simulation and experimental studies should precede the development of recommendations for practical design of electron cooling and high luminosity colliding beams.

# VI Concepts for High Luminosity

## Contents

- 6.1 Overview
- 6.2 Beam-beam effects
  - 6.2.1 Beam-beam resonances
  - 6.2.2 Beam-beam dependence on synchrotron tune
  - 6.2.3 Coherent stability
  - 6.2.4 Multiple IP interference and tuning
- 6.3 Laslett's limit on ion beam
- 6.4 Particle Scattering Processes
  - 6.4.1 Multiple intrabeam scatterings
  - 6.4.2 Touscheck effect on ion beam
  - 6.4.3 Background collision processes
- 6.5 Luminosity improvements with electron cooling
  - 6.5.1 Low beta star with short cooled bunches
  - 6.5.2 Crab crossing colliding beams
  - 6.5.3 Reduction and maintenance of transverse emittances against IBS
  - 6.5.4 Reduction of IBS by flat beam cooling
  - 6.5.5 Diminishing of Touscheck scattering and luminosity lifetime
- 6.6 Summary

## 6.1 Overview

Luminosity of an electron-ion collider is defined as

$$L = \frac{f N_e N_i}{2\pi \Sigma_x \Sigma_y}, \quad (6.1.1)$$

where  $f$  is the collision frequency of the collider,  $N_e$  and  $N_i$  are number of electrons and ions in bunch, and the effective transverse RMS spot sizes

$$\Sigma_x = \sqrt{\sigma_{xe}^2 + \sigma_{xi}^2} \quad \Sigma_y = \sqrt{\sigma_{ye}^2 + \sigma_{yi}^2} \quad (6.1.2)$$

are derived from electron and ion beams' individual RMS sizes  $\sigma_{xe}$  and  $\sigma_{ye}$ ,  $\sigma_{xi}$  and  $\sigma_{yi}$ . When a collider is designed to have the same transverse RMS spot sizes of two colliding beams, i.e.,  $\sigma_{xe} = \sigma_{xi}$  and  $\sigma_{yi} = \sigma_{ye}$ , the luminosity formula is simplified as

$$L = \frac{f N_e N_i}{2\pi \sigma_x \sigma_y}. \quad (6.1.3)$$

It is well known that the transverse beam-beam interaction at collisions is usually a dominating limiting factor of luminosity of a collider, thus the above luminosity formula can be re-cast in a more suggestive way in terms of the beam-beam tune shifts,

$$L = f \frac{\pi \gamma_e \gamma_i}{r_e r_i} \xi_x^i \xi_y^e \sqrt{\frac{\epsilon_x^i}{\beta_x^{*i}}} \sqrt{\frac{\epsilon_y^e}{\beta_y^{*e}}} \frac{(1+k)^2}{k} \quad (6.1.4)$$

where  $k = \gamma/\gamma_x$  is the aspect ratio of the beam,  $\varepsilon_x^i$  and  $\varepsilon_y^e$  are normalized beam emittance,  $\beta_x^{*i}$  and  $\beta_y^{*e}$  are beta functions at the collision points. The beam-beam tune shifts, the most important characteristic parameter of the transverse beam-beam interactions, for the ion beam in two transverse directions are defined as

$$\xi_x^i = \frac{N_e r_i}{2\pi\gamma_i} \frac{1}{\varepsilon_x^i(1+k)} \quad \xi_y^i = \frac{N_e r_i}{2\pi\gamma_i} \frac{1}{\varepsilon_y^i(1+1/k)} \quad (7.1.5)$$

There are similarly formulas for electron beam with indices  $i$  and  $e$  reversed. Here  $r_e$  and  $r_i$  are classical radii of electron and ion.

Luminosity formula of Eq. (7.1.4) displays clear linear proportional or inverse proportional dependence of an electron-ion collider luminosity on several key parameters of the colliding beams, namely, the collision frequency, transverse emittances, beta-star (optics at IPs) and beam-beam tune shifts. These dependences provide useful turning knobs or a clear roadmap to collider designers for optimizing the luminosity of the collider. It is clear that a high collision frequency, maximum beam-beam tune shifts and small beta-star values would increase the luminosity.

The concept of ultra high luminosities of ELIC has been established based on two optimizations which are very unique in comparison with other conventional colliders. The first is an ultra high collision frequency of the ELIC. Since the ELIC electron ring is filled with the 1.5 GHz CW beams from the CEBAF SRF Linac, it is possible with current technologies to design and operate an ion storage ring with a CW ion beam of the same frequency. Therefore the ELIC collision frequency can reach as high as 1.5 GHz. As a comparison, RHIC operates colliding beam at a maximum 28 MHz frequency, therefore its collision frequency is a factor of 54 smaller than ELIC. The second is ultra small transverse beam spot sizes at ELIC collision points. Since the normalized emittances of a stored beam are dictated by beam equilibrium inside storage rings, small transverse spot sizes are achieved by very short beta-stars, hence a very strong final focusing at collision points. Certainly, the largest beam-beam tune shifts which a collider can ever tolerate to pose a strong constraint for very small beam spot sizes. ELIC found an optimal solution of relative small bunch charges, very large crossing angles and continuous electron cooling of ion beams in the collider ring such that the beam spot sizes can be made as small as 1 to 6  $\mu\text{m}$ .

The ELIC high luminosity concept is set on foundation of beam physics with careful considerations of the beam-beam interactions, space charge, intrabeam scattering and electron cooling effects. Its physics can be argued as follows

1. Electron cooling in cooperation with bunching SRF resonators provides very short ion bunches (5 mm or less), thus open up the possibility to design optics near IPs with very short beta-star.
2. Reduction of transverse emittances of an ion beam by electron cooling allows one to increase beam extension in the final focusing magnet, hence, to reach a lower beta-star.
3. Short bunches open up an opportunity for implementing the crab-crossing colliding beams which help to eliminate parasitic beam-beam interactions and also can avoid beam bend at detector area while approaching a highest collision rate.

4. Reduction of bunch charge can increase the maximum tolerable beam-beam tune shifts and as well as beam stability against microwave interaction, in particularly, electron clouds.
5. Large synchrotron tune (exceeding the beam-beam tune shift) eliminates the synchrotron-betatron non-linear resonances in beam-beam interaction, thus allowing one to reach a large beam-beam tune shift.
6. Flat beams (by lowering the x-y coupling at fixed beam area) lead to reduction of intrabeam scattering growth rate against electron cooling
7. Equidistant fraction phase advance between four IPs of ELIC effectively reduces the critical beam-beam tune shift to a value normalized to one IP.

Bunch shortening was not emphasized in earlier conceptual studies of colliders with electron cooling. The reason for this was an insufficient strength RF field for bunching the beam. With high field superconducting resonators available today, it seems feasible for producing proton or ion bunch of 1 cm or even shorter with use of electron cooling. The correspondently low beta-star can be achieved by a necessarily large beam transverse extension before the final focus quadrupoles. This constraint relaxes of decrease of transverse (horizontal) emittance by the electron cooling, within the limits determined by the optics imperfections and beam alignment control

Short bunches makes crab crossing of colliding beams feasible. In this method the beams intersect at a large crossing angle, while the bunches are tilted off the beam directions by half of this angle becoming parallel to each other the collision point; thus, the parasitic collisions are avoided without loss of luminosity. The required bunch tilt can be produced by RF dipole magnetic field in superconducting resonators installed in sections of beam extension. For example, tilt angle 50 mrad in case of 150 GeV proton beam and final focal length of 4 m can be created by 1.5 GHz SRF cavities of integrated transverse magnetic field amplitude 0.1 TM which installed in a section of beam extension. Remarkably, the necessary amplitude of integrated RF field does not grow with collider energy.

Table 1: Cooled p-bunches in a ring with SRF resonators

Parameter	Unit	Value
Beam energy	GeV	150
Resonators frequency	GHz	1.5
Voltage amplitude	MV	100
Ring circumference	Km	1.2
Compaction factor	$10^{-3}$	4
Synchrotron tune		.06
Energy acceptance	%	.3
Energy spread, rms	$10^{-4}$	3
Bunch length, rms	mm	5

Table 2: Final focus of EIC with short bunches (p/e)

Beam energy	GeV	150/7
Bunch length, rms	mm	5/5
Focal length	m	4/4
Large beta	Km	3.2/3.2
Beta-star	mm	5/5
Transverse emittance, norm, rms	$\mu\text{m}$	1/100
Beam size at large beta, rms	mm	5/5
Beam size at star point, rms	$\mu\text{m}$	6/6

For ELIC electron and proton collisions, stored beams have  $10^{10}$  electrons and  $4 \cdot 10^9$  protons per bunch. The strong final focusing of ELIC is able to reduce the RMS bunch sizes to  $6 \text{ m}$  in  $x$  and  $1.2 \text{ m}$  in  $y$ . Assuming elatively large beam-beam tune shifts, namely, 0.01 for electrons and 0.086 for protons, it is found the ELIC luminosity at the top colliding energy  $7 \times 150 \text{ GeV}^2$  is about  $7.7 \cdot 10^{34} \text{ cm}^{-2}\text{s}^{-1}$  per collision point. Table 3.2.1 also gives the luminosity for two lower colliding energy settings.

Luminosities for an electron beam colliding with other ion beams depends on atomic number and net charges of ions and beam-beam tune shift, in additional to beam energies, normalized transverse emittances and the optic at IPs. It is assumed we are able to store the same ion beam currents for different species in ELIC, though this may be proved to be a challenge for some ions with large number electrons stripped. To estimate the luminosity, we assume the beam-beam tune shift of the proton-electron collision is the upper limit and will be equally tolerated at best in ELIC. Then the ion beam energy must be adjusted appropriately. Table 3.3.1 summarizes calculated luminosities for a few ion species, providing the electron beam has the same energy of 7 GeV and other beam properties of Table 3.2.1. The optics at IPs is also assumed the same for different ion species.

Table 3.3.1 Luminosity for ELIC with different ion species

ion	ener.	curr.	part.	Normalized emittance		RMS size		Beam-beam tune shift		Lumi. per IP ( $10^{34}$ )
				horiz	vert.	horiz	vert.	horiz	vert.	
	GeV/u	A	$10^{10}$	mm	mrad	m				$\text{cm}^{-2}\text{s}^{-1}$
e <sup>-</sup> /e <sup>+</sup>	7	2.4	1.04	100	4	5.6	1.1	.017	.084	
P <sup>+</sup>	150	1	.417	1	.04	6.0	1.2	.002	.01	7.8
D <sup>-</sup> /D <sup>+</sup>	75	1	.417	.5	0.02	6.0	1.2	.002	0.01	7.8
<sup>3</sup> H <sup>+</sup>	50	1	.417	.33	.013	6.0	1.2	.002	0.01	7.8
<sup>3</sup> He <sup>+2</sup>	100	1	.209	.67	.027	6.0	1.2	.002	.01	3.6
<sup>4</sup> He <sup>+2</sup>	75	1	.209	.5	.02	6.0	1.2	.002	.01	3.6
<sup>12</sup> C <sup>+6</sup>	75	1	.070	.5	.02	6.0	1.2	.002	.01	1.2

## 6.2 Beam-beam effects and Multiple IP interface

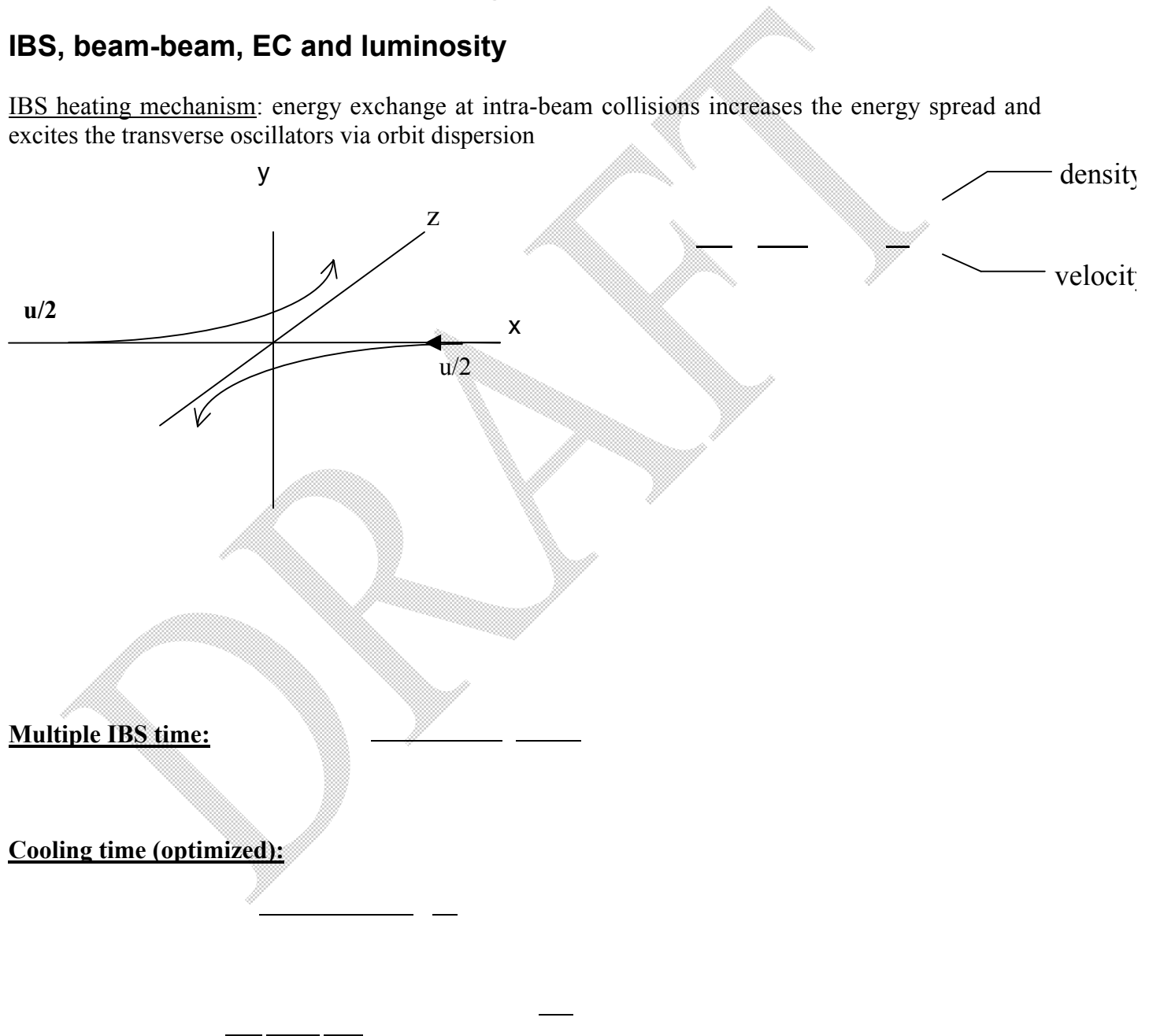
### 6.3 Laslett's limit in ion beam

### 6.4 Particle Scattering Processes

#### 6.4.1 Multiple intrabeam scatterings

##### IBS, beam-beam, EC and luminosity

IBS heating mechanism: energy exchange at intra-beam collisions increases the energy spread and excites the transverse oscillators via orbit dispersion

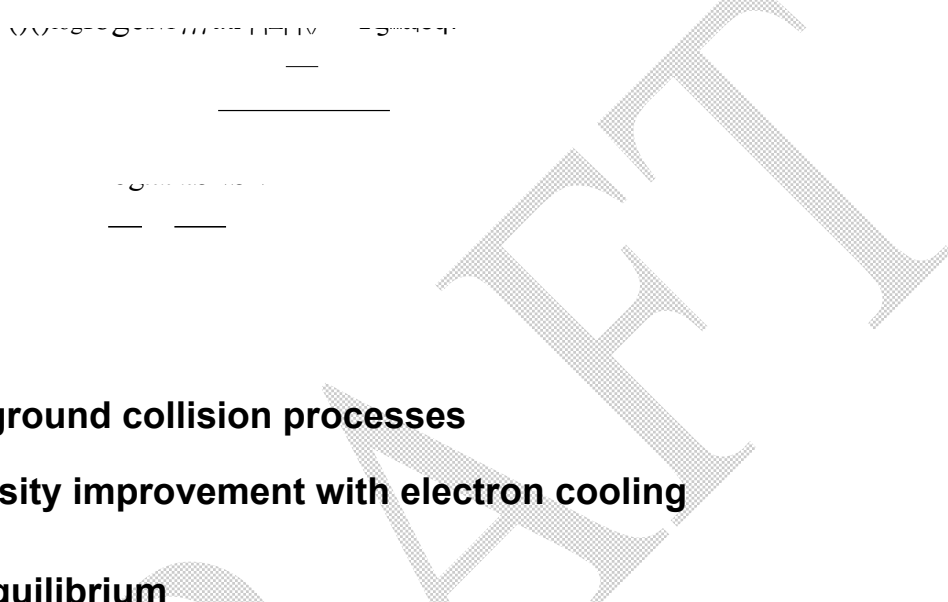


## 6.4.2 Touscheck effect in ion beam

Touschek' lifetime,  $T$

IBS at large momentum transfer (*single scattering*) drives the particles out of the beam core, limiting the luminosity lifetime.

The *optimum equilibrium* is found by equating between time of *single scattering*, *cooling time* for the scattered particles and *beam cycle* time of the collider. It results in the relationships:



## 6.4.3 Background collision processes

## 6.5 Luminosity improvement with electron cooling

### 6.5.1 IBS equilibrium

In the limit when  $\gamma \gg Q$ , where  $Q$  is “betatron tune”, the IBS times can be estimated as

$$\begin{aligned}\tau_z &\approx 8\gamma\varepsilon_6(\Delta\gamma/\gamma^2\theta_y)/N_i r_i^2 c \log_i, \\ \tau_z : \tau_x : \tau_y &\approx (\Delta\gamma/\gamma)^2 : Q^2\theta_x^2 : \gamma^2\theta_y^2 / [1 + (\gamma\kappa/Q)^2],\end{aligned}\quad (2)$$

where  $\kappa$  is the  $x$ - $y$  coupling parameter, and  $N_i$  is the number of hadrons per bunch, and  $\varepsilon_6 = \varepsilon_x \varepsilon_y \varepsilon_z$  at  $\varepsilon_\alpha$  defined as a normalized emittance:  $\langle I_\alpha \rangle = \varepsilon_\alpha$ . The *IBS cooling criterion* can be obtained by setting  $\tau_c = (\tau_\alpha)_{min}$ ; usually  $\tau_z$  is the minimum of the three cooling rates as a result of beam acceleration before cooling. *Equilibrium criterion* can be found at  $\tau_z = \tau_x = \tau_y$ , or  $(\Delta\gamma/\gamma^2\theta_x) \approx (Q/\gamma)$ ;  $(\theta_y/\theta_x) \approx [\kappa^2 + (Q/\gamma)^2]^{1/2}$ :

$$N_e > N_{cr} \approx N_i(r_i C_i \log_i / r_{el} c \log_c) [1 + (\gamma\kappa/Q)^2]^{1/2} \quad (3)$$

Thus, a minimum (possibly small)  $\kappa$  leads to a flat equilibrium, minimum  $\varepsilon_6$ , and a maximum cooling rate. Since the luminosity is determined by the product of two transverse emittances, reduction of transverse coupling to a minimum while conserving the beam area would benefit one with a decrease of energy scattering, hence, decrease of the whole the IBS impact on luminosity. Electron cooling then leads to a flat equilibrium with a large aspect ratio. In order to achieve an optimum cooling effect at equilibrium, electron beam area in solenoid should also be transformed to an elliptical one of a similar aspect ratio, applying adapting optics [2].

## 6.5.2 Luminosity lifetime due to Touschek scattering

After the cooling starts, the ion beam will shrink to a flat Fokker-Planck equilibrium, with the horizontal emittance determined by the multiple IBS and the vertical one limited by the beam-beam space charge interaction. Following this stage, an interplay between Touschek scattering and electron cooling of scattered particles will determine the core (i.e. luminosity) lifetime. At ion energies far above the transition value, area of cooling beam should frequently exceed that of the ion beam, in order to extend the ion core lifetime. To avoid the flip-flop instability of colliding beams [20], the vertical emittance due to the coupling and multiple IBS should reach the limit due to the beam-beam interaction. Using this phenomenology at a proper choice of luminosity lifetime, one can estimate an optimum set of parameters for a maximum average luminosity of a collider [9]. In particular, equating the time of Touschek scattering to the edge of electron beam with the damping time of a scattered particle and beam run duration as the luminosity lifetime,  $\tau_l$ , under condition  $(\gamma Q)^2 \gg \log_i$ ,  $\Delta\gamma_e \leq \Delta\gamma_i$ , and  $\sigma_{ze} \leq \sigma_{zi}$ , we obtain the relationships as follows:

$$(\tau_i)_{eq} = (\tau_c)_{eq} = \tau_l / (\log_i)^2, \quad (S_e / S_i) = (N_e / N_{cr}) = \log_i, \quad (4)$$

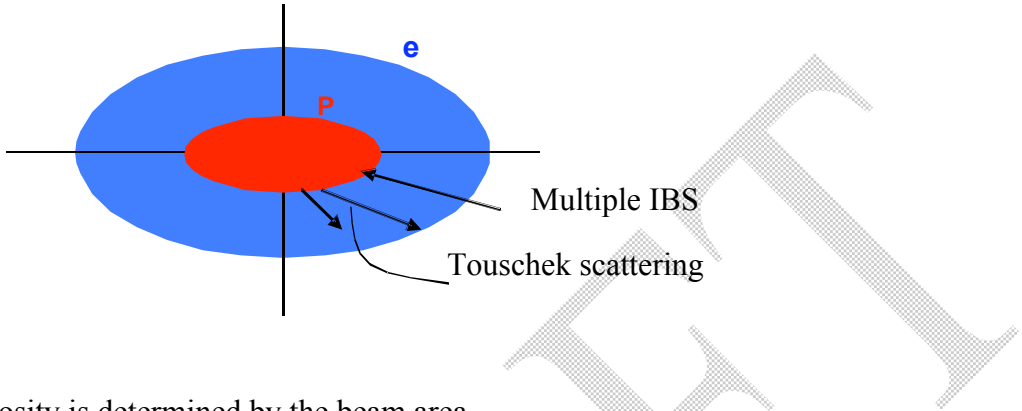
### ELECTRON COOLING AGAINST IBS

At energies above the transition value, energy exchange between two particles in intra-beam collisions leads to the horizontal emittance growing up due to the basic energy-orbit coupling, and vertical emittance due to the x-y coupling. Since the transverse temperature of a beam is large comparing to the longitudinal one, it is necessary to distinguish between *multiple IBS* (small scattering angle) and *single or Touschek scattering* that immediately drives a particle out of the beam core. Multiple scattering has a relatively large probability and responsible for (or contributing to) ion Fokker-Planck equilibrium of a beam under cooling, while Touschek scattering will limit the core and, hence, luminosity lifetime.

#### At low coupling, cooling results in flat beams

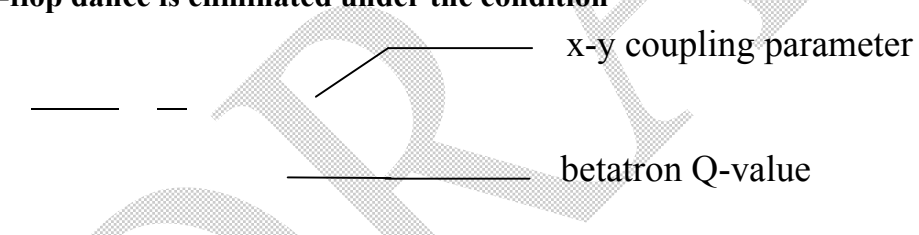
*x – emittance is determined by the IBS*

*y – emittance is limited by the beam-beam interaction*



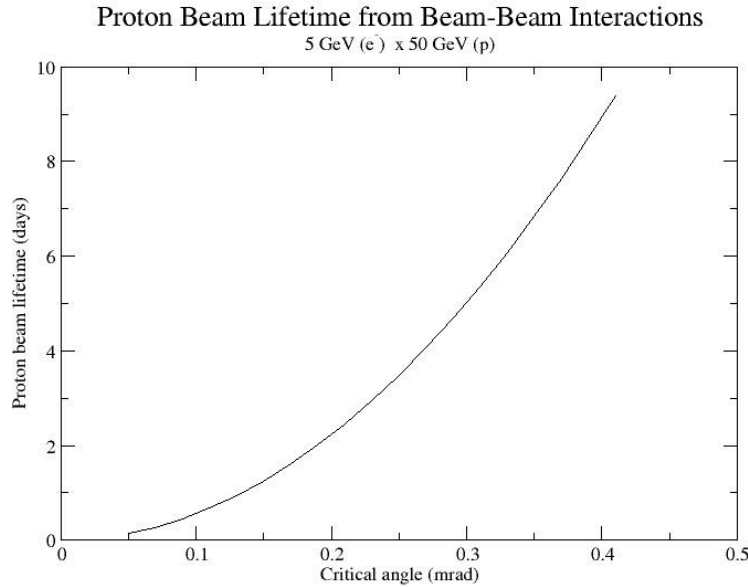
- Luminosity is determined by the beam area
- IBS effect is reduced by a factor of the aspect ratio
- Cooling effect at equilibrium can be enhanced by flattening the electron beam in cooling section solenoid

#### **Flip-flop dance is eliminated under the condition**



#### **Proton beam lifetime from small-angle elastic ep-scattering**





Contributions from inelastic processes have smaller effect by factor of ~10

### Lifetime due to Intrabeam Scattering

- IBS heating mechanism: Energy exchange at intra-beam collisions leads to x-emittance increase due to energy-orbit coupling, and y-emittance increase due to x-y coupling
- Electron cooling is introduced to suppress beam blow up due to IBS, and maintain emittances near limits determined by beam-beam interaction.
- Since  $L \propto I / \sigma_x \sigma_y$ , reduction of transverse coupling while conserving beam area, would result in decrease of impact of IBS on luminosity
- Electron cooling then leads to a flat equilibrium with aspect ratio of 100:1.
- Touschek effect: IBS at large momentum transfer (single scattering) drives particles out of the core, limiting luminosity lifetime.
- A phenomenological model which includes single scattering and cooling time of the scattered particles has been used to estimate an optimum set of parameters for maximum luminosity, at a given luminosity lifetime.

### LUMINOSITY POTENTIALS OF EIC

Let us assume the ion and electron beam sizes to be equal at collision point; then the general luminosity expression:  $L = f N_e N_i / 4\pi(\sigma_x \sigma_y)^*$  sets two formulas as follows:

$$Le^3 = (JE\xi/\beta^*)_e = (JE\xi/\beta^*)_i. \quad (5)$$

Here  $J$  is the average circulating current at  $f$  as bunch repetition rate,  $E = \gamma mc^2$ ,  $\beta^*$  is beta-function value at collision point ( $\beta^* \geq \sigma_z$ ), and  $\xi$  is the vertical beam-beam tune shift.

The luminosity increase in colliders with electron cooling is usually associated with decreased and maintained transverse emittances of hadron beams against IBS and stochastic effects related to the high order non-linear beam-beam resonances. Decrease of longitudinal emittance, that allows for bunch shortening, hence, design of a low beta-star, was not emphasized in earlier conceptual studies of colliders with electron cooling; general reason for this was an insufficient strength RF field for bunching the beam. With high field superconducting resonators available today, proton or ion *bunch length of 1 cm or even shorter* seems feasible with the use of electron cooling [11,14] (see Table 1). The correspondently *low beta-star* can be achieved by a necessarily large beam transverse extension before the final focus quadrupoles. This constraint relaxes of decrease of transverse (horizontal) emittance by the electron cooling, within the limits determined by the optics imperfections and beam alignment control (see Table 2).

Table 1: Cooled p-bunches in a ring with SRF resonators

Parameter	Unit	Value
Beam energy	GeV	150
Resonators frequency	GHz	1.5
Voltage amplitude	MV	100
Ring circumference	Km	1.2
Compaction factor	$10^{-3}$	4
Synchrotron tune		.06
Energy acceptance	%	.3
Energy spread, rms	$10^{-4}$	3
Bunch length, rms	mm	5

Table 2: Final focus of EIC with short bunches (p/e)

Beam energy	GeV	150/7
Bunch length, rms	mm	5/5
Focal length	m	4/4
Large beta	Km	3.2/3.2
Beta-star	mm	5/5
Transverse emittance, norm, rms	$\mu\text{m}$	1/100
Beam size at large beta, rms	mm	5/5
Beam size at star point, rms	$\mu\text{m}$	6/6

Short bunches also would make feasible *crab crossing* the colliding beams. In this method the beams intersect at a large crossing angle, while the bunches are tilted off the beam directions by half of this angle becoming parallel to each other at the collision point; thus, the parasitic collisions are avoided without loss of luminosity [10]. The required bunch tilt can be produced by RF dipole magnetic field

in superconducting resonators installed in sections of beam extension. [9,11,14]. For example, tilt angle 50 mrad in case of 150 GeV proton beam and final focal length of 4 m can be created by 1.5 GHz SRF cavities of integrated transverse magnetic field amplitude 0.1 TM which installed in a section of beam extension. Remarkably, the necessary amplitude of integrated RF field does not grow with collider energy [14].

Table 3: High luminosity colliding beams (p/e)

Parameter	Unit	Value
Beam energy	GeV	150/7
Energy of cooling beam	MeV	75
Bunch rep rate	GHz	1.5
Particles/bunch	$10^{10}$	0.2/1
Beam current	A	0.5/2.5
Cooling current	A	2.5
Horizontal emittance*	$\mu\text{m}$	1/100
Vertical emittance*	$\mu\text{m}$	0.01/1
Number of interaction points		4
Total beam-beam tune shift		0.04/0.16
Laslett's tune shift in p-beam		0.02
Luminosity overall IP ( $10^{35}$ )	$\text{cm}^{-2}\text{s}^{-1}$	2
Cooling/IBS time in p-beam core	min	5
Luminosity Touschek's lifetime	h	20

\* normalized rms.

A relatively high value of beam-beam tune shift,  $\xi$ , for proton beam (.01 per interaction point) is assumed taking into account an improving of the long term beam-beam stability by cooling itself and relying on the stabilizing effect of a large increase of synchrotron tune against the high order non-linear synchro-betatron beam-beam resonances. Also, a rather high current is assumed for the cooling electron beam; we consider this level achievable in a circulator-cooler ring incorporated with ERL, as discussed below.

Finally, if the colliding electron bunch length is still much shorter than that of the proton bunch, the luminosity could be additionally increased by arrangement for a traveling ion focus [16,11,14] at a proper reduction of electron emittances.

## 6.6 Interaction Points with short bunches

### 6.6.1 Low beta-star

The final focus lattice can be configured either symmetrically (DFDODFD) or anti-symmetrically (FDFODFD). The advantage of the anti-symmetric configuration is its lower sensitivity to ground motion and magnet power supply fluctuation etc. Assuming a final normalized ion beam horizontal

emittance after cooling of  $10^{-6}$   $\mu\text{m}$ , this yields the beam width in the final triplet of about 5 mm. Further, a more aggressive lattice design would assume a peak field of 9 T at the same aperture and  $\beta^{\max}$  of about 6 km, which would allow us to reduce  $\beta^*$  to about 5 mm. However, much shorter focal length of the triplet (less than 5 m) would significantly reduce free space around the interaction point available for the detector (to less than 4 m).

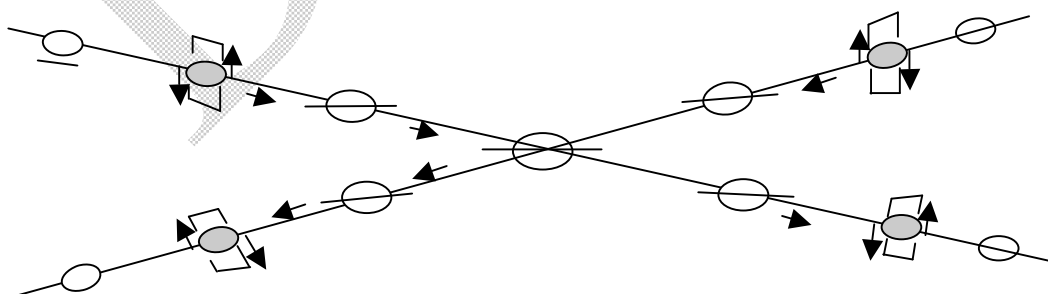
To implement very tight focusing in the ELIC interaction region, it is beneficial to use a focusing triplet (DFD or FDF) which provides a net focal length of about 5 m at the collision energy of 150 GeV. This triplet uses two types of quadrupoles: 1.12 m long defocusing one and 1.96 m long focusing one, with transverse aperture radius of 3 cm and 7.5 T peak field. The quadrupole parameter defines a maximum field gradient of 250 T/m. Our preliminary lattice design assumes  $\beta=1$  cm and  $\beta^{\max}=3800$  m. The final focus lattice can be configured either symmetrically (DFDODFD) or anti-symmetrically (FDFODFD). The advantage of the anti-symmetric configuration is its lower sensitivity to ground motion and magnet power supply fluctuation etc. Assuming a final normalized ion beam horizontal emittance after cooling of  $10^{-6}$   $\mu\text{m}$ , this yields the beam width in the final triplet of about 5 mm. Further, a more aggressive lattice design would assume a peak field of 9 T at the same aperture and  $\beta^{\max}$  of about 6 km, which would allow us to reduce  $\beta^*$  to about 5 mm. However, much shorter focal length of the triplet (less than 5 m) would significantly reduce free space around the interaction point available for the detector (to less than 4 m).

### 6.6.2 Crab Crossing

**CRAB CROSSING** To eliminate the parasitic beam-beam interaction, the colliding beams should intersect at some angle. To avoid luminosity loss, bunches then should be turned by half of the angle thus becoming parallel to each other [12]. Bunch tilt is produced by crab resonators. In our design, the crab resonators are installed before and after the outer final focus magnets, namely, they are centered at outer focus points of an experimental area with two interaction points. Then, the colliding bunches do not rotate, while the crab tilt becomes compensated after the second resonator. In our estimates, dipole magnetic field resonator with effective 1.5 GHz SRF voltage about 80 MV is sufficient to create 50 mrad bunch tilt for 150 GeV proton beam yet fit the free space near final focus magnets.

Short bunches make Crab Crossing feasible.

SRF deflectors at 1.5 GHz can be used to create a proper bunch tilt.



Figure

Parasitic collisions are avoided without loss of luminosity.

Short bunches also make feasible the introduction of crab crossing that allows one practically to remove parasitic beam-beam interactions without loss of luminosity, attain a highest bunch collision frequency (up to 1.5 GHz) and release more space for detectors [11]. With ion bunches 0.5 cm as short, applying SRF deflectors of integrated magnetic field amplitude 600 G by 4 m to effect 100 GeV ion beam, one can obtain bunch tilt 0.05 rad (corresponding crossing angle 0.1 rad) at final focus parameter 3 m (Fig.4). Bend-related rotation of electron spin can be preventively compensated by Wien filter or in other way.

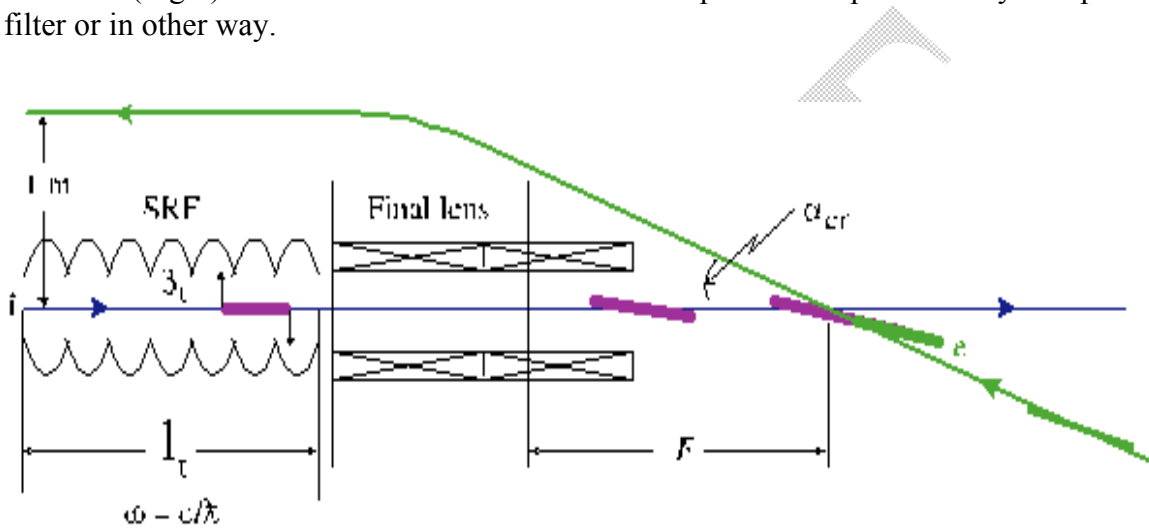


Fig.4. Crab crossing for EIC

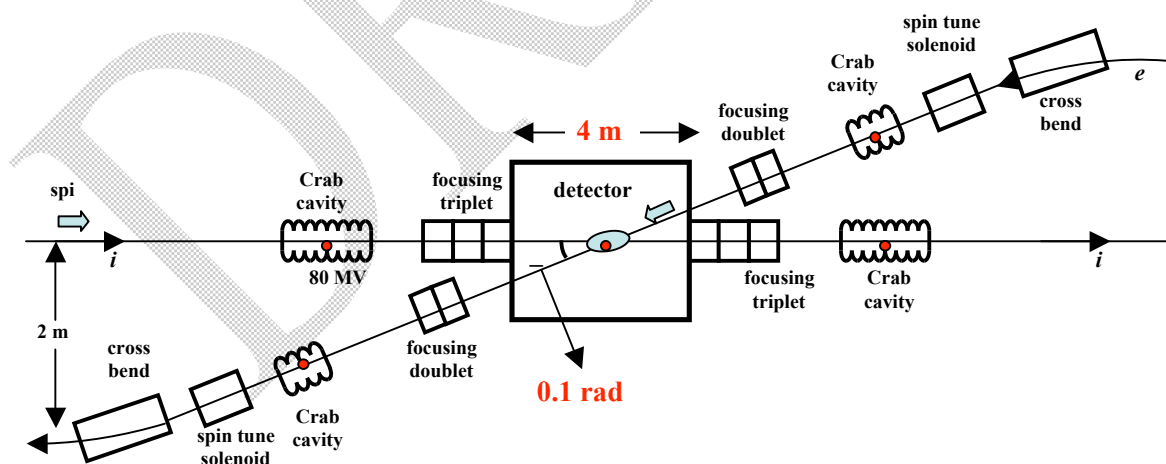


Fig.2: Crab crossing interaction region of ELIC

## CRAB CROSSING

To eliminate the parasitic beam-beam interactions, the colliding beams should intersect at some angle. To avoid luminosity loss, bunches then should be turned by half of the angle thus becoming parallel to each other. The designed bunch length of 0.5 mm makes this feasible. Bunch tilt has to be produced by deflecting resonators. The peak dipole field required to generate a 50 mrad bunch tilt for 150 GeV proton beam is estimated from

$$V = \frac{\lambda_{RF} E}{2\pi\sqrt{\beta\beta^*}} \tan \frac{\theta}{2}$$

where  $\beta$  and  $\beta^*$  are beta parameters at the cavity location and the collision point, respectively (which are to be separated by 90 degree in betatron phase to be most effective). Also,  $\lambda_{RF}$  is the wavelength of the operating mode of the deflecting cavity and  $\theta$  is the beam crossing angle, and  $E$  is the beam energy. Therefore, approximately 100 MV is required to create the necessary bunch tilt for a crab crossing assuming  $\beta$  of about 1 km at the cavity and  $\beta^*$  of 5 mm. For 7 GeV electron beam the dipole voltage needed is much more modest 5 MV. After the collision two beams are required to return to initial unperturbed states. This is achieved by a second deflecting cavity located 90 degree in betatron phase away from the collision point. However, if the cancellation of kicks is not perfect, the residual effect is an excitation of betatron motion which could lead to synchro-betatron resonances with resulting beam quality degradation [paper by Wei].

Near the resonance  $Q_x \pm mQ_s = p$  (where  $m, p$  are integers and  $Q$ 's are tunes, i.e. the synchrotron tune  $Q_s = \omega_s/\omega_0$ , etc.), changes in beam emittances due to the resonances can be estimated from

$$\frac{1}{\epsilon_x} \frac{d\epsilon_x}{dt} = eV \frac{2\omega_0 mc_m}{\pi E} \sqrt{\frac{2\beta_x}{\epsilon_x}} \left[ \left( \frac{\delta V}{V} \right)^2 + (\delta\phi)^2 \right]^{1/2}$$

$$\frac{1}{S} \frac{dS}{dt} = eV \frac{2\omega_0 m^2 c_m}{Sc} \sqrt{2\beta_x \epsilon_x} \left[ \left( \frac{\delta V}{V} \right)^2 + (\delta\phi)^2 \right]^{1/2}$$

where

$$c_m \approx \left[ \frac{\eta\omega_{RF}^2 S}{64\pi\omega_s E} \right]^{m/2}$$

Low order synchro-betatron resonances are likely in ELIC proton beam since  $Q_s$  is rather large 0.06. For example, consider  $m = 4$  resonance. Assuming the average beta of 13 m and the revolution frequency of 0.25 MHz the horizontal emittance growth rate is about 0.045/second when  $\delta V/V$  or  $\delta\phi$  = 0.01 for the 150 GeV proton beam. The maximum bunch length is assumed to be 25 degree in RF phase in this estimate.

Constrains for RF amplitude and phase fluctuations also come from the fact that the bunch spot size is about 6 micron at the collision point and bunch tilts and transverse offsets must be controlled to ensure the collision of two bunches. From a qualitative consideration we find that the amplitude fluctuation can be a few percent but the RF phase must be maintained within about 0.2 degree.

# VI The Interaction Region

## Contents

- 7.1 *Detector design considerations*
- 7.2 *Final focusing and crab crossing*
- 7.3 *Lattice optics design and special elements*
- 7.4 *Technical issues*

## 7.1 The IR organization in general

The ELIC interaction region is designed to accommodate up to four detectors for different nuclear physics experiments simultaneously at four collision points located symmetrically on the two straight sections of the beam line around the center of the figure-8 collider ring (see Fig. 3.2.1). To attain the highest luminosity, the beams have to be focused at the collision points as tightly as possible. The focusing principle for colliding beams is similar to focusing of light beams in optical microscopes and electron beams in electron microscopes. The scheme generally includes a relatively long section of beam transverse extension and final focusing lenses (quadrupole doublet or triplet magnets). These lenses transform the large beam size (obtained after the extension) to a maximum beam angle divergence and, correspondently, a minimum size at the *collision point*. In addition to the final focusing principle, other considerations of the IR design include detector instrumentation, beam separation after the collisions, synchrotron radiation at the IPs, beam polarization.

## 7.2 Interaction region geometry

The electron and ion storage rings of ELIC are stacked vertically in the same tunnel with the electron ring on top. While the ion ring lies entirely within a horizontal plane, the electron beam emerging from the arcs is bent vertically near the first IP to collide with the ion beam, then is bent back vertically to cross the second IP before entering the next arc of the electron ring. The distance between the two IPs on the straight section of the beam line is 60 meters. Due to the very close bunch spacing (20 cm) for both colliding beams, a relatively large crossing angle, 0.1 rad or 5.8 degrees, will be used in order to avoid parasitic collisions. Such a large crossing angle eliminates the need for separation dipoles required in conventional IPs with small crossing angles and thus makes the design of ELIC IP's greatly simplified. The present design makes provision for a 4 meter (with the possibility of extension to 6 m) free space around each interaction point for physics detectors.

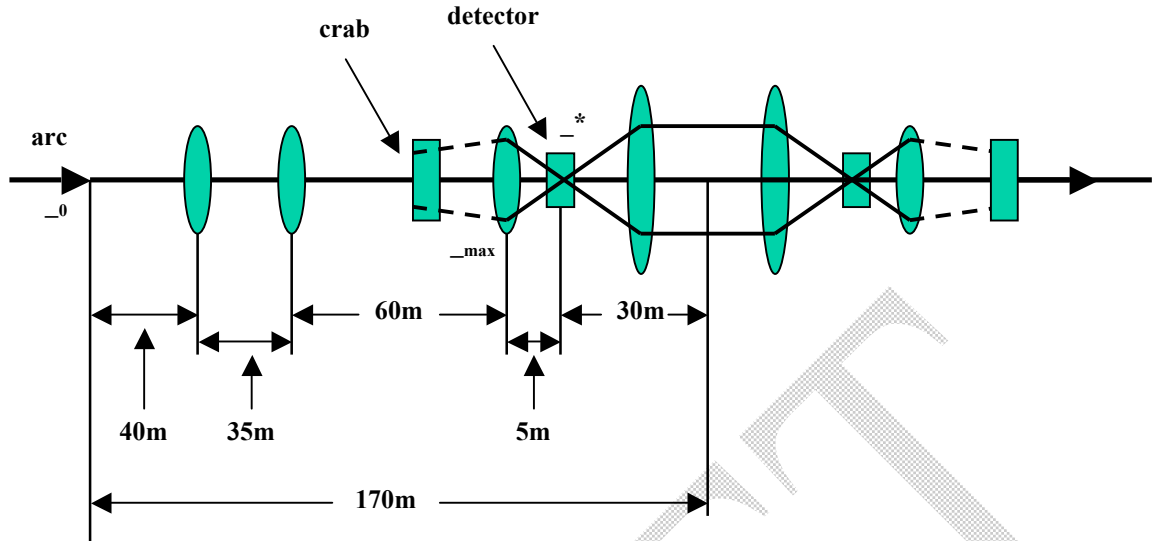


Figure 6.1. Interaction Region of ELIC: global scheme with two Interaction Points (in each of two crossing straights)

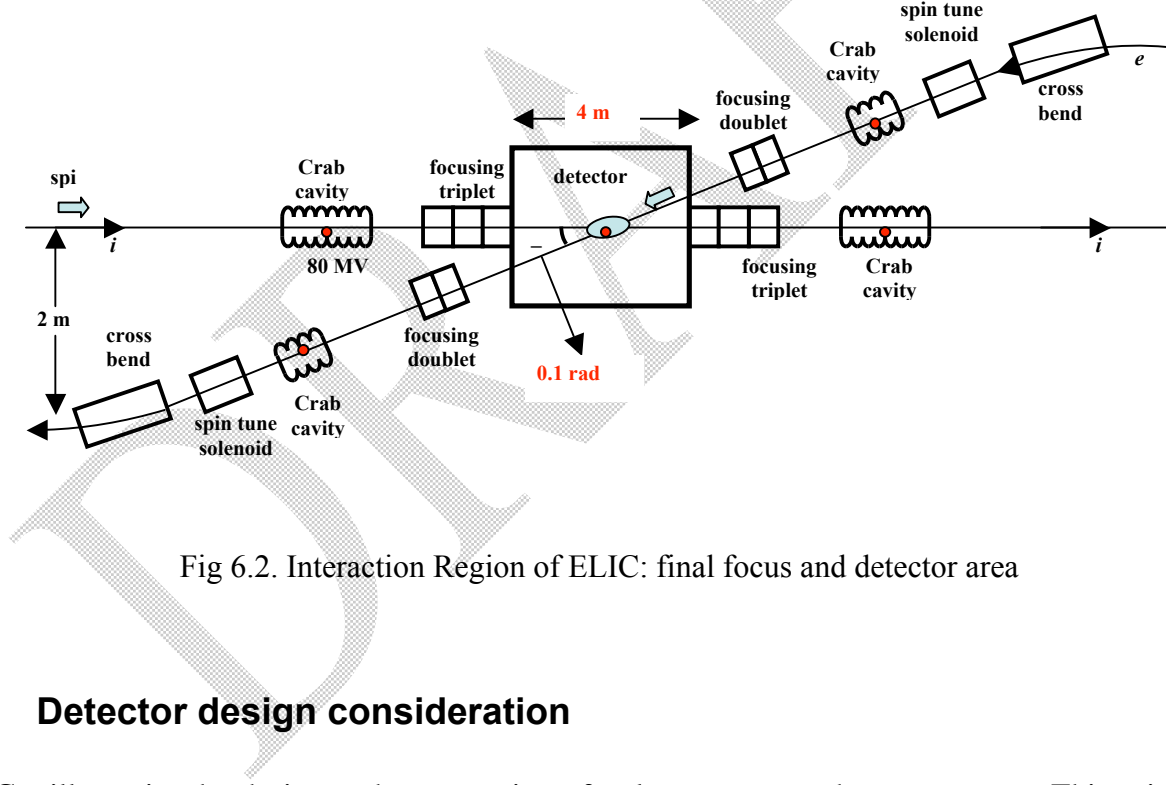


Fig 6.2. Interaction Region of ELIC: final focus and detector area

### 7.3 Detector design consideration

ELIC will require the design and construction of at least one new detector system. This primary detector should be integrated into the machine lattice and cover something close to the full angular acceptance. One possible design is based on the experience gained from the H1 and ZEUS detectors operated at the HERA collider at DESY. Here a hermetic inner and outer tracking system including an electromagnetic section of a barrel calorimeter is surrounded by an axial magnetic field. The forward calorimeter is subdivided into hadronic and electromagnetic sections while rear and barrel electromagnetic calorimeters could possibly consist of segmented towers, e.g. a tungsten-silicon type. This would allow a fairly compact configuration.

In addition the physics program at ELIC will require identification of pions, kaons and protons over a large momentum range and the capability to separate primary and secondary vertices for e.g. decays of charmed mesons. At present no comprehensive design incorporating these requirements exists. However, the following minimal requirements on a future ELIC detector can be made:

- Precision measurement of the energy and angle of the scattered electron (to determine the kinematics of the DIS reaction)
- Measurement of hadronic final state (to provide additional constraints on the kinematics of the DIS reaction, to allow jet studies, flavor tagging, fragmentation studies and the study of heavy flavor physics)
- Separation of primary and secondary vertices (for heavy flavor studies)

In addition to those demands on a central detector, the following forward and rear detector systems are crucial:

- A zero-degree photon detector to control radiative corrections and measure bremsstrahlung photons for luminosity measurements (absolute and relative with respect to different ep spin combinations)
- An electron tagger under very small angles ( $<1^\circ$ ) to measure the kinematics of quasi-real photoproduction and to study the non-perturbative and perturbative QCD transition region
- A tagging detector for forward particles (to study diffraction and nuclear fragments)

Optimizing all of the above requirements is a challenging task and will need detailed Monte Carlo studies of the required momentum resolution, angular coverage of the particle identification system and possible realization of a trigger system.

In addition, the study of exclusive processes might require a separate detector system with better resolution and the capability to detect the recoiling proton.

## 7.4 Final focusing

To implement very tight focusing in the ELIC interaction region, it is beneficial to use a focusing triplet (DFD or FDF) which provides a net focal length of about 5 m at the collision energy of 150 GeV. This triplet uses two types of quadrupoles: 1.12 m long defocusing one and 1.96 m long focusing one, with transverse aperture radius of 3 cm and 7.5 T peak field. The quadrupole parameter defines a maximum field gradient of 250 T/m. Our preliminary lattice design assumes  $\beta^* = 1$  cm and  $\beta^{\max} = 3800$  m. The final focus lattice can be configured either symmetrically (DFDODFD) or anti-symmetrically (FDFODFD). The advantage of the anti-symmetric configuration is its lower sensitivity to ground motion and magnet power supply fluctuation etc. Assuming a final normalized ion beam horizontal emittance after cooling of  $10^{-6}$   $\mu\text{m}$ , this yields the beam width in the final triplet of about 5 mm. Further, a more aggressive lattice design would assume a peak field of 9 T at the same aperture and  $\beta^{\max}$  of about 6 km, which would allow us to reduce  $\beta^*$  to about 5 mm. However, much

shorter focal length of the triplet (less than 5m) would significantly reduce free space around the interaction point available for the detector (to less than 4 m).

## 7.5 Crab crossing

### 7.5.1 Crab crossing principle

Short bunches also make feasible the introduction of crab crossing that allows one practically to remove parasitic beam-beam interactions without loss of luminosity, attain a highest bunch collision frequency (up to 1.5 GHz) and release more space for detectors [11]. With ion bunches 0.5 cm as short, applying SRF deflectors of integrated magnetic field amplitude 600 G by 4 m to effect 100 GeV ion beam, one can obtain bunch tilt 0.05 rad (corresponding crossing angle 0.1 rad) at final focus parameter 3 m (Fig.4). Bend-related rotation of electron spin can be preventively compensated by Wien filter or in other way.

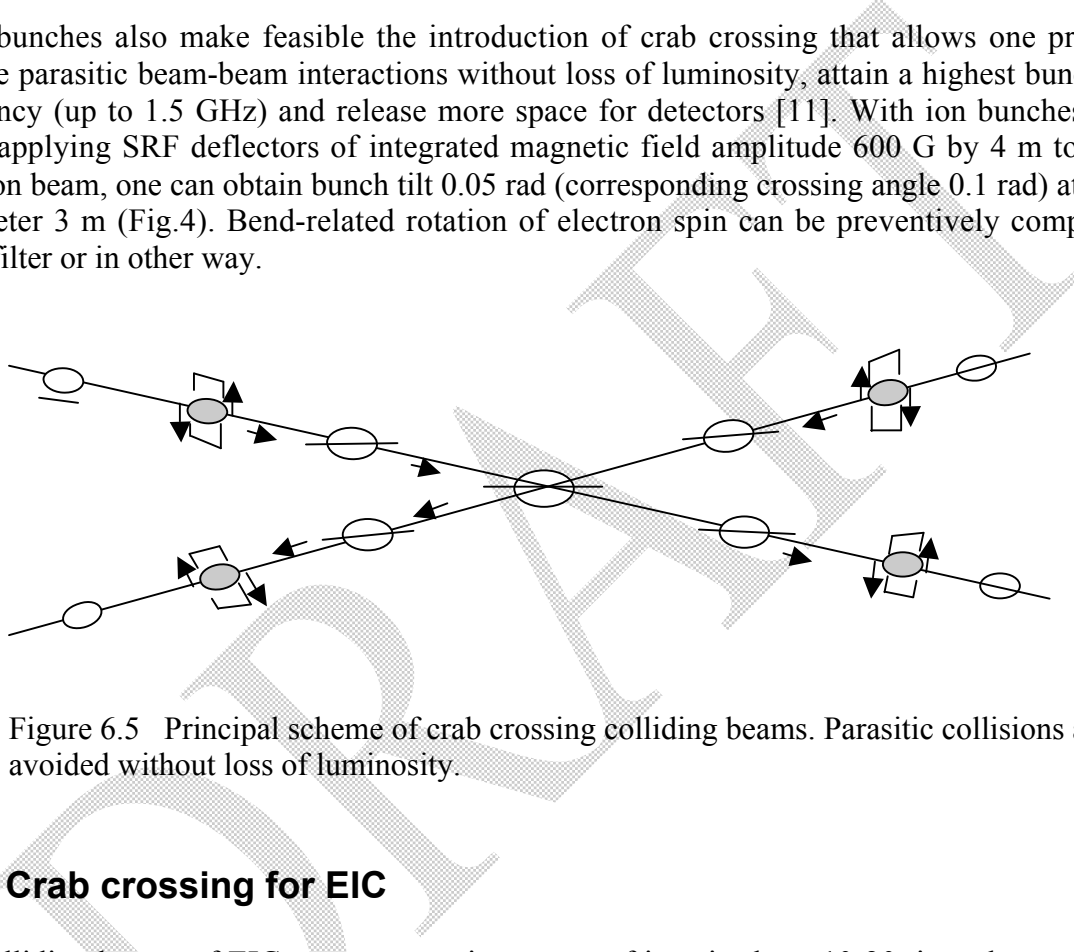


Figure 6.5 Principal scheme of crab crossing colliding beams. Parasitic collisions are avoided without loss of luminosity.

### 7.5.2 Crab crossing for EIC

The colliding beams of EIC are asymmetric, energy of ions is about 10-20 times larger than that of electrons. Therefore, the crossing beams can be designed with bend for only electron beam, but crab kick angle and tilt still required have equal magnitude for two beams (see Figure 6.4). Though electron bend is associated with the synchrotron radiation issue for detector area, it is located far away of the detector internal zone and is much less intense than at “conventional” design with beam bend inside and near the detector. Ultimately, one can consider the crossing with no bend of electron beam, bending only the ion beam. Such design is more expensive considering cost of bend dipoles for ion beam, although this bend is relatively small. Here, however, does appear a conceptual issue concerning the ion spin rotation by the cross bend, thus requiring a specific spin transport design around the IR, at least. Next stage study of the conceptual design might include the IR design with ion bends for the purpose of reaching an achromatic beam focus at Interaction Point, if needed; such considerations should take into account spin rotation by involved dipoles. At this stage of conceptual studies, ELIC IR is designed with bend of only the electron beam. Even at this approach, electron spin rotation by the cross bends is significant. In the described Ring-Ring design of ELIC, this rotation is

naturally included in design of electron spin transformation from the vertical polarization in arcs to the longitudinal one at IP, maintaining beam orbit constant with energy (see Part 3.8).

The schematic layout and basic parameters of the crab crossing beams of ELIC for crossing angle 0.1 radian are presented in Figure 6.4 and Table 6.3. An important feature of this design is that the crab resonator are installed outside the final focusing quadrupole sections at centered at the inverted focal points of focusing triplets (or doublets), thus not consuming space of the detector area. Also, the beam tilt is not evolving and the tilted bunches do not rotate in the detector zone. After that the tilted bunches have passed two Interaction points with two detectors, the crab tilt is compensated in a symmetrically located crab resonators, thus not propagating outside the detectors zone.

Table 7.3 Main parameters of ELIC Crab Crossing design.

Parameter	Unit	Ions	Electrons
Energy	GeV	150	7.5
Beam bend angle	rad	0	0.1
Bunch tilt angle at IP	rad	0.05	0.05
SRF Crab resonator frequency	GHz	1.5	1.5
Integrated amplitude of dipole SRF magnetic field	TM	0.24	0.01
Equivalent voltage	MV	80	4
Characteristic particle angle tilt in crab resonator	mrad	0.2	0.2
Crab cavity length	m	4	4

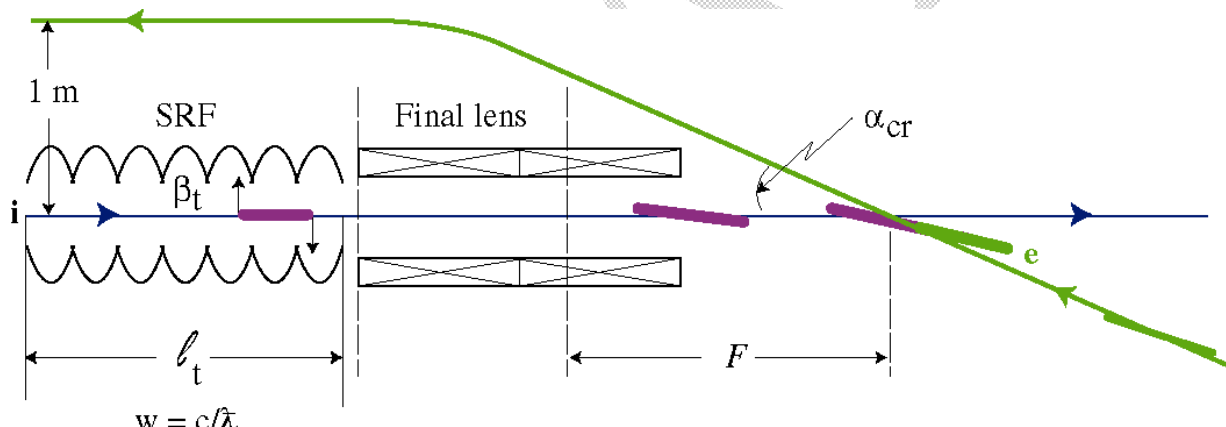


Fig.4. Crab crossing for EIC (crab resonator for electron beam is not shown)

### 7.5.3 Crab crossing tolerances

To eliminate the parasitic beam-beam interactions, the colliding beams should intersect at some angle. To avoid luminosity loss, bunches then should be turned by half of the angle thus becoming parallel to each other. The designed bunch length of 0.5 mm makes this feasible. Bunch tilt has to be produced by deflecting resonators. The peak dipole field required to generate a 50 mrad bunch tilt for 150 GeV proton beam is estimated from

$$V = \frac{\lambda_{RF} E}{2\pi\sqrt{\beta\beta^*}} \tan \frac{\theta}{2}$$

where  $\beta$  and  $\beta^*$  are beta parameters at the cavity location and the collision point, respectively (which are to be separated by 90 *degree* in betatron phase to be most effective). Also,  $\lambda_{RF}$  is the wavelength of the operating mode of the deflecting cavity and  $\theta$  is the beam crossing angle, and  $E$  is the beam energy. Therefore, approximately 100 MV is required to create the necessary bunch tilt for a crab crossing assuming  $\beta$  of about 1 km at the cavity and  $\beta^*$  of 5 mm. For 7 GeV electron beam the dipole voltage needed is much more modest 5 MV. After the collision two beams are required to return to initial unperturbed states. This is achieved by a second deflecting cavity located 90 *degree* in betatron phase away from the collision point. However, if the cancellation of kicks is not perfect, the residual effect is an excitation of betatron motion which could lead to synchro-betatron resonances with resulting beam quality degradation [paper by Wei].

Near the resonance  $Q_x \pm mQ_s = p$  (where  $m, p$  are integers and  $Q$ 's are tunes, i.e. the synchrotron tune  $Q_s = \omega_s/\omega_0$ , etc.), changes in beam emittances due to the resonances can be estimated from

$$\frac{1}{\epsilon_x} \frac{d\epsilon_x}{dt} = eV \frac{2\omega_0 mc_m}{\pi E} \sqrt{\frac{2\beta_x}{\epsilon_x}} \left[ \left( \frac{\delta V}{V} \right)^2 + (\delta\phi)^2 \right]^{1/2}$$

$$\frac{1}{S} \frac{dS}{dt} = eV \frac{2\omega_0 m^2 c_m}{Sc} \sqrt{2\beta_x \epsilon_x} \left[ \left( \frac{\delta V}{V} \right)^2 + (\delta\phi)^2 \right]^{1/2}$$

where

$$c_m \approx \left[ \frac{\eta\omega_{RF}^2 S}{64\pi\omega_s E} \right]^{m/2}$$

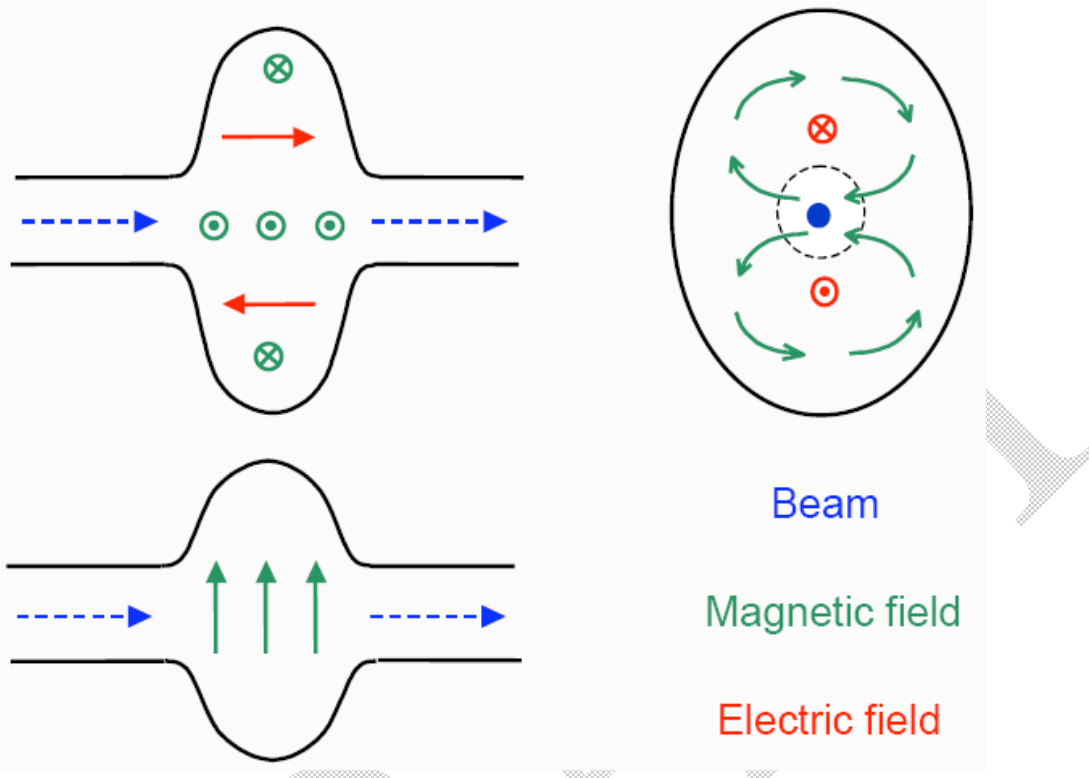
Low order synchro-betatron resonances are likely in ELIC proton beam since  $Q_s$  is rather large 0.06. For example, consider  $m = 4$  resonance. Assuming the average beta of 13 m and the revolution frequency of 0.25 MHz the horizontal emittance growth rate is about 0.045/*second* when  $\delta V/V$  or  $\delta\phi$  = 0.01 for the 150 GeV proton beam. The maximum bunch length is assumed to be 25 *degree* in RF phase in this estimate.

Constraints for RF amplitude and phase fluctuations also come from the fact that the bunch spot size is about 6 *micron* at the collision point and bunch tilts and transverse offsets must be controlled to ensure the collision of two bunches. From a qualitative consideration we find that the amplitude fluctuation can be a few percent but the RF phase must be maintained within about 0.2 *degree*.

#### 7.5.4 Crab Cavity

A crab cavity is similar to an accelerating cavity but is operated in the  $TM_{110}$  dipole mode instead of the usual  $TM_{010}$  monopole mode. On avis, the dipole mode has a zero electric field but a large transverse magnetic field. The Lorentz force resulting from the longitudinal velocity and the transverse magnetic field imparts a transverse kick to a particle proportional to  $\sin(\phi - \phi_0)$  where  $\phi$  is the phase of the rf magnetic field when the particle reaches the center of the cavity. Operating the cavity

such that when the center of the bunch reaches the center of the cavity produces transverse kick of opposite direction for the head and the tail of the bunch *i.e.* the bunch is rotated.



The effect of the electric and magnetic field on a relativistic particle traversing the cavity parallel to the axis can be obtained from

The radial kick on the particle is then given by

where  $E$  is the energy of the particle.

Dipole mode cavities at 3.9 GHz have been designed at Fermilab for Kaon separation [1] and similar cavities are under study for the ILC [2]. In these cavities, at the design transverse gradient of 5 MV/m, the peak surface electric field is 18.5 MV/m and the peak surface field is 77 mT. If the ongoing R&D program in support of the ILC comes to fruition, it is not unreasonable to assume a design transverse gradient of 8 MV/m which would correspond to a peak surface electric field of 29.6 MV/m and a peak surface magnetic field of 1230 mT.

At a frequency of 1.5 GHz, the required voltage of 80 MV would imply 10 m of cavity or about 10 m of accelerator. In this case the crab tilt design should take into account that crab resonator will be centered not at the inverse focal point of the triplet but before it. Then, a specific design should be developed in order to prevent or compensate the dynamic mismatch between the ion and electron bunch tilt at collision point.

Alternatively, one may consider operating the crab cavities at 3 or even 4.5 GHz in order to reduce the length of the crab cavities. Such high frequencies, however, will introduce significant non-linear transverse and longitudinal tilt aberrations and stringent requirements on the timing and stability of the rf system for the cavities. They would also exacerbate the generation and control of the HOMs and the cooling of the cavities.

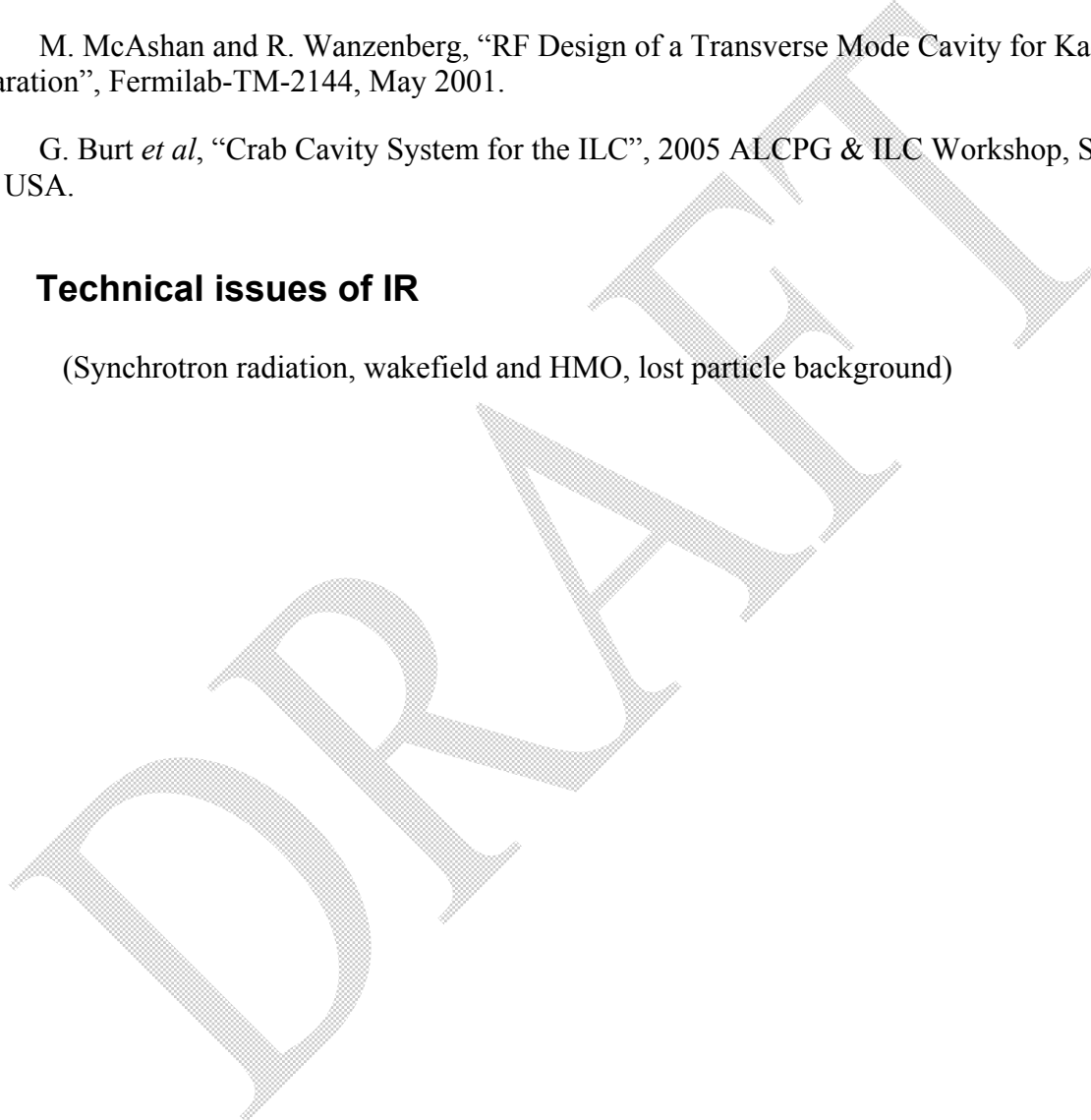
Note, that the SRF crab technology is implemented now at the KEKB (crab cavity has been installed in the beam line).

[1] M. McAshan and R. Wanzenberg, “RF Design of a Transverse Mode Cavity for Kaon Separation”, Fermilab-TM-2144, May 2001.

[2] G. Burt *et al*, “Crab Cavity System for the ILC”, 2005 ALCPG & ILC Workshop, Snowmass, CO, USA.

## 6.6 Technical issues of IR

(Synchrotron radiation, wakefield and HMO, lost particle background)



## **IX R&D Issues**

DRAFT

## X Summary

DRAFT

## **Appendix A**

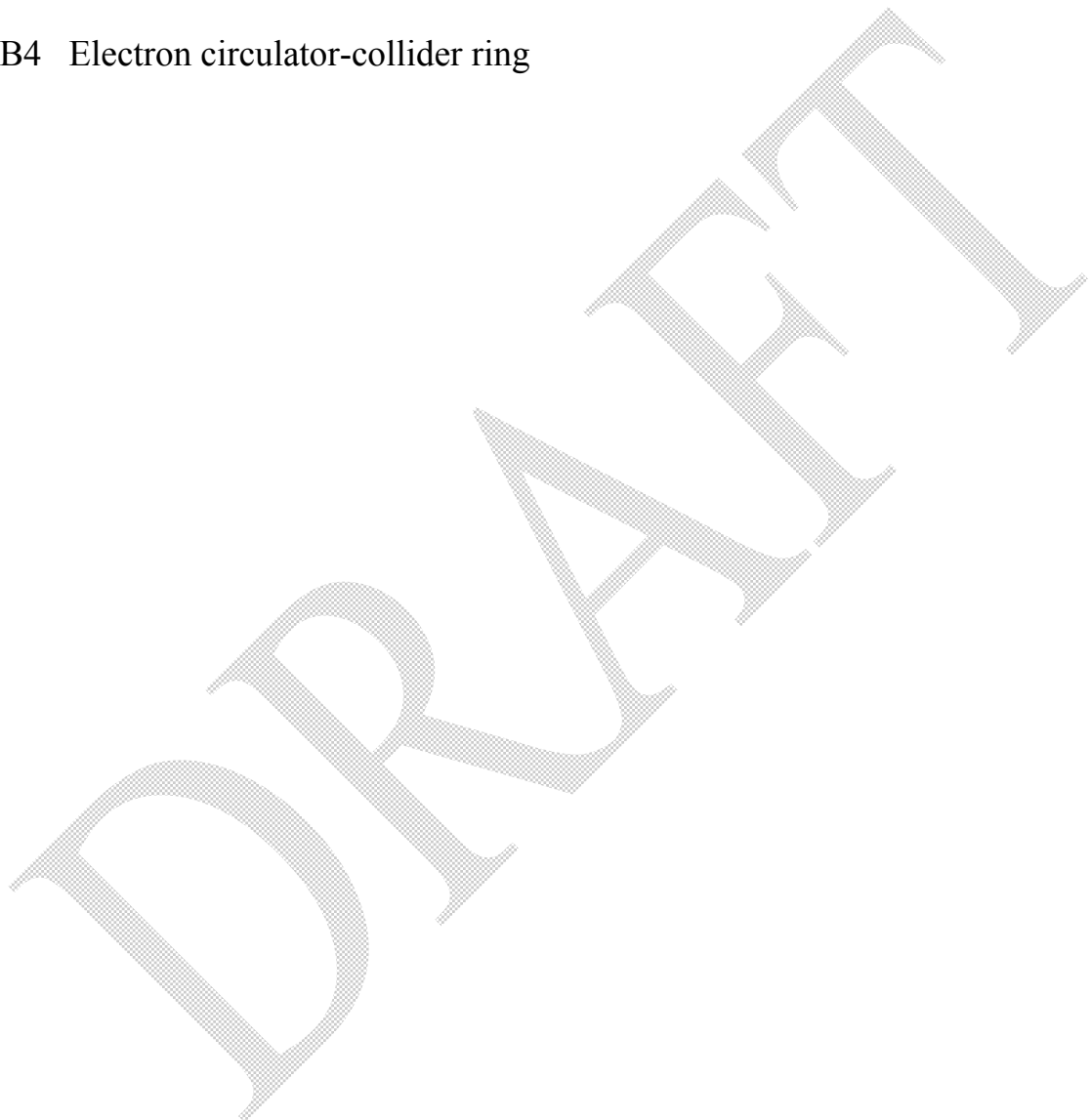
A1 Complete ELIC parameter list

A2 Site Map



## **Appendix B: ELIC Linac-Ring: Advantages and Technical Challenges**

- B1 Design consideration: ring-ring vs. linac-ring
- B2 High average current polarized electron source and injector
- B3 Energy recovery linac
- B4 Electron circulator-collider ring



## Appendix C: A High Luminosity Polarized $e^-e^-$ Collider

DRAFT

## **Appendix D: Applications**

### D1 An Advanced Ion Facility for Carbon Therapy and Injector for ELIC

